Proximal tibial subchondral bone microarchitecture: regional variations and associations with *in vivo* joint loading in end-stage knee osteoarthritis

Bryant Christopher Roberts
BAppSc (Human Movement), BEng (Biomedical) (Hons I)

A thesis submitted to the College of Science and Engineering
in total fulfilment of the requirements of the degree of
Doctor of Philosophy

Principal Supervisor: Dr Egon Perilli
Associate Supervisors: Professor Karen Reynolds, Associate Professor Dominic Thewlis

June 9, 2017

Contents

List of Figures ix

List of Tables xiii

Abbreviations xv

Abstract xvii

Declaration xix

Acknowledgements xxi

Statement of Ethical Conduct xxiii

Publications xxv

1 Introduction 1

1.1 Motivation 1

1.2 Aims and significance of research 3

1.3 Outline of the thesis 4

2 Background: Anatomy of the knee and proximal tibia subchondral bone microarchitecture 7

2.1 Anatomy and function of the knee . . . 7
2.1.1 Meniscus . . . 8
2.1.2 Articular cartilage . . . 9
2.2 Proximal tibial subchondral bone microarchitecture . . . 10
2.2.1 Subchondral bone plate (SBP) . . . 12
2.2.2 Subchondral trabecular bone (STB) . . . 13
2.2.3 Image analysis of tibial subchondral trabecular bone . . . 14
2.3 Summary . . . 18

3 Background: Gait biomechanics and knee osteoarthritis 21
3.1 Gait biomechanics changes with knee osteoarthritis . . . 21
3.1.1 Spatiotemporal parameters . . . 22
3.1.2 Gait kinematics . . . 22
3.1.3 Gait kinetics . . . 23
3.2 Gait biomechanics and knee joint structures . . . 26
3.2.1 Joint loading and variations in tibial subchondral bone . . . 27
3.3 Summary . . . 28

4 Study 1: Systematic mapping of the subchondral bone 3D microarchitecture in the human tibial plateau: variations with joint alignment 29
4.1 Introduction . . . 32
4.2 Methods . . . 33
4.2.1 Bone specimens . . . 33
4.2.2 Mechanical joint alignment from radiographic data . . . 33
4.2.3 Micro-computed tomography (micro-CT) imaging . . . 34

4.2.4 Defining the medial and lateral condylar tibia regions 35

4.2.5 Image binarization (thresholding) 35

4.2.6 Separation of subchondral bone plate (SBP) and subchondral trabecular bone (STB) in each condylar region 35

4.2.7 Systematic mapping: grid of 11 subvolumes of interest in the SBP and STB of each condyle 39

4.2.8 Morphometric Analysis 40

4.2.9 Statistical Analysis 40

4.3 Results 41

4.3.1 Within-condylar differences in STB and SBP morphometric parameters 41

4.3.2 Between-condylar (medial-to-lateral) differences in STB and SBP morphometric parameters 42

4.3.3 Associations between STB and SBP morphometric parameters 42

4.4 Discussion 54

4.4.1 Within-condylar differences in STB and SBP morphometric parameters 54

4.4.2 Between-condylar difference in STB and SBP morphometric parameters 55

4.4.3 Associations between STB and SBP morphometric parameters 56

5 Study 2: Relationships between *in vivo* dynamic knee joint loading, static alignment and tibial subchondral bone microarchitecture in end-stage knee osteoarthritis 59

5.1 Introduction 62

5.2 Methods 63

5.2.1 Participants 63

5.2.2 Gait Analysis 64

5.2.3 Clinical and radiographic data 65

5.2.4 Micro-computed tomography (micro-CT) imaging and morphometric analysis . . . 66

5.2.5 Statistics . . . 67

5.3 Results . . . 70

5.3.1 Subchondral trabecular bone microarchitecture . . . 70

5.3.2 Relationships between joint loading and tibial subchondral trabecular bone microarchitecture . . . 73

5.3.3 Relationships between knee joint loading and tibial condyle BV/TV ratios among subregions . . . 74

5.3.4 Multiple regression analysis . . . 74

5.4 Discussion . . . 80

6 Study 3: Joint loading and proximal tibia subchondral trabecular bone microarchitecture differ with walking gait patterns in end-stage knee osteoarthritis 85

6.1 Introduction . . . 88

6.2 Methods . . . 89

6.2.1 Participants, gait analysis, clinical and radiographic data, and micro-CT and morphometric analysis . . . 89

6.2.2 Cluster Analysis . . . 89

6.2.3 Statistical Analysis . . . 90

6.3 Results . . . 91

6.3.1 Comparison in loading indices among gait subgroups . . . 92

6.3.2 Comparison in morphometric parameters among gait subgroups . . . 93

6.4 Discussion . . . 100

6.4.1 Comparison in loading indices among gait subgroups . . . 101

6.4.2 Comparison in morphometric parameters among gait subgroups . . . 101

7 Conclusions and Future Recommendations **105**

7.1 Principal Findings 106

7.1.1 Regional heterogeneity of proximal tibia subchondral bone microarchitecture differs with variations in static knee joint alignment 106

7.1.2 Knee joint loading is associated with proximal tibia subchondral trabecular bone microarchitecture 106

7.1.3 Knee joint loading and subchondral trabecular bone microarchitecture varies among end-stage knee OA patients with different walking gait patterns 107

7.2 Significance to OA research 108

7.3 Recommendations for future research 109

7.3.1 Characterising regional variations in the osteochondral unit in both osteoarthritic and non-pathological joints 109

7.3.2 Exploring a causal link between knee joint loading and knee osteoarthritis progression 110

7.3.3 Elucidate the significance of the rotational moments to joint loading and structural variations in the knee joint 111

7.4 Concluding Statement 112

References **113**

A Patient Recruitment & Study Allocation **131**

List of Figures

2.1 Anterior view of the bones that comprise the knee 8

2.2 Lateral view of the knee illustrating soft tissue structures within the knee joint 9

2.3 The medial and lateral menisci shown upon the tibial plateau 10

2.4 Histological section of the articular surface 11

2.5 Subchondral bone plate thickness distribution across the medial and lateral tibial condyles 13

2.6 Within-condyle subchondral trabecular bone regions of interest selected for 2D histology analysis 17

3.1 Average external knee moments over the stance phase of the gait cycle 24

3.2 The external knee adduction moment impulse over the stance phase of the gait cycle 25

4.1 Excised tibial plateau specimen (right knee, view from top), and a specimen pair, wrapped in cling-film and fixed on the carbon scanning bed of the micro-CT system 34

4.2 Micro-CT triaxial cross-section images of a tibial plateau specimen and grey-level histogram showing threshold level used for segmentation of the bone . . . 37

4.3 3D micro-CT image of an excised tibial plateau from a right knee showing locations of 22 tibial condyle subvolumes of interest 38

4.4 Selection of subchondral bone plate and subchondral trabecular bone regions of interest for morphometric analysis 39

4.5 Regional distribution of STB BV/TV, SBP thickness and SBP porosity 48

4.6 3D micro-CT images of STB and SBP from two lateral condyle subregions showing variable bone microarchitecture 49

4.7 Bar graphs reporting average values and standard deviations of STB BV/TV, SBP thickness and SBP porosity in the 11 subregions of interest within the medial and lateral tibial condyles 50

4.8 Scatter plots with best-fit line for regions of interest with strongest correlations between STB BV/TV, SBP thickness and SBP porosity 52

5.1 3D micro-CT image of an excised tibial plateau from a right knee showing locations of four tibial condyle subvolumes of interest 69

5.2 Average external knee moment curves and standard deviation (shaded area) over the stance phase of the gait cycle for all knee OA patients (n = 25) . . . 71

5.3 Univariate scatter and box and whisker plots of 3D STB morphometric parameters in the four subregions of interest within the tibial plateau, in all OA patients and for the neutral-varus and valgus OA subgroups 72

5.4 3D micro-CT images of cylindrical STB volumes examined from the anterior-medial and anterior-lateral subregions of interest 73

5.5 Heatmap of Pearson's correlations "knee joint loads vs. subregional subchondral trabecular bone microarchitecture parameters" 75

5.6 Heatmap of Pearson's correlations "knee joint loads vs. subregional subchondral trabecular bone microarchitecture parameters" for neutral-varus subgroup (n = 18) 76

5.7 Heatmap of Pearson's correlations "knee joint loads vs. subregional subchondral trabecular bone microarchitecture parameters" for neutral-varus subgroup (n = 7) 77

5.8 Scatter plots and best-fit line for Pearson's correlations between "knee joint loads vs. subregional subchondral trabecular bone microarchitecture" 78

6.1 3D micro-CT image of an excised tibial plateau from a right knee showing locations of four tibial condyle subvolumes of interest 91

6.2 Average 3D knee moment curves for each gait subgroup in knee OA 95

6.3 Bar graphs reporting average values and standard deviations of knee loading indices in each gait subgroup in knee OA 97

6.4 Average knee flexion angle curves and standard deviation (shaded area) for each gait subgroup in knee osteoarthritis 98

6.5 Bar graphs reporting average values and standard deviations of subregional bone volume fraction (BV/TV) and BV/TV ratios among subregions for the gait subgroups in knee OA 100

A.1 Flowchart showing patient recruitment and study allocation 132

List of Tables

4.1 Varus aligned knee joints (n = 17): 3D bone morphometric parameters in the 11 regions of interest (ROIs) in the medial and lateral condyle 44

4.2 Non-varus aligned knee joints (n = 8): 3D bone morphometric parameters in the 11 regions of interest (ROIs) in the medial and lateral condyle 46

4.3 r-values for region-specific correlations between STB BV/TV and SBP Pl.Th and Pl.Po 51

4.4 r-values for correlations between subchondral trabecular bone (BV/TV, SMI, Tb.Th, Tb.SP, Pl.Th) and subchondral bone plate morphometric parameters (Pl.Th, Pl.Po) for values averaged over the 11 subregions of interest within each condyle 53

5.1 Physical characteristics of total knee arthroplasty patients 64

5.2 Summary of stepwise multiple linear regression, considering covariates that influence medial condyle joint forces and medial-to-lateral load distribution . . . 79

6.1 Summary of patient characteristics and WOMAC data for the gait subgroups in knee osteoarthritis (OA) 94

6.2 Summary of kinematic and joint loading parameters for the gait subgroups in knee osteoarthritis (OA) 96

6.3 Summary of subchondral trabecular bone microarchitectural parameters (average ± SD) for the gait subgroups in knee osteoarthritis (OA) 99

Abbreviations

AL	anterior-lateral
AM	anterior-medial
BMC	bone mineral content
BMD	bone mineral density
BV/TV	bone volume fraction
CT	computed tomography
DXA	dual X-ray absorptiometry
ERM	knee external rotation moment
IRM	knee internal rotation moment
JRF	joint reaction force
KAM	knee adduction moment (1st (KAM_1), 2nd (KAM_2) peak)
KEM	knee extension moment
KFM	knee flexion moment
MAD	mechanical axis deviation
micro-CT	X-ray micro-computed tomography
M:L	medial-to-lateral ratio
MPTA	medial proximal tibial angle
MRI	magnetic resonance imaging
OA	osteoarthritis
OCU	osteochondral unit

PCA	principal component analysis
PL	posterior-lateral
Pl.Po	plate porosity
Pl.Th	plate thickness
PM	posterior-medial
HR-pQCT	high resolution peripheral quantitative computed tomography
ROI	region of interest
SBP	subchondral bone plate
SMI	structure model index
STB	subchondral trabecular bone
Tb.N	trabecular number
Tb.Th	trabecular thickness
Tb.Sp	trabecular separation
TKA	total knee arthroplasty
VOI	volume of interest
WOMAC	Western Ontario & McMaster Universities Osteoarthritis Index

Abstract

Knee osteoarthritis (OA) is a debilitating disease characterised by major structural changes to all joint tissues including the subchondral bone. Biomechanical factors, including knee loads during gait, have been related to variations in these joint structures. However, their relationship with proximal tibia subchondral bone plate (SBP) and trabecular bone (STB) microarchitecture remains unclear. The overall aims of this thesis were, on end-stage knee OA patients undergoing total knee arthroplasty, (1) to characterise regional variations in subchondral bone microarchitecture; and (2) to explore associations between bone microarchitecture and joint loading parameters during walking gait.

The first study in this thesis characterised the spatial distribution of proximal tibia SBP thickness, porosity, STB microarchitectural parameters and relationships among them, in OA tibiae of varying joint alignment (varus and non-varus knees). Significant within-condylar and between condylar (medial vs. lateral) differences ($p < 0.05$) were found. In varus, STB bone volume fraction (BV/TV) was consistently high throughout the medial condyle, whereas in non-varus, medially it was more heterogeneously distributed. Regions of high BV/TV were co-located with regions of high STB BV/TV underneath. In varus, BV/TV was significantly higher medially than laterally, however, not so in non-varus. These findings suggesting that joint alignment influences both the between- and within-condylar distribution of joint loads, generating a corresponding bony response.

The second study explored relationships between *in vivo* dynamic knee joint loading measured during walking, static alignment and proximal tibia STB microarchitecture quantified with 3D micro-CT, on the same patient. The strongest relationships that were observed were between the external rotation moment (ERM) during early stance and the anterior-medial BV/TV ($r = -0.74$, $p < 0.01$). Medial-to-lateral BV/TV ratios correlated most strongly with ERM ($r = -0.74$) and static alignment (mechanical axis deviation, $r = 0.74$, $p < 0.001$). Relationships with ERM remained significant also after controlling for potentially confounding factors that influence joint loads (walking speed, knee adduction moment (KAM) and static alignment). Reductions in ERM may potentially indicate increased mechanical stresses in the anterior-

medial condyle, resulting in greater BV/TV in this region. These findings also suggest that ERM and rotational moments in general, under-reported in the scientific literature, warrant further exploration.

The final study identified three OA patient subgroups with distinct walking gait patterns (biphasics, flexors, counter-rotators), and evaluated differences in knee joint loading and STB microarchitecture among them. The KAM and KAM impulse were higher in the biphasic subgroup compared with flexors and counter-rotators (-0.65, -0.40 and -0.21 Nm/kg and 43.8, 25.6, and 15.2 Nm.s/kg, respectively). Despite higher KAM indices, the STB medial-to-lateral BV/TV ratio, however, did not differ between biphasics and flexors, though it was significantly lower in counter-rotators (2.15, 1.92 and 1.04, respectively). Although this study was cross-sectional in design, and hence it is impossible to conclude direct cause-effect relationship, these findings could suggest that between flexors and biphasics there may be different mechanisms for generating comparable (non-differing) loads, as indicated by the comparable medial-to-lateral BV/TV ratios as a bony response.

Findings from this thesis augment our understanding of the mechanics-structure relationship in knee OA. Significant associations between subregional proximal tibia bone microarchitecture and *in vivo* dynamic knee joint loads during walking gait measured on the same patients, were revealed for the first time, further highlighting the possible contribution of biomechanical factors in the disease. Future work is required to elucidate, if present, possible causative links between knee joint loading and microarchitectural changes in tibial subchondral bone, to identify potential biomechanical factors that may be targets for non-invasive therapies.

Declaration

I certify that this thesis does not incorporate without acknowledgement any material previously submitted for a degree or diploma in any university; and that to the best of my knowledge and belief it does not contain any material previously published or written by another person except where due reference is made in the text.

Bryant Christopher Roberts

March 1, 2017

Acknowledgements

First and foremost, I wish to thank my principal PhD supervisor Dr Egon Perilli for his continuous support throughout my candidature. Egon you were always willing to share your immense expertise in bone imaging and biomechanics and continually challenged me during my research to always pursue *good science*. Thank you also for providing numerous opportunities to expand my experiences beyond the scope of my thesis, towards building a competitive research record for the future. I hope that going forward in my career I continue to share even just a little of the tremendous enthusiasm you demonstrate for your work.

I also wish to thank Professor Karen Reynolds, first for encouraging me to pursue a PhD, and her invaluable guidance throughout this experience. Karen you retained a balanced view of my work and always reminded me to keep my focus on the end-goal.

Thanks also to Dr Dominic Thewlis. Although our meetings were as irregular as they were infrequent, your critical input and insights helped me to take significant steps towards producing publishable research and towards the completion of this thesis.

I also extend my thanks to Professor Bogdan Solomon who continuously drove patient recruitment efforts through the Royal Adelaide Hospital, and whom always made himself available to collect patient data, even at short notice and despite a very busy schedule. Thanks to Drs John Arnold and Francois Fraysse, University of South Australia who assisted in patient recruitment and collection of gait data, and to Annika Theodoulou, Repatriation General Hospital and the staff at the Royal Adelaide Hospital for coordinating collection of bone specimens. I also acknowledge the contribution of an Australian Government Research Training Program Scholarship that supported me to undertake the research within this thesis.

A thanks also to the many friends I made along the way, who come from lands near and many more from lands afar: members of Engineering Room 340 – Diana Pham, Fabian Lim, Laura Diment, Mel Ryan, Emily Anderson and Aaron Mohtar – and the Tonsley crew – Dermot O'Rourke, Albert Ruiz Vargas, Rowan Pivetta, Maged Awadalla, Dhara Amin, Mark Gardner, Laura Gell, the many, many visiting scholars and others I am sure I have forgotten – we shared

many exciting research and, mostly non-research related experiences together, which made my time at Flinders University infinitely more enjoyable. A special thanks, in particular, to the many international friends I made during this time, whom were always very eager to share their culture and teach me their language. You have inspired me to pursue a future in scientific research abroad. ¡Gracias! Grazie! Danke sehr!

To all my family and friends, without whom all my achievements to date would not have been possible. Your continuous help, encouragement and unparalleled support was worth more than I can express on paper, and for this I am grateful. Thanks especially to Mum for always encouraging me to follow my own path.

Finally, to *Kelly*, my partner, my fiancée and now my wife, to whom I dedicate this thesis. We have shared many wonderful experiences over the past 4 years as I pursued my doctorate. I graciously thank you for your patience, encouragement and unwavering support and look forward to spending many more years together, chasing many new and exciting adventures.

Statement of Ethical Conduct

Ethical approval for research undertaken in this thesis was obtained from the Southern Adelaide Clinical Human Research Ethics Committee (Approval ID: 107.13) and the Royal Adelaide Hospital Human Research Ethics Committee (Reference Number: HREC/13/SAC/402). All patients provided written informed consent prior to their involvement.

Publications

A number of publications and conference presentations have or will arise from the work presented in this thesis and are listed below. Publications are noted individually at the beginning of each relevant chapter.

Research articles in peer-reviewed journals

1. **Roberts BC**, Thewlis D, Solomon LB, Mercer G, Reynolds KJ and Perilli E 2016. Systematic mapping of the subchondral bone 3D microarchitecture in the human tibial plateau: variations with joint alignment, Journal of Orthopaedic Research, doi: 10.1002/jor.23474. In press.

2. **Roberts BC**, Solomon LB, Mercer G, Reynolds KJ, Thewlis D and Perilli E. Relationships between *in vivo* dynamic knee joint loading, static alignment and tibial subchondral bone microarchitecture in end-stage knee osteoarthritis, Osteoarthritis and Cartilage. *In revision*. May 2017.

3. **Roberts BC**, Solomon LB, Mercer G, Reynolds KJ, Thewlis D and Perilli, E 2017 Joint loading and proximal tibia subchondral trabecular bone microarchitecture differs with walking gait patterns in end-stage knee osteoarthritis. Osteoarthritis and Cartilage. doi: 10.1016/j.joca.2017.06.001. In press.

National and International Conferences

1. **Roberts BC**, Thewlis D, Solomon LB, Mercer G, Reynolds KJ and Perilli E. Joint loading and subchondral bone microarchitecture with varying walking patterns in medial knee osteoarthritis. 10th Australasian Biomechanics Conference, 2016, December 4 - 6, Melbourne, Australia. *Podium presentation*.

2. **Roberts BC**, Thewlis D, Solomon LB, Mercer G, Reynolds KJ and Perilli E. Variations in joint loading and subchondral bone microarchitecture with walking patterns in medial knee osteoarthritis. Australian and New Zealand Orthopaedic Research Society 22nd Annual Scientific Meeting, 2016, October 13 - 15, Melbourne, Australia. *Podium presentation*.

3. **Roberts BC**, Thewlis D, Solomon LB, Mercer G, Reynolds KJ and Perilli E. Linking proximal tibia bone microarchitecture to *in vivo* dynamic knee joint loads in end-stage knee osteoarthritis. Australian Society of Medical Research South Australian Annual Scientific Meeting, 2016, June 8, Adelaide, Australia. *Poster presentation*.

4. **Roberts BC**, Thewlis D, Solomon LB, Mercer G, Reynolds KJ and Perilli E. A systematic mapping of tibial plateau bone microarchitecture in end-stage knee osteoarthritis. Osteoarthritis Research Society International 2016 World Congress, March 31 - April 3, Amsterdam, The Netherlands. *Poster presentation*. In *Osteoarthritis and Cartilage*, vol. 24, no. S1, pp. S248-S249.

5. **Roberts BC**, Thewlis D, Solomon LB, Mercer G, Reynolds KJ and Perilli E. Linking proximal tibia bone microarchitecture to *in vivo* dynamic knee joint loads in end-stage knee osteoarthritis. Osteoarthritis Research Society International 2016 World Congress, March 31 - April 3, Amsterdam, The Netherlands. *Poster presentation*. In *Osteoarthritis and Cartilage*, vol. 24, no. S1, pp. S98.

6. **Roberts BC**, Thewlis D, Solomon LB, Mercer G, Reynolds KJ and Perilli E. Systematic mapping of tibial plateau bone microarchitecture in end-stage knee osteoarthritis. Orthopaedic Research Society 62nd Annual Meeting, 2016, March 5 - 8, Orlando, Florida, USA. *Poster presentation*.

7. **Roberts BC**, Thewlis D, Solomon LB, Mercer G, Reynolds KJ and Perilli E. Linking regional proximal tibia bone microarchitecture to *in vivo* dynamic joint loads in end-stage knee osteoarthritis. Orthopaedic Research Society 62nd Annual Meeting, 2016, March 5 - 8, Orlando, Florida, USA. *Podium presentation*. **Recipient Force and Motion/ORS Young Scientist Travel Grant**.

8. **Roberts BC**, Thewlis D, Solomon LB, Mercer G, Reynolds KJ and Perilli E. Regional variations in proximal tibia bone microarchitecture and joint loads in end-stage knee osteoarthritis. Australian and New Zealand Orthopaedic Research Society 21st Annual Scientific Meeting, 2015, October 2 - 4, Auckland, New Zealand. *Podium presentation*. **PhD Award Finalist**.

9. **Roberts BC**, Thewlis D, Solomon LB, Mercer G, Reynolds KJ and Perilli E. Systematic mapping of proximal tibia subchondral bone microarchitecture in end-stage knee

osteoarthritis. Australian and New Zealand Orthopaedic Research Society 21st Annual Scientific Meeting, 2015, October 2 - 4, Auckland, New Zealand. *Podium presentation*.

10. **Roberts BC**, Thewlis D, Solomon LB, Mercer G, Teague, D, Reynolds KJ and Perilli E. Relationships between proximal tibia bone microarchitecture and dynamic joint loads in end-stage knee osteoarthritis - a preliminary study. Australian and New Zealand Orthopaedic Research Society 20th Annual Scientific Meeting, 2014, September 21 - 23, Adelaide, Australia. *Podium presentation*.

Chapter 1

Introduction

1.1 Motivation

Osteoarthritis (OA) is a debilitating disease of the joint characterised by major structural changes to all joint tissues including articular cartilage and the underlying subchondral bone (Loeser et al., 2012). A leading cause of disability worldwide, OA occurs most commonly in the joints of the lower limb, with an estimated 3.8% and 0.85% of the global population affected by knee and hip OA respectively (Busija et al., 2010; Cross et al., 2014). OA is more common in women than in men, and prevalence rises significantly with age. Prevalence rates of radiographic knee OA greater than 37% have been observed in populations 60 years or older (Lawrence et al., 2008). In Australia, 1.9 million people currently live with OA of some severity (Arthritis and Osteoporosis Victoria, 2013), and over 250 million people worldwide are estimated to be affected by OA at the knee, with the incidence of the disease increasing annually (Murray et al., 2013). In many developed countries OA carries high economic costs. In Australia 40.9% of all direct health care expenditure associated with the treatment of musculoskeletal conditions were attributed to OA, a value exceeding 3.7 billion AUD in 2012. In the USA the annual cost of OA was estimated to have exceeded 185 billion USD in 2007 (Kotlarz et al., 2009).

The physical symptoms of OA include joint pain, stiffness and loss of joint function which result in difficulties performing activities of daily living. In addition to the physical symptoms of the disease, OA also has adverse social and psychological consequences including greater absenteeism and unemployment and higher incidence of depression and anxiety (Arthritis and Osteoporosis Victoria, 2013). OA was previously characterised primarily as a disease of the articular cartilage, however, it is now recognised that abnormal remodelling may occur in all joint tissues including the subchondral bone (Loeser et al., 2012). Subchondral bone

integrity is important for joint health, as this structure functions as a mechanical shock absorber that protects the overlying articular cartilage from excessive joint loads (Imhof et al., 1999). Alterations in the subchondral bone are suggested to play an important role in the initiation and progression of OA (Radin & Rose, 1986), with changes in subchondral bone microarchitecture shown to precede changes in other joint tissues (Weinans et al., 2012).

OA is of complex aetiology, and multiple systematic, intrinsic and extrinsic factors contribute in the development of the disease (Felson, 2004). The development of OA is itself heterogeneous and the sequence in which disease symptoms and structural changes occur at the affected joint has been shown to vary among individuals (Driban et al., 2010). In most OA patients, symptoms may progress gradually over many years or decades, while in others progression towards the end stages of the disease can occur rapidly (Felson et al., 2013; Riddle et al., 2016). The identification of modifiable risk factors, which could predict the rate of disease progression, is a priority area in OA research (Conaghan et al., 2014; Felson, 2014). The combination of risk factors that contribute in the progression of OA, however, still remains unclear.

Biomechanical factors, including obesity, joint malalignment, joint loading and level of physical activity, are suggested to be implicit in the development of OA. In particular, indirect estimates of knee joint loads - defined by knee adduction moment parameters (Kutzner et al., 2013; Schipplein & Andriacchi, 1991) - have been linked with structural variations, or osteoarthritic progression of joint tissues. Much of this research, however, either has a cartilage-centric focus (Bennell et al., 2011; Chang et al., 2015; Chehab et al., 2014), or when the subchondral bone has been considered, has examined macroscopic variations in this tissue (e.g. bone mineral density (BMD) (Thorp et al., 2006b; Wada et al., 2001) or subchondral bone articulating surface area (Creaby et al., 2010; Vanwanseele et al., 2010)). Developments in modern x-ray micro-computed tomography (micro-CT) systems enable scanning of large human bone segments as big as the human tibial plateau, and at high image resolution, permitting quantification of the trabecular bone microarchitecture (Ab-Lazid et al., 2014; Briggs et al., 2010; Fields et al., 2009; Perilli et al., 2012; Wen et al., 2013). However, the relationships between local mechanical factors at the knee joint (such as knee moments during gait or joint malalignment) and regional variations in the subchondral bone microarchitecture within the load-bearing condyles of the tibial plateau, remain to be investigated. Through a better understanding of how joint loading is related to local changes in subchondral bone microarchitecture in knee OA, it may be possible to better describe the role of both of these factors in the disease.

There is currently no cure for OA and without successful disease modifying treatments, many OA patients ultimately undergo total knee arthroplasty (TKA). With the increasing incidence of knee OA, a concomitant increase in annual TKA surgeries has been observed, resulting in a

significant increase in health care related costs for management of the disease (Hunter et al., 2014; Le Pen et al., 2005). Numerous non-surgical treatments do attempt to delay progression of OA by reducing or redistributing joint loads upon the knee (Erhart et al., 2008; Hinman et al., 2008; Jones et al., 2015). However, the inter-individual responses to conservative treatments are highly variable, and in some patients the use of these treatments, for example prescription of lateral wedge insoles, have resulted in a paradoxical increase in the KAM (Chapman et al., 2015; Hinman et al., 2012). Moreover, to date, these interventions do not appear to attenuate disease related changes in joint structures (Bennell et al., 2011; Pham et al., 2004). Such unsatisfactory outcomes, it is suggested, may be a consequence of a 'one size fits all' approach that fails to account for heterogeneity within the knee OA cohort to whom the intervention has been prescribed (Arnold et al., 2015). The need for a more individualised/patient-specific approach to management of OA is thus growing. Accordingly, an emerging evidence base is attempting to identify OA phenotypes for whom treatments would be most beneficial (Bijlsma et al., 2011; Karsdal et al., 2014; McAlindon et al., 2014). However, there remains a paucity of studies characterising and exploring for homogeneous biomechanical phenotypes among OA patients.

1.2 Aims and significance of research

The overall aims of the research conducted in this thesis were to describe, in end-stage knee OA patients who underwent total knee arthroplasty: (1) regional variations in subchondral bone microarchitecture; and (2) to explore associations between bone microarchitecture and joint loading parameters during walking gait.

More specifically, the aims were:

Aim 1: In the condyles of entire tibial plateaus retrieved from end-stage knee OA patients with varying joint alignment (varus or non-varus subgroups) (a) to characterise the spatial distribution of subchondral bone plate thickness, plate porosity and underlying subchondral trabecular bone microarchitecture, (b) to map region-specific associations among these 3D microarchitectural parameters between these two compartments.

Aim 2: To study, on end-stage knee OA patients undergoing total knee arthroplasty, the relationships between *in vivo* dynamic knee joint loads measured preoperatively using 3D gait analysis, static alignment and the proximal tibial subchondral trabecular bone microarchitecture of their excised knees quantified with 3D micro-CT.

Aim 3: (a) To identify subgroups with distinct walking gait patterns in end-stage knee os-

teoarthritis (OA) patients; (b) to compare measures of joint loading and proximal tibia subchondral trabecular bone microarchitecture among them.

The results presented in this thesis will expand upon the current understanding of the mechanics-structure relationship in the OA knee joint. Describing regional variations in the 3D microarchitecture of the proximal tibia subchondral bone plate and subchondral trabecular bone, and of the relationships between compartments, may provide novel insights into the loading history of the knee joint. Further, comparing the microarchitecture between both varus and non-varus knees will further shed light on the contribution of joint malalignment to biomechanics within the knee. Moreover, establishing relationships between *in vivo* measures of knee joint loading, obtained using clinical 3D gait analysis, and proximal tibia regional subchondral trabecular bone microarchitecture, may aid to identify modifiable biomechanical factors (e.g. knee moments), that in future could be targeted using non-invasive therapies to alleviate progression or symptoms of the disease. Finally, a stratification of knee OA subgroups with distinct walking patterns could help to better understand why certain OA patients may or may not respond to such treatments.

1.3 Outline of the thesis

The thesis is structured as follows:

Chapter 1 is an introduction highlighting the motivation, specific aims and the outline of this thesis.

Chapter 2 describes the anatomy and function of the knee, including the tibial subchondral bone microarchitecture as quantified via histomorphometric or 3D image analysis.

Chapter 3 is a review of the published scientific literature describing changes in gait biomechanics occurring in knee OA. Previous studies exploring relationships between joint loading and structural variations at the knee are also described.

Chapter 4 presents Study 1 in which the influence of joint alignment on the within and between condyle spatial distribution of subchondral bone plate thickness, plate porosity, subchondral trabecular bone microarchitecture and relationships among parameters, is explored (**Aim 1**).

Chapter 5 presents Study 2 that examined the relationships between dynamic knee joint loading during walking gait, static alignment and regional subchondral trabecular bone

microarchitecture as measured with 3D micro-CT, in end-stage knee OA patients (**Aim 2**).

Chapter 6 presents Study 3, which explores whether knee loading indices and subchondral bone microarchitecture differ with different walking gait patterns in end-stage knee OA (**Aim 3**).

Chapter 7 concludes this thesis. Principal findings and significance of this work to OA research, study limitations and recommendations for future work are presented.

Chapter 2

Background: Anatomy of the knee and proximal tibia subchondral bone microarchitecture

2.1 Anatomy and function of the knee

The knee, the largest joint in the human body, is a modified hinge type synovial joint that permits predominantly flexion and extension, in addition to limited abduction/adduction and internal/external rotation. In addition to these angular motions, the knee joint also experiences anteroposterior translation of both the medial and lateral condyles relative to the femur, and to a lesser extent, medial and lateral translations in response to varus and valgus loading (Levangie & Norkin, 2011). The distal femur, the proximal tibia, proximal fibula and the patella comprise the osseous portion of the knee joint (Fig. 2.1). The knee is commonly viewed as consisting of two articulations: at the tibiofemoral and at the patellofemoral joints (Blackburn & Craig, 1980). The tibiofemoral joint contains two separate articulations, between the medial or lateral femoral condyles and the corresponding condyles of the tibial plateau. In the patellofemoral joint a single articulation is present between the patella and the patella surface of the femur (Levangie & Norkin, 2011).

Between and surrounding the articulating bones of the knee, exist a variety of soft tissue structures (Fig. 2.2 and 2.3). These include the quadriceps muscle group, that serves as a major component of the extensor mechanism of the knee; tendons and ligaments, that stabilise the knee joint by reducing translational and rotational movements; fat pads, fluid filled sacs (bursa) and the synovial fluid, that each provide lubrication and thus reduce friction, between

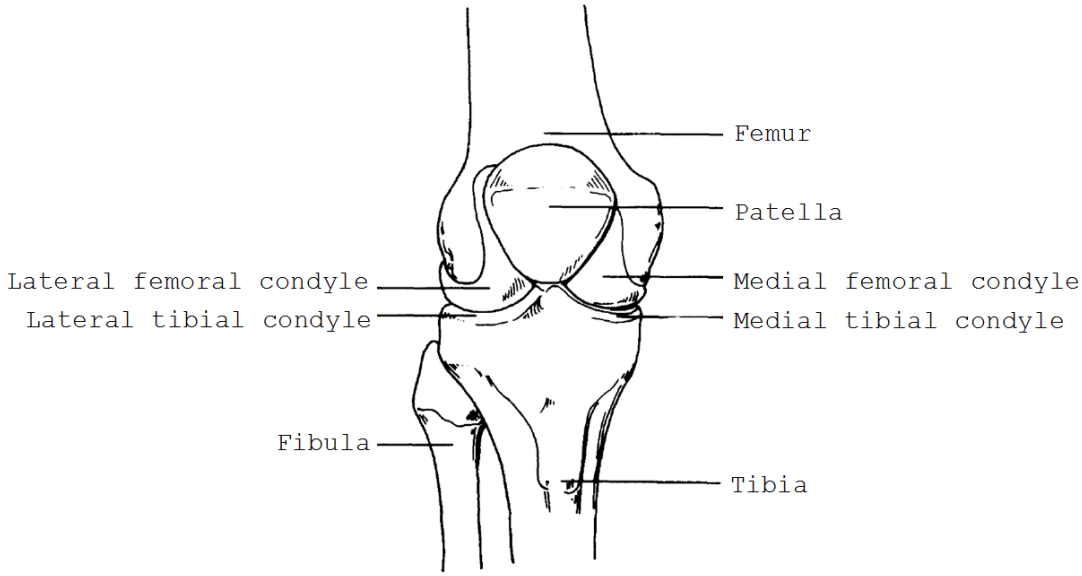

Figure 2.1: Anterior view of the bones that comprise the knee. Modified with permission from Oxford University Press, from Blackburn & Craig (1980).

moving parts in the joint. Synovial fluid also cushions shocks in joints that are subject to compressive loads. Its circulation also provides nutrients and a waste disposal pathway for the chondrocytes of the articular cartilage. Key soft tissue structures of particular importance in tibiofemoral joint OA include the menisci and articular cartilage.

2.1.1 Meniscus

Between the articular surfaces of the femoral and tibial condyles lies a pair of fibrocartilage pads, the medial and lateral menisci (Fig. 2.3). The menisci are primarily composed of 70% water and approximately 20% type I collagen. The remaining matter is composed of types II, III and IV collagen and noncollagenous proteins (Brindle et al., 2001). Each meniscus, which extends the superior surface of the tibia, attaches at the intercondylar eminence of the tibial plateau. Both menisci are roughly wedge-like, with the medial meniscus more of a crescent shape that covers between 51-74% of the medial condyle, while the lateral meniscus is circular and covers between 75-93% of the lateral condyle (Clark & Ogden, 1983). The superior surface of each meniscus is concave and thus conforms to the convex shape of the femoral condyles. This improves joint congruity between the flat surface of the tibial plateau and the distal femur (Blackburn & Craig, 1980). The major functions of the menisci are to distribute loads across the knee during weight bearing, provide shock absorption, reduce joint contact stresses and facilitate joint gliding through lubrication and nutrition of the articular cartilage (Brindle et al., 2001; Makris et al., 2011). The menisci reduce forces across the articular cartilage by

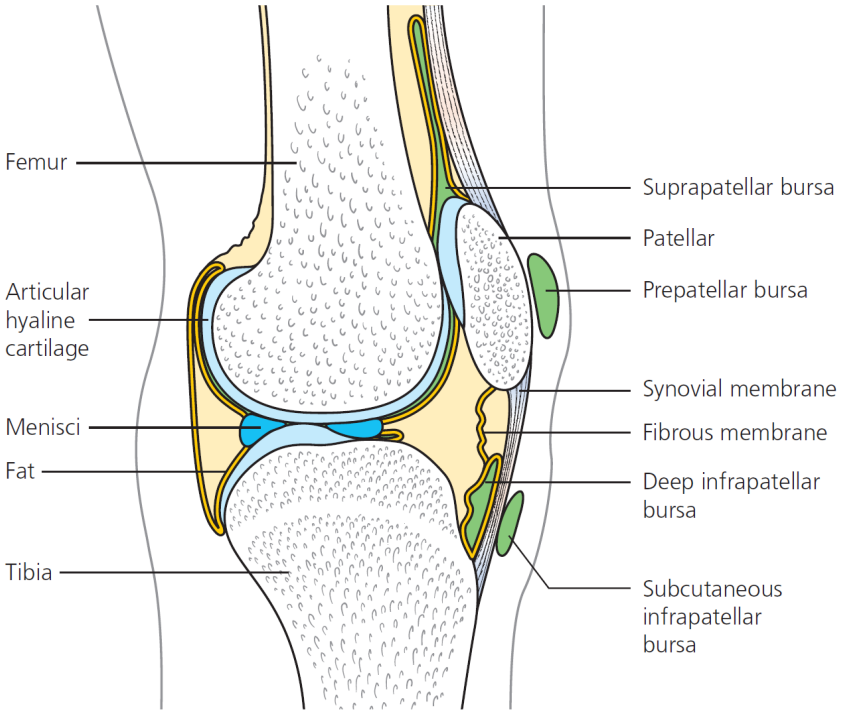

Figure 2.2: Lateral view of the knee illustrating soft tissue structures within the knee joint. Reproduced with permission from Conaghan & Nelson (2012). Copyright ©fastfacts.com

converting a compressive axial load into a tensile strain which is dispersed by the collagen fibres (Bullough et al., 1970).

2.1.2 Articular cartilage

Articular cartilage is a specialised hyaline cartilage that lines the articular surfaces within synovial joints (Fig. 2.2). Articular cartilage is up to a few millimetres thick with variations in thickness, chondrocyte density and mechanical properties, common within the same joint, across joints and between genders (Buckwalter & Mankin, 1998). Chondrocytes are the only cells comprising hyaline cartilage. These cells however are rather sparse, contributing approximately 5% of the tissue volume. The chondrocytes produce a well hydrated extracellular matrix, comprised of 70-80% water, collagen, proteoglycans and noncollagenous proteins (Conaghan & Nelson, 2012). Histologically, the cartilage may be divided into four layers, or zones, distinguished by the orientation of collagen fibrils. In the superficial layer (zone I), collagen tends to be oriented tangentially to the articular surface, whilst in the intermediate and deep zones (zones II and III), collagen is gradually re-oriented perpendicular to the surface. Deep to these zones is a layer of calcified cartilage (zone IV), which is separated from the articular cartilage by a tidemark. The calcified cartilage adjoins the corticalised subchondral bone plate (SBP),

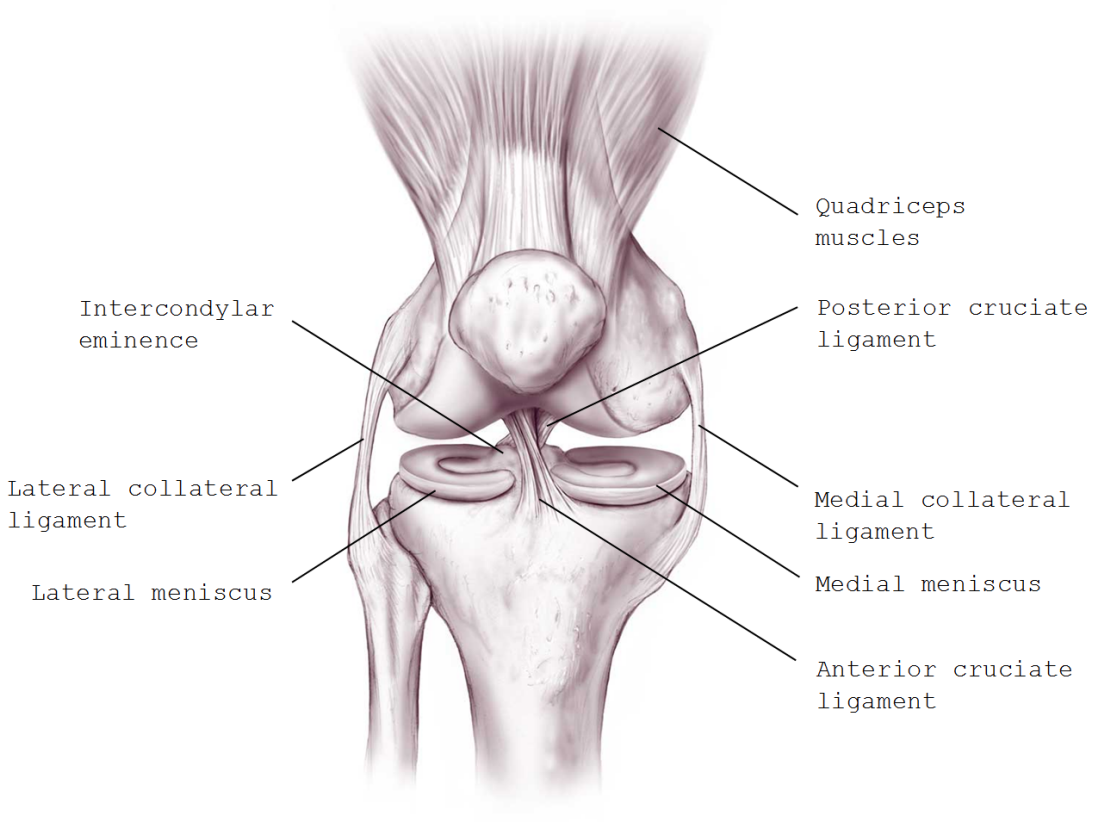

Figure 2.3: The medial and lateral menisci shown upon the tibial plateau. Reproduced with permission from Oxford University Press, from Blackburn & Craig (1980).

and from beneath the plate, the subchondral trabecular bone (STB) emerges (Fig. 2.4). Due to the arrangement of collagen, articular cartilage is able to withstand tensile and shear stresses at the surface and compressive stress in the deeper cartilage layers. Thus it exhibits an exceptional ability to distribute load and consequently minimise peak stresses on the underlying subchondral bone (Burr, 2004).

2.2 Proximal tibial subchondral bone microarchitecture

Subchondral bone is the term used to define the region of bone extending from the calcified cartilage to the bone marrow. Subchondral bone is formed from the subchondral bone plate and the underlying subchondral trabecular bone (Fig. 2.4). Unlike the articular cartilage, the subchondral bone has dense vascular and neural networks that are important in maintaining homeostasis via bone remodelling. Together, the articular cartilage and underlying subchondral bone form a single functional structure: the osteochondral unit (OCU). The OCU is important to the maintenance of joint health with pathological changes to one structure shown to lead to

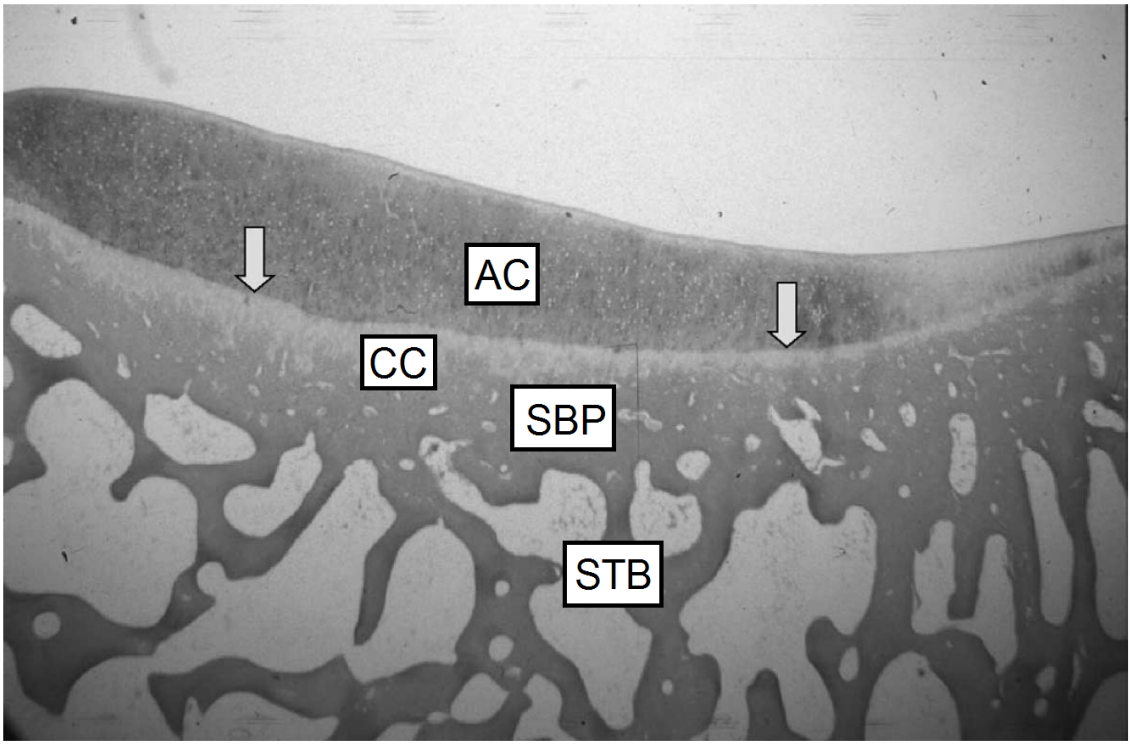

Figure 2.4: Histological section of the articular surface from rabbit proximal tibia. The articular cartilage (AC) is separated from the calcified cartilage (CC) by the tidemark (arrows). The calcified cartilage bounds the subchondral bone plate (SBP) and deeper subchondral trabecular bone (STB). Original magnification = 6.25x. Reproduced with permission from Elsevier, from Burr (2004).

abnormal remodelling of the other (Burr & Gallant, 2012; Mahjoub et al., 2012). Despite the importance of both tissues in OA, the remainder of this chapter is concerned with discussion of the subchondral bone, which is the tissue of primary interest in this thesis. The structure and function of subchondral bone, as well as how subchondral bone microarchitecture varies with and without OA, are described in the following section.

2.2.1 Subchondral bone plate (SBP)

The subchondral bone plate is a corticalised lamellar structure that adjoins the calcified cartilage. Like the articular cartilage, the thickness of the SBP varies within the joint and tends to be thicker in the higher weight-bearing regions on the tibial plateau (Fig. 2.5) (Duncan et al., 1987; Milz & Putz, 1994). These regions, typically located at the centre of the medial and lateral tibial condyles, are areas that correspond to places within the joint where stress is assumed to be greatest (Madry et al., 2010). The calcified cartilage keys into, somewhat like a jigsaw puzzle, the irregular surface of the SBP to form the osteochondral junction. The arrangement of the osteochondral junction permits transformation of large shear forces into compressive and tensile stress. The SBP functions to attenuate and distribute forces, transmitted through the menisci and cartilage, to the underlying STB (Imhof et al., 1999). The SBP is porous with a dense network of marrow cavities and capillaries extending from the STB through the SBP. A minority of these channels open into the calcified cartilage and are believed to contain vessels that provide pathways for communication between the articular cartilage and subchondral bone marrow (Findlay & Kuliwaba, 2016; Yuan et al., 2014). Studies in mice have shown, using fluorescent dyes, the diffusion of small molecules across the SBP, between bone marrow and articular cartilage, highlighting the possibility of a direct signalling pathway between both tissues within the OCU (Pan et al., 2012). SBP pores have been shown to vary in size between 10 and 180 μm (Clark, 1990; Wen et al., 2013). In non-pathological joints, medially, pores appear more frequently at the periphery of the condyle, in regions covered by the meniscus and where the SBP is thin (Clark & Huber, 1990; Duncan et al., 1987). The SBP remodels itself in response to changes in the local mechanical and biochemical environment and with knee OA, changes in the SBP have been shown to precede changes in the underlying STB (Burr & Gallant, 2012). In an animal model of post-traumatic OA, SBP becomes thinner and pore density increases in the early stages of the disease, while in late OA SBP thickness increases and the previously formed perforations disappear (Botter et al., 2011).

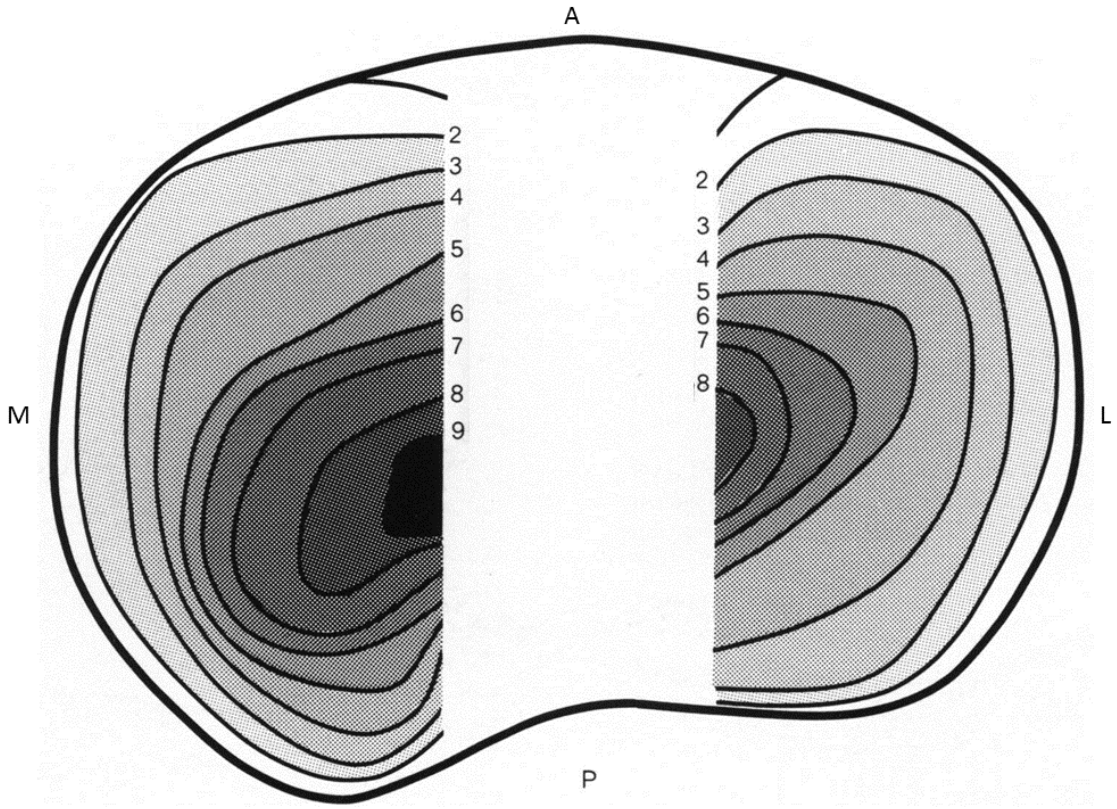

Figure 2.5: Subchondral bone plate thickness distribution across the medial (M) and lateral (L) tibial condyles. A: anterior; P: posterior; SBP thickness is indicated by numbers - 2: 200 μm to 9: 900 μm. Modified with permission from Wiley, from Milz & Putz (1994).

2.2.2 Subchondral trabecular bone (STB)

Inferior to the SBP emerges the subchondral trabecular bone. STB is a heterogeneous structure where individual trabeculae are oriented in different directions. STB differs from the SBP in that it is not only more porous, but it also exhibits different mechanical properties (e.g. a lower elastic modulus (Choi et al., 1990; Rho et al., 1993)), adapting to mechanical loads in different ways (Burr, 2004; Choi et al., 1990). An important function of STB is the attenuation of joint loads imposed upon the articulating surfaces of the joint and transmission of these loads from the joint surface to the tibial diaphysis (McKinley et al., 2003). STB continually remodels itself, in part, in response to imposed mechanical loads (Turner, 1998). The local mechanical environment is thus important to the health of the STB. *In vivo* measures of knee joint loads (knee moments) from 3D gait analysis, have been shown to differ from normal, in subjects with knee OA (see **Chapter 3, Section 3.1** for details). STB microarchitecture has also been shown to differ in the OA human knee, when compared to non-pathological joints. In the following section, common 3D microarchitectural parameters for characterising subchondral trabecular bone are first described. Then, differences in proximal tibial STB microarchitecture,

in the OA and non-pathological human knee, are discussed.

2.2.3 Image analysis of tibial subchondral trabecular bone

Trabecular bone microarchitectural parameters

Quantification of trabecular bone microarchitecture in two (2D) or three dimensions (3D) may be performed using several methods, applied to 2D histological slices or three-dimensional reconstructions of x-ray images obtained from micro-computed tomography (micro-CT) or other imaging modalities capable of imaging trabecular bone, in 3D and at high-resolution (e.g. high-resolution peripheral quantitative computed tomography (HR-pQCT)).

3D microarchitectural parameters, commonly reported in the scientific literature, include:

- Bone volume fraction (BV/TV, %): the ratio of bone volume to the total volume of a region of interest (ROI). Calculated as the number of voxels segmented as bone within the ROI, divided by the number of voxels constituting the examined ROI (Perilli et al., 2012).
- Trabecular thickness (Tb.Th, μm): average thickness of trabeculae within the examined ROI. Computed in 3D directly by using local sphere-fitting methods (Hildebrand & Rüegsegger, 1997a; Perilli et al., 2006).
- Trabecular number (Tb.N, 1/mm): a measure of the number of trabeculae per unit length (Parfitt et al., 1987).
- Trabecular separation (Tb.Sp, μm): average distance between trabeculae within the examined ROI. Computed in 3D directly by using local sphere-fitting methods (Hildebrand & Rüegsegger, 1997a).
- Structure model index (SMI, unitless): a measure describing the ratio of rod- to plate-like trabecular structures, ranging in value from 0 (ideal plate-like structure) to 3 (ideal rod-like structure), with intermediate values indicating a mixed structure (Hildebrand & Rüegsegger, 1997b; Perilli et al., 2006). In ROIs of high BV/TV, negative values of SMI can be found, attributed to high prevalence of concave surfaces within the examined tissue.

Between-condylar differences in STB microarchitecture

Ex vivo studies, using histological or micro-CT image analysis, reveal that STB microarchitecture varies between the medial and lateral tibial condyles. In both OA and non-pathologic joints the medial tibia has higher STB BV/TV (Bobinac et al., 2003; Ding et al., 2003; Matsui et al., 1997; Patel et al., 2003), higher Tb.Th (Bobinac et al., 2003; Ding et al., 2003; Matsui et al., 1997; Patel et al., 2003) and Tb.N (Bobinac et al., 2003; Patel et al., 2003) and lower Tb.Sp (Bobinac et al., 2003; Patel et al., 2003) compared with laterally. Medial STB is also more plate-like as indicated by a lower SMI (Ding et al., 2003; Patel et al., 2003). Higher medial tibial bone mass has also been observed with dual X-ray absorptiometry (DXA), reported as areal bone mineral density (aBMD) or bone mineral content (BMC) (Akamatsu et al., 2012; Clarke et al., 2004; Madsen et al., 1994; Wada et al., 2001) and with peripheral quantitative computed tomography (pQCT, measuring volumetric BMD, vBMD) (Bennell et al., 2008). However, the magnitude of the detected differences between condyles may depend on variations in joint alignment in the cohort examined, or on differences in the methodologies used to detect them (e.g. location of selected ROI). Christensen et al. (1982) noted that medial bone volume was higher only within varus-aligned joints, whilst in valgus-aligned knees the bone volume was higher laterally. Findings from Hulet et al. (2002) further support this, revealing that greater differences between medial and lateral condyle aBMD are associated with greater varus malalignment, as indicated by a decreasing hip-knee-ankle angle. Moreover, Bennell et al. (2008) highlighted that significant differences in vBMD between condyles, observed *in vivo*, were detectable only with subregional analysis of the tibial STB.

Within-condylar and depth dependent differences in STB microarchitecture

STB microarchitecture has also been shown to vary depending on the anatomical location within the medial and lateral tibial condyles. In the medial condyle, BV/TV, Tb.Th and Tb.N were highest and Tb.Sp lowest in more central to anterior regions, compared with more posterior ROIs (Bobinac et al., 2003; Kamibayashi et al., 1995). In the lateral condyle, internal and more centrally located ROIs were also found to exhibit higher BV/TV and Tb.Th compared with all other regions examined (Bobinac et al., 2003; Matsui et al., 1997). However, the study by Bobinac et al. (2003) did not make statistical comparisons between each of the four regions examined within the tibial condyles. The ROIs examined in the aforementioned studies are illustrated in Figure 2.6. Within-condylar differences in vBMD, as measured with CT and pQCT, have also been reported, albeit without statistical comparisons. Results from pQCT show higher bone volume more medially compared with peripherally in the medial condyle in an OA cohort (Bennell et al., 2008), while results from CT observed higher vBMD in central

to anterior regions of the medial condyle within control subjects (Johnston et al., 2009). In both OA and controls, higher vBMD was observed central-to-posteriorly in the lateral condyle (Bennell et al., 2008; Johnston et al., 2009).

With increasing depth from the articulating surface of the tibial condyles, decreases in BV/TV, Tb.Th and Tb.N and an increase in Tb.Sp has been observed (Kamibayashi et al., 1995; Matsui et al., 1997; Patel et al., 2003). Additionally, significant increases in the SMI, indicating a more rod-like structure, have been reported (Patel et al., 2003). Below 6 mm from the articulating surfaces no statistically significant depth-dependent microarchitectural changes are evident (Patel et al., 2003). This finding suggests that STB microarchitectural variations, which are influenced by biochemical and mechanical interactions at the joint, are likely to be confined between the SBP and this distance.

Variations in subchondral bone architecture with osteoarthritis

Tibial STB BV/TV has been shown to significantly decrease with age in knees without evidence of macroscopic pathological changes or history of musculoskeletal disease (Ding et al., 2002). With knee OA however, numerous cross-sectional *ex vivo* studies reveal higher BV/TV and Tb.Th in the medial condyle, compared with age-matched controls (Bobinac et al., 2003; Ding et al., 2003; Kamibayashi et al., 1995). Ding et al. (2003) also report a significant decrease in the SMI, indicating that osteoarthritic bone is more plate-like than in controls. Conflicting results, however, revealing lower STB BV/TV and Tb.Th and higher SMI in severe OA specimens compared with controls, have also been documented (Patel et al., 2003). In the lateral condyle, micro-CT image analysis revealed no significant differences in STB microarchitecture between OA and non-pathological joints (Ding et al., 2003). Meanwhile *in vivo* studies, using magnetic resonance imaging (MRI) for examination of STB, reveal medially, significantly lower apparent BV/TV, albeit in mild to moderate OA subjects, compared with controls (Beuf et al., 2002; Bolbos et al., 2008), and no differences in medial STB microarchitecture between a severe OA and control cohort (Beuf et al., 2002). Laterally, lower measures of BV/TV have been observed with OA, compared with controls (Bolbos et al., 2008). These reported discrepancies between *in vivo* and *ex vivo* studies, in particular for medial condyle bone microarchitecture, may largely be attributed to methodological differences, in part, due to differences in the depth of the subchondral bone regions examined. *In vivo* research, conducted using MRI, has examined subchondral bone regions greater than 10 mm inferior to the articulating surfaces of the tibial plateau. *Ex vivo* research, meanwhile, has examined bone immediately subjacent to the joint surfaces, where microarchitectural changes that are influenced by the mechanical environment of the joint are most likely to occur (Patel et al., 2003). Moreover, discrepancies among studies may arise potentially due to differences in measures of knee joint alignment be-

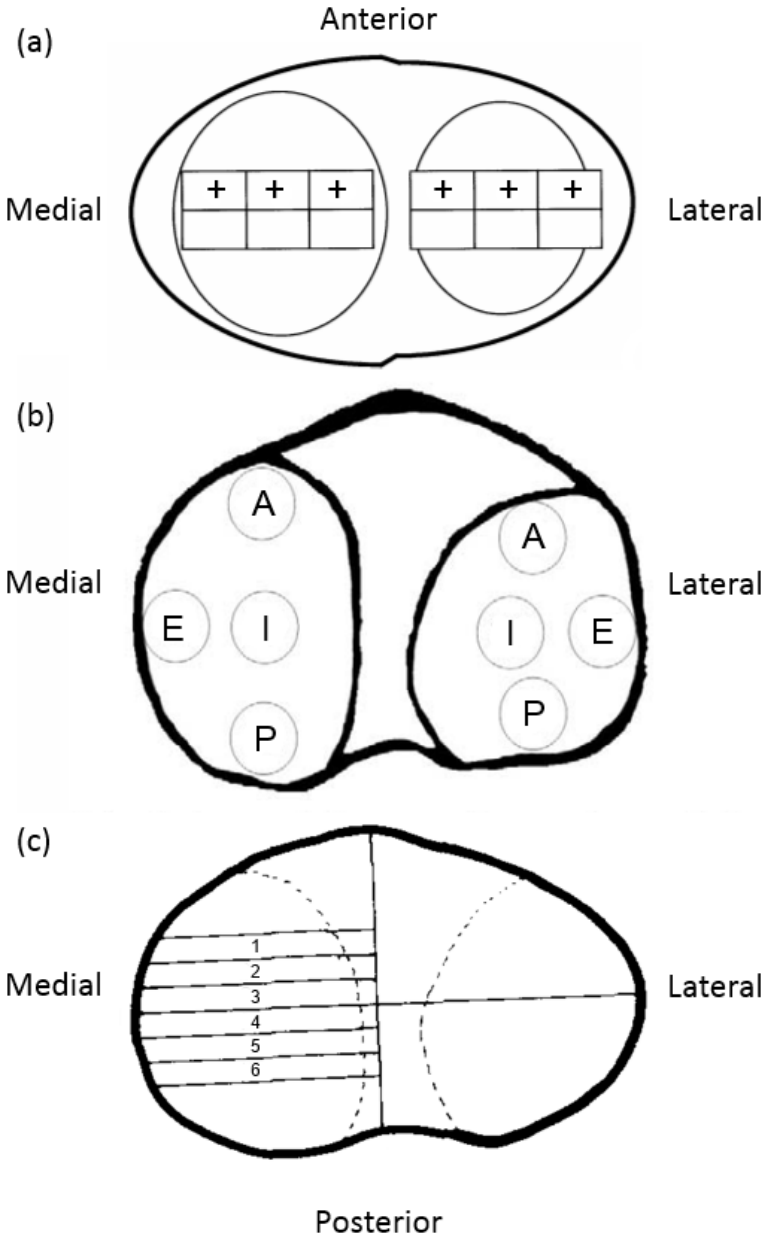

Figure 2.6: Within-condyle subchondral trabecular bone regions of interest selected for 2D histology analysis, shown within a right tibial plateau; (a) modified with permission from Wiley, from Matsui et al. (1997), regions examined are indicated by cross (+), (b) modified with permission from Elsevier, from Bobinac et al. (2003), A: anterior, E: external, I: internal, P: posterior, (c) modified with permission from Elsevier, from Kamibayashi et al. (1995).

tween patient cohorts examined, shown previously to influence BMD distribution (Hulet et al., 2002).

With increasing clinical measures of OA disease severity, changes in STB microarchitecture are also evident. Chiba et al. (2012) found that knee OA subjects with moderate to severe radiographic OA (Kellgren-Lawrence (KL) grade II-IV) had higher measures of medial tibia apparent BV/TV and Tb.Th, as determined from MRI *in vivo*, compared with subjects with mild disease severity (KL grade 0-II). Higher measures of apparent BV/TV and Tb.Th have also been reported in moderate OA patients, compared with patients with mild OA (Beuf et al., 2002). Higher measures of apparent BV/TV and Tb.Th have also been associated with decreasing cartilage area (i.e. cartilage loss) in the medial tibia (Chiba et al., 2012), while increases in BV/TV and Tb.Th, assessed histologically, have been observed with increasing cartilage degeneration determined using Mankin's grading system (Bobinac et al., 2003). Increases in medial-to-lateral (M:L) aBMD ratio have also been observed with advancing stages of radiographic disease severity (Madsen et al., 1994; Wada et al., 2001), attributed largely to an increase in medial aBMD (Madsen et al., 1994).

STB microarchitecture also varies with proximity to structural features of OA, such as subchondral bone marrow lesions (BML) or bone cysts. In the presence of a BML, higher BV/TV, but reduced tissue mineral density, and lower SMI has been observed, compared with STB ROIs or tibiae in which no BMLs were evident (Hunter et al., 2009; Muratovic et al., 2016). STB ROIs that contained a bone cyst similarly exhibited higher BV/TV, as well as higher Tb.N and lower tissue mineral density and SMI in the surrounding bone, compared with regions without a cyst, in OA specimens (Chen et al., 2015).

2.3 Summary

The microarchitecture of the proximal tibia subchondral bone, as determined from scientific literature, using *ex vivo* 2D histology and 3D micro-CT or *in vivo* MRI image analysis, was described. Present literature highlights that subchondral bone plate and subchondral trabecular bone microarchitecture differs both within and between the medial and lateral tibial condyles. Microarchitectural adaptations occur with OA, with regions of subchondral trabecular bone located up to 5 mm from the subchondral bone plate being most affected by the disease. STB BV/TV tends to be higher in the medial condyle compared with laterally, in both OA and non-pathological joints. Furthermore, higher medial tibia STB BV/TV, characterised by thicker and more plate-like trabeculae, has been observed in osteoarthritic knee joints when compared with age-matched controls.

Challenges: The tibia specimens examined *ex vivo* are typically from cadavers of unknown medical history, or have been obtained from end-stage knee OA patients following total knee arthroplasty for whom patient history is limited. To date, regional variations in bone microarchitecture within these tibia have mainly been examined by 2D histology, restricted to three or four regions of interest per condyle. Furthermore, these studies have not considered the influence of differences in joint alignment between patients, which has previously been associated with altered distribution of bone mass across the tibial condyles, and that could potentially explain conflicting findings in the scientific literature. Moreover, whereas only a few studies quantify the microarchitecture of the SBP, the relationships between SBP (plate porosity and plate thickness) and STB parameters remain still to be investigated. **Chapter 4** presents original research, undertaken in this thesis on 25 knee OA patients, that extends upon the current understanding of tibia subchondral bone microarchitecture with OA. The aims of that study were to characterise, in the medial and lateral tibial plateau, the spatial distribution of SBP thickness, SBP porosity, STB microarchitecture and the relationships among them. The study presented considers the influence of joint alignment, examining tibial plateaus from end-stage knee OA patients with and without varus joint alignment.

Chapter 3

Background: Gait biomechanics and knee osteoarthritis

Walking is a common functional activity of daily living and experimental data indicate that adults accumulate on average between 5,100 – 8,700 walking steps per day (Bassett et al., 2010; Rosenberg et al., 2010). During walking gait, individuals impart peak joint reaction forces (JRFs) between 2 – 3 body weights across the tibial plateau during single stance, approximately 70% of which pass through the medial tibial condyle (Fregly et al., 2012; Schipplein & Andriacchi, 1991). With varus or valgus malalignment, an increased percentage of the tibiofemoral JRF may be imparted upon the medial or lateral tibial condyles respectively, increasing risk for knee OA progression (Niu et al., 2009; Sharma et al., 2001). Walking gait has thus been of particular interest within the scientific literature, to understand the role of habitual loading in the development of knee OA. In the following section, changes in gait biomechanics with knee OA, as well as associations between joint loading parameters and structural changes in the knee joint, are described.

3.1 Gait biomechanics changes with knee osteoarthritis

A growing number of studies indicate that patients with knee OA exhibit significantly different spatiotemporal, joint kinematic and kinetic features during gait compared with healthy controls (Mills et al., 2013). These gait alterations, present in those with knee OA, may represent compensatory movement strategies that attempt to reduce joint loads for alleviation of joint pain (Henriksen et al., 2006) or compensate for joint instability (Farrokhi et al., 2012). In this section, differences in spatiotemporal, joint kinematic and kinetic parameters, with knee OA,

are described.

3.1.1 Spatiotemporal parameters

In general, patients with knee OA have been found to demonstrate a significant reduction in preferred walking speeds compared with healthy controls, though the magnitude of differences varies with disease severity (Al-Zahrani & Bakheit, 2002; Astephen et al., 2008; Creaby et al., 2012; Deluzio & Astephen, 2007; Gök et al., 2002; Kaufman et al., 2001; Zeni & Higginson, 2009). However, no statistically significant differences in walking speeds between controls and patients with mild to moderate knee OA have also been documented (Landry et al., 2007; Mündermann et al., 2005). Where reductions in walking speed are evident, gait is characterised by decreased stride length, shorter step length, lower cadence, longer stride time and a more prolonged stance phase during the gait cycle (Al-Zahrani & Bakheit, 2002; Astephen et al., 2008; Gök et al., 2002). Reductions in walking speed have also been observed among radiographic stages of disease severity (Astephen et al., 2008). In a recent systematic review, Mills et al. (2013) found consistent evidence in the literature reporting an increase in stride duration and decrease in cadence in severe OA compared with controls. Moderate evidence for longer stride duration in severe OA compared with mild/moderate disease, was also found, while conflicting outcomes were documented for other spatiotemporal parameters (Mills et al., 2013).

3.1.2 Gait kinematics

Numerous studies have reported significantly different sagittal plane knee kinematics during walking gait in knee OA patients, compared with healthy controls. In knee OA subjects, significantly lower knee flexion-extension range of motion during gait has been observed (Baliunas et al., 2002; Deluzio & Astephen, 2007; Ko et al., 2011). Knee OA subjects also exhibited significantly smaller peak knee flexion angles during both the stance (Astephen et al., 2008; Creaby et al., 2012; Huang et al., 2008) and swing phases of the gait cycle (Astephen et al., 2008; Weidow et al., 2006). A waveform analysis of sagittal plane knee kinematics revealed that the magnitude of the flexion angle was reduced throughout the gait cycle in OA patients (Deluzio & Astephen, 2007). Astephen et al. (2008) furthermore found that the peak knee flexion angle during stance decreased with increasing disease severity. In a systematic review, Mills et al. (2013) however, highlight that the largest differences in joint kinematics between OA and healthy controls are evident for comparisons involving individuals with severe knee OA. In contrast, a number of studies have reported no differences in knee motion between knee OA and control groups (Landry et al., 2007; Mündermann et al., 2005). Where no differences

were detected, patients either suffered from bilateral OA (Mündermann et al., 2005), or were compared with controls who significantly differed in body mass and age (Landry et al., 2007).

3.1.3 Gait kinetics

No methods currently exist for the direct non-invasive measurement of JRFs across the tibial plateau during gait. The external knee moments (Fig. 3.1), representing surrogate measurements of the tibiofemoral JRFs, are thus frequently examined. The external knee adduction moment (KAM) and more recently KAM impulse have to date been of most interest in understanding gait adaptations in the development and progression of knee OA. Previous research suggests that the KAM, typically reported as first or overall peak, is a useful surrogate measurement for the medial-to-lateral (M:L) distribution of JRFs across the tibial plateau (M:L JRF ratio) (Schipplein & Andriacchi, 1991). The peak KAM may also be predictive of the peak medial joint reaction force (mJRF) during stance (Zhao et al., 2007), though data from instrumented knee prostheses suggests that the predictive ability of the KAM for mJRF is limited (Kutzner et al., 2013; Walter et al., 2010).

A typical KAM curve is characterised by two distinct peaks, the first and generally largest, is present during midstance, while a second peak is recorded during the terminal stance phase of gait. With increasing knee OA severity the prevalence of subjects with a definitive second peak however is reduced (Hurwitz et al., 2002; Rutherford et al., 2008). Numerous studies reveal that a higher KAM is present in knee OA subjects compared with asymptomatic controls (Baliunas et al., 2002; Hurwitz et al., 2002; Mündermann et al., 2005; Thorp et al., 2006a) and that KAM increases with increasing disease severity (Mündermann et al., 2005; Sharma et al., 1998). Conflicting findings, reporting no differences in KAM among control and OA subgroups, have however also been documented (Astephen et al., 2008; Kaufman et al., 2001; Messier et al., 2005; Zeni & Higginson, 2009). Findings from a recent systematic review suggest that only patients with mild knee OA consistently exhibit larger KAM compared with controls within the scientific literature (Mills et al., 2013). Conflicting findings, for comparisons between moderate or severe knee OA and controls, were attributed to a high amount of heterogeneity among studies (e.g. high variability in mechanical alignment of knee joints among the cohorts examined) (Mills et al., 2013). Increasing interest has also been given to examination of the KAM impulse, as this measure has shown improved ability, compared with peak KAM, to distinguish between radiographic stages of disease severity (Kean et al., 2012; Thorp et al., 2006a). The KAM impulse, defined as the area under the KAM curve (Fig 3.2), provides a measure of the cumulative load imposed upon the knee during the stance phase of gait. The KAM impulse is higher in knee OA compared with controls (Maly et al., 2013) and has consistently been shown to progressively increase with increasing disease severity (Henriksen

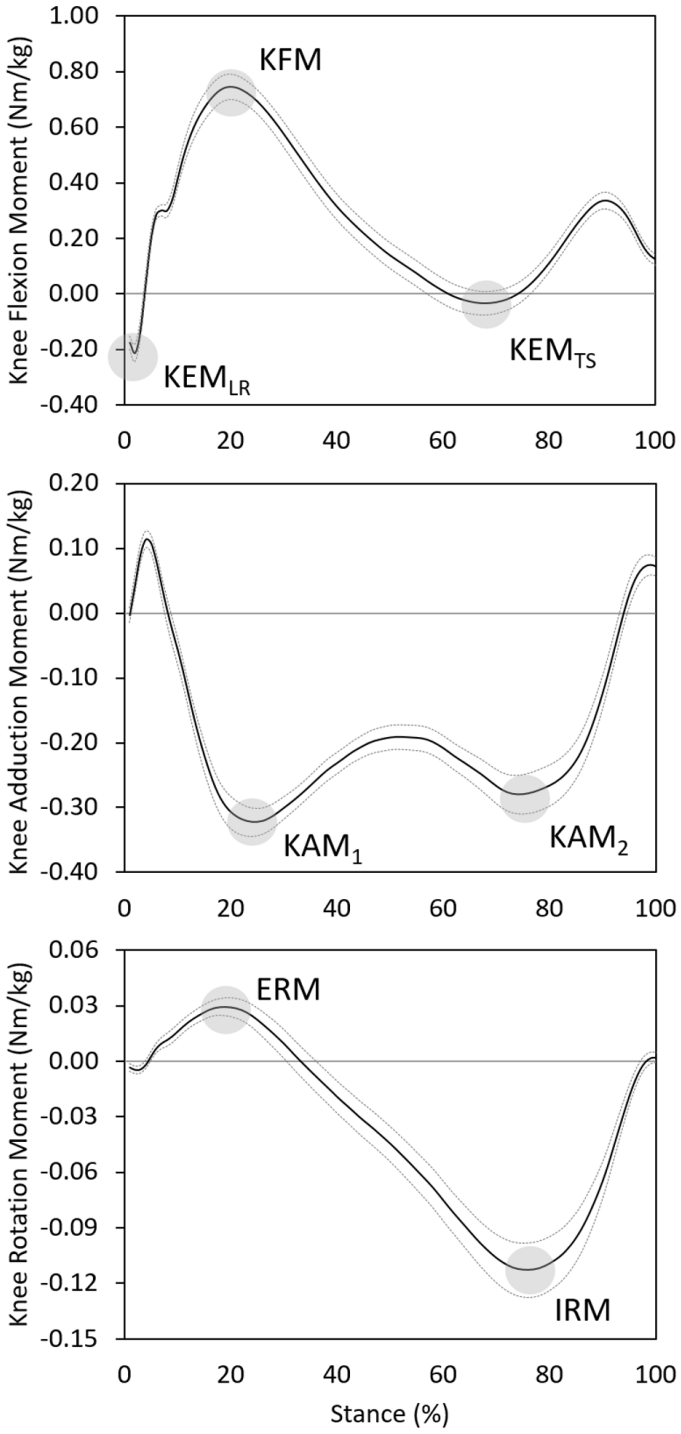

Figure 3.1: Average external knee moments (black line, ± standard error (dashed line)) over the stance phase of the gait cycle. Frequently reported peak knee moments are highlighted: KEM – knee extension moment; KFM – knee flexion moment; KAM – knee adduction moment; ERM – external rotation moment; and IRM – internal rotation moment. Subscripts LR and TS denote peak KEM during loading response (LR) and terminal stance (TS), respectively. Subscripts 1 and 2 correspond with first and second peak KAM

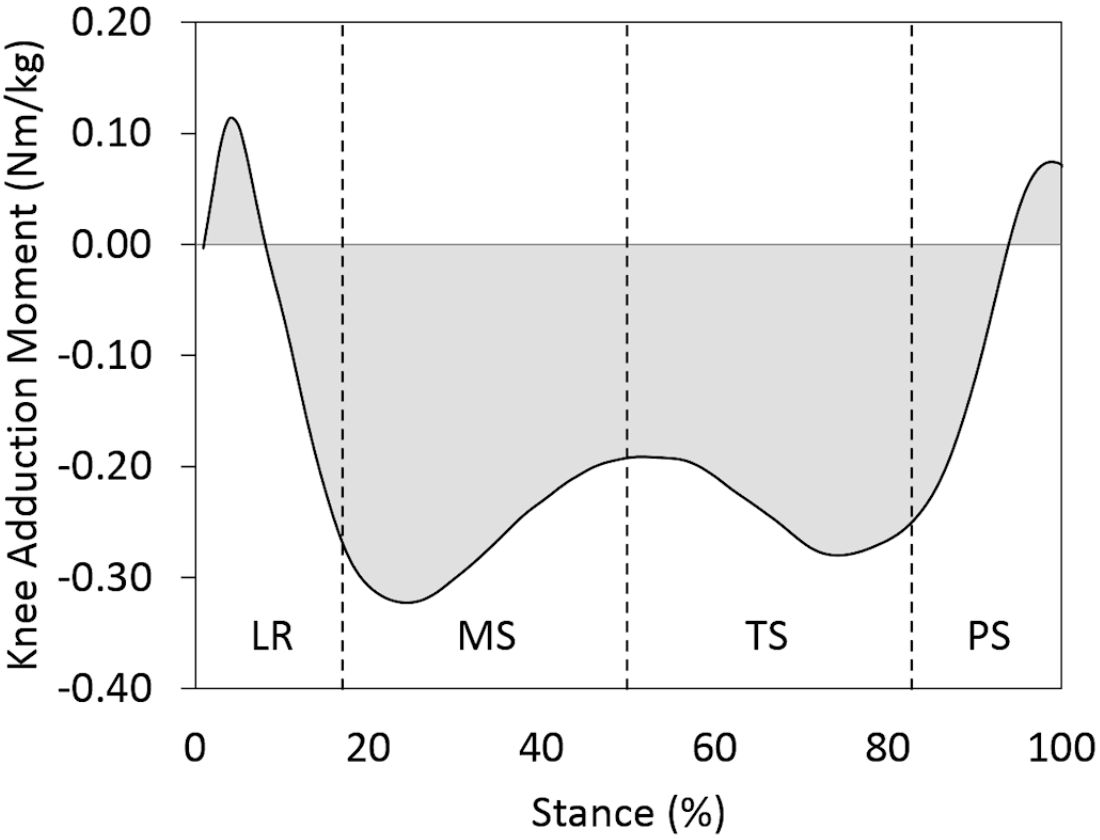

Figure 3.2: The external knee adduction moment impulse (shaded area) over the stance phase of the gait cycle. The phases of stance, as described by Perry & Burnfield (1992) are indicated: LR – loading response (0-16% of stance), MS – midstance (17-50%), TS – terminal stance (51-83%), PS – preswing (84-100%).

et al., 2012; Kean et al., 2012; Kito et al., 2010; Thorp et al., 2006a).

Differences in peak moments have also been observed in the sagittal and transverse planes. Numerous studies have reported lower peak knee flexion (KFM) (Astephen et al., 2008; Landry et al., 2007; Zeni & Higginson, 2009) and peak extension moments (KEM) (Astephen et al., 2008; Gök et al., 2002; Weidow et al., 2006) in knee OA subjects compared with healthy controls. A lower KFM has also been observed with increasing disease severity (Astephen et al., 2008). A biphasic flexion-extension moment curve (as shown in Fig 3.1) is considered characteristic of normal knee function and is observed most frequently in healthy control subjects (Smith et al., 2004). However, with knee OA, abnormal gait patterns in which the flexion-extension moment either remains predominantly in flexion (a quadriceps overuse gait pattern), or predominantly within extension (quadriceps avoidance), become more prevalent (Smith et al., 2004). Peak KFM has been linked with tibiofemoral joint load. In combination with peak KAM, it has been shown to be the best predictor of the mJRF during stance,

measured directly in instrumented knees, or indirectly using an electromyography (EMG)-driven musculoskeletal model (Manal et al., 2015; Walter et al., 2010). The KFM is balanced by an internal quadriceps moment. When active, the quadriceps impart compressive forces upon the tibiofemoral joint (Andriacchi, 1990). The reduction in the peak KFM in OA patients may thus be a result of compensatory strategies that attempt to reduce forces within the knee during gait. For rotation moments in the transverse plane, there is currently a paucity of studies exploring differences with knee OA. Conflicting findings, revealing no significant difference, as well as a higher or lower peak internal rotation moment (IRM) occurring during terminal stance, have been documented in knee OA patients compared with healthy controls (Astephen et al., 2008; Gök et al., 2002; Weidow et al., 2006). No differences, as well as a lower external rotation moment (ERM) occurring during early stance, have also been reported with OA, compared to non-pathological controls (Landry et al., 2007; Weidow et al., 2006). The contribution of the rotation moments to loading within the knee are less clear, than for the KAM and KRM.

3.2 Gait biomechanics and knee joint structures

In both non-pathological and OA knees, measures of joint loading have previously been associated with variations in joint structures, including the subchondral bone. In OA subjects, higher KAM indices during stance (e.g. a larger overall peak KAM and/or KAM impulse) have been associated with increased presence of cartilage defects (Creaby et al., 2010) and bone marrow lesions (Bennell et al., 2010), lower medial tibial condyle cartilage thickness (Erhart-Hledik et al., 2015; Maly et al., 2015) and decreasing M:L cartilage thickness ratios (Andriacchi et al., 2009; Erhart-Hledik et al., 2015). Conversely, in healthy knees, a higher KAM was associated with increasing cartilage thickness ratios (Andriacchi et al., 2009; Koo & Andriacchi, 2007). Prospective cohort studies of durations from 1 to 6 years, have also found that higher baseline measures of KAM or KAM impulse are predictive of greater rate of structural changes (cartilage thinning, cartilage volume loss) within the knee joint. Miyazaki et al. (2002) revealed that baseline measures of KAM were associated with rate of disease progression, with results in their study suggesting that a 1% increase in KAM increased risk for progression of OA 6.46 times. A higher baseline KAM has also been associated with greater subregional medial tibial cartilage thinning over a 2 year period, measured with MRI *in vivo* (Chang et al., 2015), but not with medial cartilage volume loss over a 12 month or 5 year period (Bennell et al., 2011; Chehab et al., 2014). A higher baseline KAM impulse, however, was shown to be predictive of both greater medial condyle cartilage thinning and volume loss (Bennell et al., 2011; Chang et al., 2015). Associations between joint loading and tibial subchondral bone changes reported in the scientific literature are discussed in detail within the following section.

3.2.1 Joint loading and variations in tibial subchondral bone

Commonly reported measures of subchondral bone include medial and lateral aBMD or BMC measured with DXA, as well as subchondral bone articulating surface area as measured with MRI. Several studies reveal that higher measures of peak KAM are significantly associated with higher M:L aBMD (or BMC) ratio, in both healthy and OA subjects (range r-values: 0.30 – 0.52) (Hudson et al., 2007; Hurwitz et al., 1998; Thorp et al., 2006b; Wada et al., 2001). This association was found within relatively homogeneous cohorts (healthy subjects (Hudson et al., 2007; Hurwitz et al., 1998), patients with mild to moderate radiographic knee OA (Kellgren Lawrence (KL) grade II – III) (Thorp et al., 2006b)) and within a more heterogeneous knee OA patient group (subjects with mild to severe radiographic knee OA (KL grade I – IV) (Wada et al., 2001)). Thorp et al. (2006b) also found that the second peak KAM explained greater variance in BMD ratio than first or overall peak KAM values (r-values 0.44, 0.31 and 0.30 respectively, $p < 0.01$). Additionally, a significant positive association "KAM impulse vs. M:L BMD ratio" has been reported, which was stronger compared with "peak KAM vs. M:L BMD ratio" ($r = 0.43$, $p < 0.01$ compared with $r = 0.31$, $p < 0.01$) (Thorp et al., 2006b). A positive association between M:L JRF and M:L BMD ratios has also been reported in healthy knees (Hurwitz et al., 1998). In knee OA, KAM and KAM impulse were positively associated with M:L tibial bone area ratio and KAM impulse also with medial condyle bone area (Creaby et al., 2010; Vanwanseele et al., 2010). Neither the peak KFM, nor peak KEM, was associated significantly with aBMC ratios in a non-pathological cohort (Hurwitz et al., 1998). Relationships between peak flexion moments and subchondral bone structure, in the OA knee however, are yet to be explored. Moreover, relationships between peak rotational moments and variations in any knee joint structures (soft tissues (i.e. cartilage) or subchondral bone), in the pathological or non-pathological knee joint, have not yet been investigated.

Static alignment has previously been associated with dynamic markers of load (e.g. KAM (Hurwitz et al., 2002)) and thus may provide a static surrogate for forces across the knee joint during gait. Greater measures of static alignment, as determined by the mechanical axis, tibial condylar angle or hip-knee-ankle angle, indicating greater varus alignment, have been associated with higher M:L BMD and bone area ratios and were equal if not better predictors of M:L BMD ratio compared to KAM (range r-values: 0.41 – 0.53) (Eckstein et al., 2009; Thorp et al., 2006b; Wada et al., 2001). Notably, among all reported studies, no significant relationships were observed between static or dynamic markers of load and BMD measures in a more distal ROI located within the tibial shaft (Hurwitz et al., 1998; Thorp et al., 2006b), nor did markers of joint loading explain variance in anterior-posterior BMD distribution (Wada et al., 2001).

DXA, used in the described studies, is a two-dimensional (2D) projection-imaging technique with low spatial resolution. It cannot differentiate between cortical and trabecular bone, nor among different subregions within the same condyle, and is unable to quantify the subchondral (trabecular and cortical) bone microarchitecture (see **Chapter 2** for details). To date, relationships with knee joint loading (knee moments, joint reaction force and static alignment) and the tibial subchondral bone microarchitecture, are yet to be explored.

3.3 Summary

The reviewed scientific literature highlights that, with OA, knee joint kinematics and kinetics differ from healthy controls. In particular, knee OA subjects present with a higher KAM impulse, which increases with radiographic disease severity. A higher KAM has also been observed in knee OA subjects, though evidence is conflicting. The KAM and KAM impulse were further found to be significantly associated with variations in proximal tibia subchondral bone, in patients with medial knee OA. In particular, significant positive relationships between tibial subchondral aBMD or bone area ratios and knee adduction moment parameters, static alignment or estimations of joint forces were revealed. As bone adaptation occurs in response to the dynamic loads imposed upon it, the higher subchondral BMD and bone area ratios observed with increased KAM or KAM impulse (surrogates of joint loading), could thus reflect changes in subchondral bone structure to variations in load distributions. However, these loads likely only affect periarticular measures of BMD, as forces are attenuated and become more evenly distributed with increasing distance from the articulating surfaces of the joint.

Challenges: Due to the low spatial resolution of *in vivo* imaging modalities previously employed (DXA), relationships between knee joint loading and subchondral bone microarchitecture, remain yet to be explored. Moreover, much of this research has focused on relationships between frontal plane loading indices (static alignment, KAM) and structural variations in the OA knee, despite differences in flexion-extension and rotational moments between OA patients and controls reported in the scientific literature. In **Chapters 5** and **6**, two research studies undertaken in this thesis are presented, extending upon the discussed literature. **Chapter 5** examines, on 25 end-stage OA patients undergoing total knee arthroplasty, relationships between *in vivo* dynamic knee joint loads (including the full 3D knee moments), static alignment and subregional proximal tibia subchondral bone microarchitecture of their excised knees. **Chapter 6** describes differences in knee joint loading and subchondral bone microarchitecture among OA subgroups who exhibited different walking gait patterns. Through a better understanding of how joint loading is related to local changes in subchondral bone micro-architecture in knee OA, it may be possible to better describe the role of these factors in the disease.

Chapter 4

Study 1: Systematic mapping of the subchondral bone 3D microarchitecture in the human tibial plateau: variations with joint alignment

The study presented in this chapter is the subject of the following paper:

Roberts BC, Thewlis D, Solomon LB, Mercer G, Reynolds KJ and Perilli E 2016. Systematic mapping of the subchondral bone 3D microarchitecture in the human tibial plateau: variations with joint alignment, Journal of Orthopaedic Research. doi: 10.1002/jor.23474. In press.

Abstract:

Tibial subchondral bone plays an important role in knee osteoarthritis (OA). Microarchitectural characterisation of subchondral bone plate (SBP), underlying trabecular bone (STB) and relationships between these compartments, however, is limited. The aim of this study was to characterise the spatial distribution of SBP thickness, SBP porosity and STB microarchitecture, and relationships among them, in OA tibiae of varying joint alignment. Twenty-five tibial plateaus from end-stage knee-OA patients, with varus (n = 17) or non-varus (n = 8) alignment were micro-CT scanned (17 μm/voxel). SBP and STB microarchitecture was quantified via a systematic mapping in 22 volumes of interest per knee (11 medial, 11 lateral). Significant within-condylar and between-condylar (medial vs. lateral) differences ($p < 0.05$) were found. In varus, STB bone volume fraction (BV/TV) was consistently high throughout the medial condyle, whereas in non-varus, medially, it was more heterogeneously distributed. Regions of high SBP thickness were co-located with regions of high STB BV/TV underneath. In varus, BV/TV was significantly higher medially than laterally, however, not so in non-varus. Moreover, region-specific significant associations between the SBP thickness and SBP porosity and the underlying STB microarchitecture were detected, which in general were not captured when considering the values averaged for each condyle. As subchondral bone changes reflect responses to local mechanical and biochemical factors within the joint, our results suggest that joint alignment influences both the medial-to-lateral and the within-condyle distribution of force across the tibia, generating corresponding local bony responses (adaptation) of both the subchondral bone plate and underlying subchondral trabecular bone microarchitecture.

4.1 Introduction

Osteoarthritis (OA) is a major cause of disability, occurring most commonly at the knee joint (Cross et al., 2014). Worldwide estimates suggest that 3.8% of the adult population are affected by knee OA, with direct health care expenditure exceeding $185 billion in the US annually (Cross et al., 2014; Kotlarz et al., 2009). Previously considered a primary disorder of articular cartilage, it is now recognised that OA involves the whole joint, including the bone. The pathophysiology of OA is multifactorial and subchondral bone has been suggested to play an important role in onset and progression of OA (Radin & Rose, 1986; Weinans et al., 2012).

The subchondral bone in the tibial plateau is a mechanical shock absorber of the knee joint (Imhof et al., 2000). It has a heterogeneous microarchitecture, varying between, and within, the medial and lateral condyles (Bobinac et al., 2003; Ding et al., 2003; Kamibayashi et al., 1995; Matsui et al., 1997). Despite the increase in published studies investigating the proximal tibia, the quantitative characterisation of the regional distribution of the tibial plateau subchondral trabecular bone (STB) microarchitecture, and of the thickness and porosity of the overlaying subchondral bone plate (SBP), is still limited. A systematic mapping of the regional distribution of the STB and SBP 3D-microarchitectural parameters within the medial and lateral tibial plateau, and of the relationships among these, may aid to better understanding subchondral bone changes occurring in pathologies affecting the knee, such as OA.

To date, regional variations in bone microarchitecture within the tibial condyles have mainly been examined by two-dimensional (2D) histomorphometry, restricted to three to four regions of interest per condyle (Bobinac et al., 2003; Matsui et al., 1997). Three-dimensional (3D) analysis using micro-computed tomography (micro-CT) has been limited, particularly for examination of intra-condylar variations in bone 3D microarchitecture; typically, only one or very few bone cores were physically extracted per condyle. The bone microarchitecture data was then pooled from the multiple core locations and averaged for analysis (Ding et al., 2003, 2002; Hunter et al., 2009). Furthermore, these studies have not considered the influence of differences in joint malalignment within patients, which has previously been associated with altered distribution of bone mass across the tibial condyles (Christensen et al., 1982; Hulet et al., 2002). Developments in micro-CT systems enable scanning of large human bone segments, including the tibial plateau (Ab-Lazid et al., 2014; Briggs et al., 2010; Fields et al., 2009; Perilli et al., 2012; Wen et al., 2013). However, to the best of the authors' knowledge, no study has performed a systematic examination (mapping) of a dense grid of subvolumes of the entire tibial condyle bone microarchitecture. Moreover, whereas only few studies did quantify the microarchitecture of the cortical SBP (Hunter et al., 2009; Milz & Putz, 1994; Wen et al., 2013), the relationships between STB and SBP parameters remain still to be investigated in

humans.

The aim of this study, conducted in human tibial plateaus retrieved from end-stage knee-OA patients with varying joint alignment categorised into varus and non-varus subgroups, was to 1) characterise the spatial distribution of SBP thickness and porosity and the underlying STB 3D microarchitecture (bone volume fraction, trabecular thickness, trabecular number, structure model index, trabecular separation); 2) to map region specific relationships among these 3D microarchitectural parameters between the two compartments. To this purpose, a systematic spatial mapping method of the cortical SBP and STB microarchitecture was developed and performed via micro-CT image analysis.

4.2 Methods

4.2.1 Bone specimens

Twenty-five entire tibial plateaus (Fig. 4.1(a)) were retrieved from patients with end-stage knee OA who underwent total knee arthroplasty surgery (13 right, 12 left knees). Patients (10 males, 15 females) were of age 67.3 $\pm$ 7.1 years (average $\pm$ standard deviation), height 1.66 $\pm$ 0.08 m, body mass 90.1 $\pm$ 18.9 kg. Tibial plateaus were retrieved following surgery and fixed in 70% ethanol solution. Approval to use specimens for research purposes was granted by Southern Adelaide Clinical and Royal Adelaide Hospital Human Research Ethics Committees. All patients gave written informed consent.

4.2.2 Mechanical joint alignment from radiographic data

Prior to surgery, the degree of varus-valgus mechanical alignment was quantified in the affected joints by measure of the mechanical axis deviation (MAD), obtained from full-length anterior-posterior weight-bearing radiographs by an experienced examiner (LBS). MAD is defined as the perpendicular distance (in mm) from the knee joint centre to the mechanical axis, where the mechanical axis is the line connecting the centre of the femoral head to the centre of the ankle joint. Valgus alignment was defined as $>$ 0 mm lateral deviation, neutral alignment between 0-15 mm medial deviation and varus as $>$ 15 mm medial deviation (Paley, 2002).

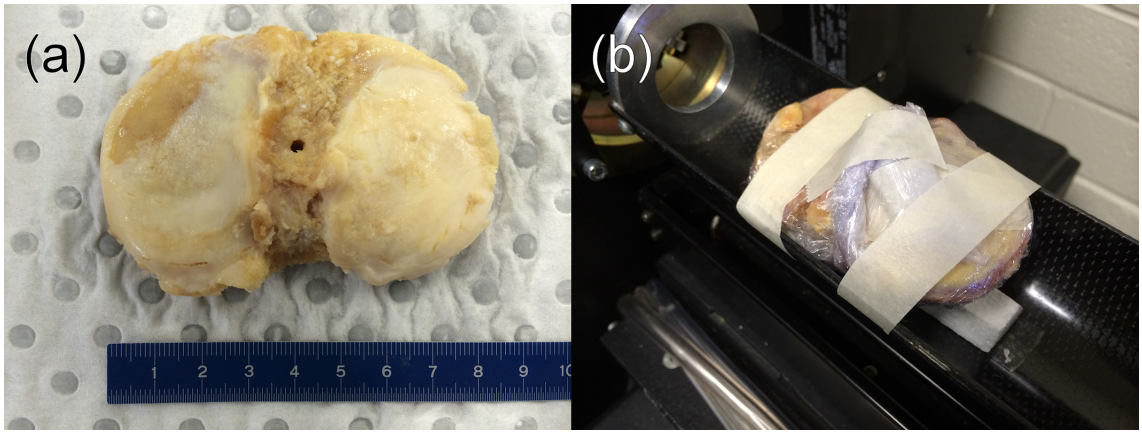

Figure 4.1: (a) Excised tibial plateau specimen (right knee, view from top), and (b) a specimen pair, wrapped in cling-film and fixed on the carbon scanning bed, with the medial-lateral axis of the specimens aligned with the rotation axis of the system.

4.2.3 Micro-computed tomography (micro-CT) imaging

Micro-CT examination of the tibial plateaus was performed using a desktop micro-CT scanner (Skyscan 1076, Skyscan-Bruker, Kontich, Belgium). Prior to scanning, specimens were removed from the ethanol solution and individually wrapped in cling-film. Scans were performed with the tibial plateau fixed on a carbon bed, the medial-lateral axis of each specimen aligned with the system's rotation axis (Fig. 4.1(b)). As specimens had one flat surface (resection surface) and were relatively thin (up to 10 mm), the field of view (68 mm diameter) was large enough to fit two specimens at once. Hence, specimens were scanned in pairs, with the flat surfaces facing each other, separated by polystyrene (transparent to X-rays) (Fig. 4.1(b)). Scanner settings: 17.4 μm isotropic pixel size, source voltage 100 kVp, current 90 μA, rotation step 0.4°, 180°rotation, exposure time 590 ms, 4 frames averaging (Perilli et al., 2012). A 0.5 mm-thick aluminium filter was used for beam hardening artefact reduction. Each scan was performed in six consecutive automated steps, imaging one-sixth of the specimen's medial-lateral length at each step (18.2 mm). For each tibial plateau pair this produced a total of 3162 X-ray projection images (527 projections per step), each image 3936 x 1048 pixels (68.5 x 18.2 mm) in size, saved in 16-bit Tiff format, generating a projection dataset of 24.3 GB, scan duration 7 hours.

The cross-section images were then reconstructed using a filtered back-projection algorithm (NRecon software, v1.6.9.8, Skyscan-Bruker) and saved as 8-bit bitmap format images (256 grey-levels, bmp value of 0 = air, 255 = mineralised tissue). For each specimen pair, a stack of up to 4997 consecutive cross-sections was reconstructed (corresponding to 86.9 mm length), slice thickness of 1 pixel (17.4 μm), producing a dataset of 70 GB, reconstruction time 4

hours (workstation: Intel Xeon CPU E5-2630v2 @2.60 GHz, 128 GB memory, OS Windows 7 64-bit). The reconstructed images were then rotated in 3D and saved with the anatomical superior-inferior axis of each plateau aligned with the z-axis of the image stack (DataViewer software, v1.5.1.2, Skyscan-Bruker) (Fig. 4.2). The resultant axial cross-section images were of size 4997 x 3936 pixels each (86.9 x 68.5 mm) (Fig. 4.2).

4.2.4 Defining the medial and lateral condylar tibia regions

Within the axial image dataset of each tibial plateau, the medial and lateral tibial condylar regions were defined by selecting the largest possible elliptical region of interest (ROI) within each condyle (software CT Analyser, v1.14.4.1, Skyscan-Bruker) (Bennell et al., 2008). The major axis of each ellipse corresponded to the anterior-posterior length of the condyle; the minor axis was contained within the outer margin of the intercondylar tubercles (inner condylar boundary) and the most external (medial or lateral) condylar edge (outer condylar boundary), excluding osteophytes, respectively (Schmidt et al., 2005) (Fig. 4.3). By using these elliptical ROIs, image datasets containing only the medial or lateral condyles were saved.

4.2.5 Image binarization (thresholding)

A 3D-median filter was applied to the medial and lateral cross-section image datasets for noise reduction. Images were then binarised using uniform thresholding (Perilli et al., 2007a,b). The uniform threshold value was the average of threshold values determined from the histograms of a subset of six representative specimens and then applied consistently on all the specimens (Perilli et al., 2007b). Pixels representing bone tissue (grey-level values between 87 and 255) were segmented as solid and those representing non-bone tissue (grey-level values from 0 to 86, marrow spaces and air) as background (Fig. 4.2).

4.2.6 Separation of subchondral bone plate (SBP) and subchondral trabecular bone (STB) in each condylar region

Subchondral bone plate (SBP) (Fig. 4.4(a,b)): On the binarised images (bone = white pixels, background = black pixels) of the tibial condyles, the SBP was separated from the underlying STB as follows (software CT Analyser). Within the stack of coronal images (Fig. 4.4(a)), the SBP was selected by manually contouring the plate boundaries every 15 images (0.26 mm); images in between had the ROI automatically interpolated (software CT Analyser) (Perilli et al., 2015a). The superior surface, defined as the first black pixel above the SBP, was traced

by following the bordering pixels of the plate (Fig. 4.4(a)). Similarly, the inferior surface of the SBP was contoured, defined as the first black pixel laying below the SBP. Trabecular struts adjoining the SBP were removed by tracing the ROI boundary across the trabeculae, hence connecting the neighbouring marrow spaces (Fig. 4.4(a)). Then the 'ROI shrink-wrap' plug-in was applied (CT Analyser), which automatically conformed the ROI boundaries to the plate border (Fig. 4.4(b)). From the resulting stack of ROIs, an image dataset containing only the SBP was saved.

Subchondral trabecular bone (STB) (Fig. 4.4(c)): The STB ROI had its superior boundary in common with the inferior boundary of the previously saved SBP ROI, whereas the STB inferior boundary was contoured following the anatomy of the inferior border of the plate and selecting subchondral trabecular bone within the first 5 mm. Only STB within the first 5 mm below the inferior SBP was considered, as it has been reported that microarchitectural differences in tibial condyles are most prominent within this distance (Patel et al., 2003). From these ROIs an image dataset containing only the STB was saved.

From the saved SBP and STB datasets, subvolumes of interest (VOI) for morphometric analysis were then selected, as follows.

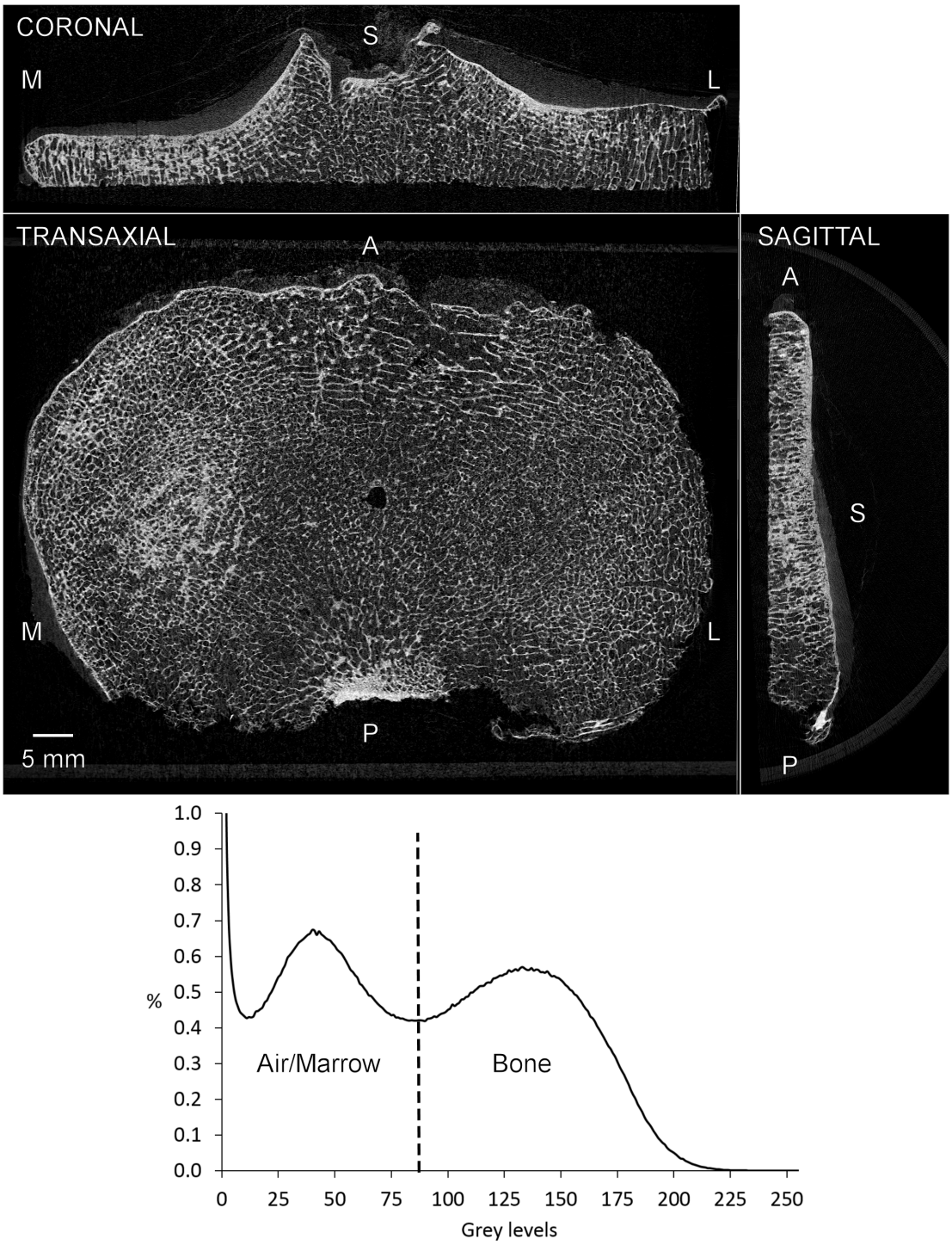

Figure 4.2: Micro-CT cross-section images of a tibial plateau specimen at 17.4 μm pixel size in coronal, transaxial and sagittal view. The grey-scale images show the bone (in bright grey colour), surrounded by background (bone marrow, cartilage, air, in dark grey). The transaxial cross-section images are 4997 x 3936 pixels in size (corresponding to 86.9 x 68.5 mm, width x height). M: medial; L: lateral; A: anterior; P: posterior; S: superior. A grey-level histogram (256 grey levels) is shown (*bottom*), with the threshold level used for segmentation of the bone indicated by a dashed line (value = 87).

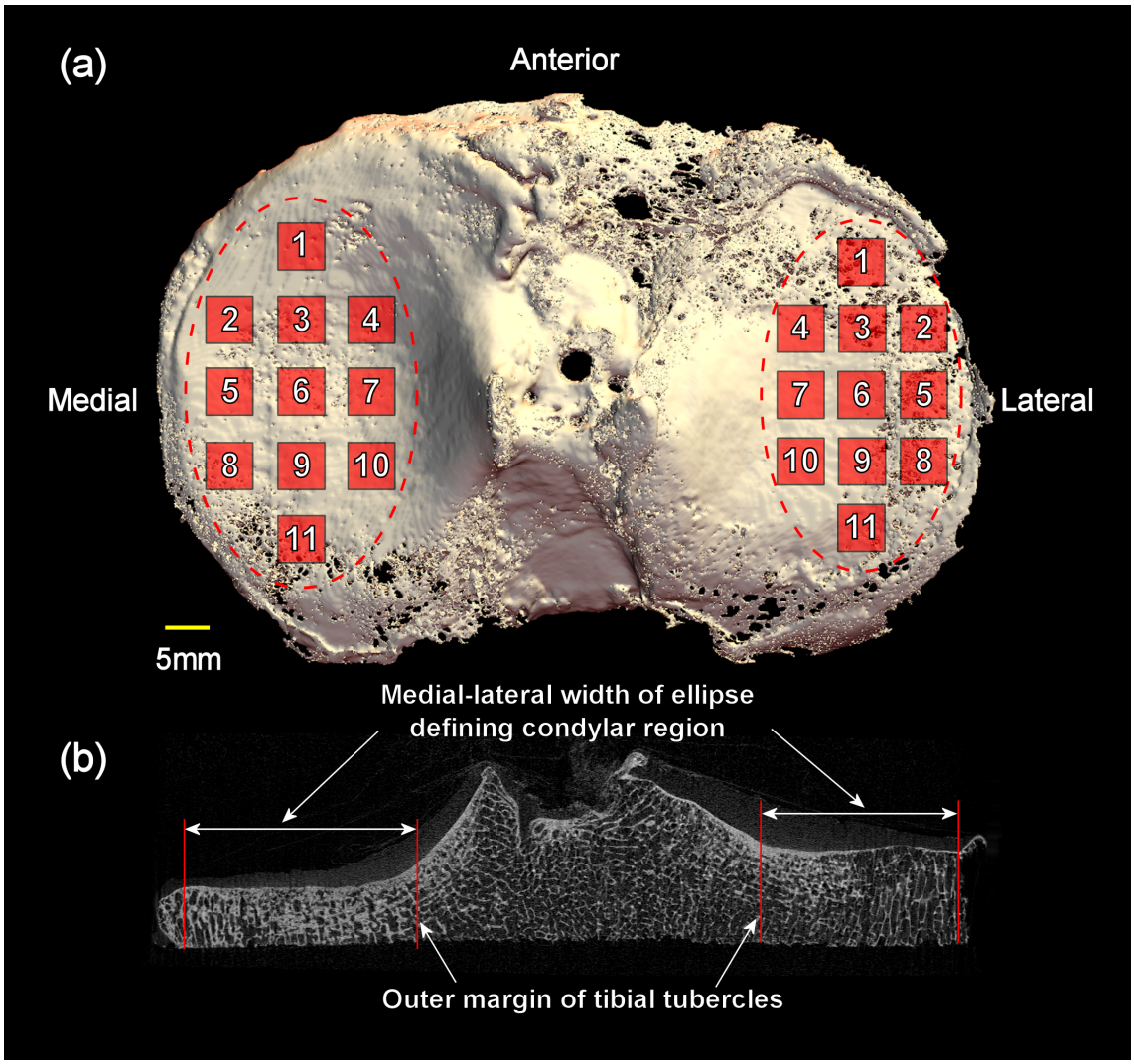

Figure 4.3: (a) 3D micro-CT image of an excised tibial plateau from a right knee (view from the top). The ellipses defining the medial and lateral tibial condyles are shown (dashed lines), containing the locations of the 22 tibial condyle subvolumes of interest (VOIs, red squares, 11 per condyle); (b) 2D coronal micro-CT cross-section image of the tibial plateau with medial and lateral boundaries of the ellipses indicated by red lines.

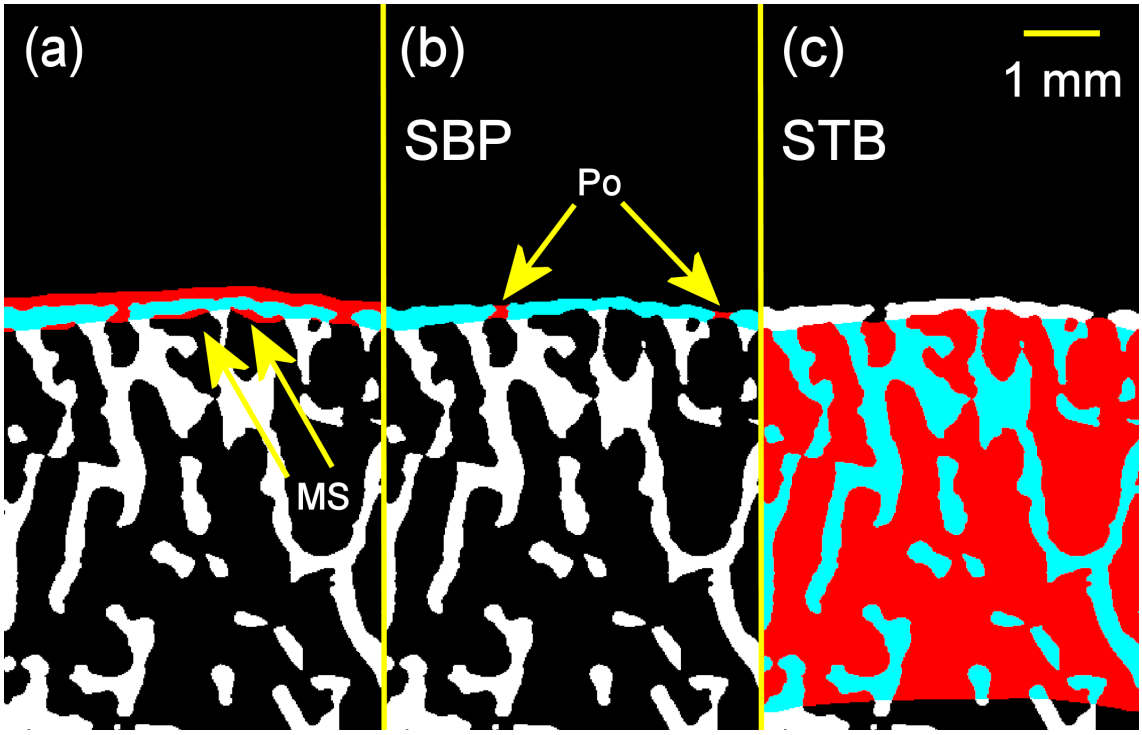

Figure 4.4: Contouring of the subchondral bone plate (SBP) and the subchondral trabecular bone (STB) on thresholded coronal micro-CT cross-section images within the tibial condyle (software CT Analyser, Bruker): (a) SBP ROI semiautomatically traced to the subchondral bone plate; blue pixels in the ROI are classified as bone, red pixels in ROI as background. The neighbouring marrow spaces (MS, indicated by arrows) were manually connected to remove trabecular struts adjoined to the SBP; (b) final SBP ROI, after the application of the "ROI shrink-wrap" plug-in (software CT Analyser); this process shrinks the ROI to the surfaces of the SBP (in blue colour) and stretches the ROI over pores (Po, in red colour) (setting: up to 20 voxels diameter (346 μm)); (c) STB ROI, of 5 mm height, containing bone (blue) and marrow space (red).

4.2.7 Systematic mapping: grid of 11 subvolumes of interest in the SBP and STB of each condyle

In the STB and SBP axial image datasets of each condyle, 11 VOIs were selected (22 VOIs per tibia). The VOI location was standardised by using a template grid (custom written MATLAB code; Mathworks, Natick, MA), normalised to the size of the ellipse defining each condyle, ensuring that the VOIs were centred about the same anatomical locations in all specimens (Fig. 4.3). VOIs were parallelepipeds with a 5 x 5 mm^2 square cross-section, with height corresponding to the entire plate thickness for the SBP and to 5 mm for the STB. The STB VOIs were cubes of 5 mm side length, to satisfy the continuum assumption for 3D morphometric analysis of trabecular bone (Harrigan et al., 1988; Tassani & Perilli, 2013).

4.2.8 Morphometric Analysis

Over each STB VOI the following morphometric parameters were calculated (CT Analyser, v1.14.4.1): bone volume fraction (BV/TV, %), trabecular thickness (Tb.Th, μm), trabecular separation (Tb.Sp, μm), trabecular number (Tb.N, 1/mm) and structure model index (SMI). BV/TV was calculated as the voxels segmented as bone within the VOI, divided by the voxels constituting the examined VOI (Perilli et al., 2012). The Tb.Th, a 3D measure of the average thickness of the trabeculae, and the Tb.Sp, a 3D measure of the mean distance between the trabeculae, were both computed by using the local sphere-fitting method (Hildebrand & Rüegsegger, 1997a; Perilli et al., 2006). The Tb.N, the number of trabecular plates per unit length (Parfitt et al., 1987), was calculated as is implemented in CT Analyser software (Tb.N = (BV/TV)/Tb.Th) (Guggenbuhl et al., 2006; Perilli et al., 2012, 2015b). The SMI describes the ratio of rod- to plate-like trabecular structures, ranging in value from 0 (ideal plate-like structure) to 3 (ideal rod-like structure), with intermediate values indicating a mixed structure (Hildebrand & Rüegsegger, 1997b; Perilli et al., 2006). For each SBP VOI, the 3D subchondral plate thickness (Pl.Th, μm) and plate porosity (Pl.Po, %) were calculated. Pl.Th was calculated using the local sphere-fitting method (Hildebrand & Rüegsegger, 1997a). Plate porosity, the percentage pore volume to tissue volume (Perilli et al., 2015a), was calculated as the number of voxels segmented as pores (background) within the SBP VOI, divided by the number of voxels constituting the VOI examined.

4.2.9 Statistical Analysis

All morphometric parameters were tested for assumptions of normality (Shapiro-Wilks test). Differences in morphometric parameters among the 11 regions within each condyle, and between corresponding regions in the medial and lateral condyles, were assessed using two-way repeated measures ANOVA. Where for a given parameter F values were found significant for a "region by condyle interaction effect", the simple "region effect" and "condyle effect" were investigated using one-way repeated measures ANOVA, followed by paired t-tests with Bonferroni adjustment for multiple comparisons. Correlations between SBP (Pl.Th, Pl.Po) and STB microarchitecture (BV/TV, Tb.Th, Tb.Sp, Tb.N, SMI) were examined using Pearson's correlation. Significance level was set to $p < 0.05$. Statistical analysis were performed using SPSS Statistics 22 (IBM Corp., Armonk, NY, USA).

4.3 Results

Specimens were split into two subgroups, categorised as exhibiting either varus (n = 17) or non-varus (n = 8) joint alignment based on their MAD. This classification provided subgroup sizes that were sufficient for further analysis (n > 6). Of the 25 entire tibial plateaus examined, two medial and one lateral condylar region, each from non-varus knees, were excluded as the height of the STB compartment suitable for analysis in these specimens was too thin to satisfy the continuum assumption for trabecular bone (height < 3 mm) (Harrigan et al., 1988).

For each subgroup, the "region effect", "condyle effect" and "region by condyle interaction effect" were significant ($p < 0.05$). Thus, the SBP and STB microarchitecture differed significantly within and between the tibial condyles, with the patterns of the within-condylar differences dependent on the condyle examined (medial or lateral).

4.3.1 Within-condylar differences in STB and SBP morphometric parameters

Within each subgroup, statistically significant differences in morphometric parameters among ROIs within the tibial condyles were found (Tables 4.1 and 4.2). Figure 4.5 shows 3D micro-CT images of a human tibial plateau with a heat map visualizing the subregional distribution of BV/TV, Pl.Th and Pl.Po within the medial and lateral condyles, averaged over the 17 varus (on left in figure) and 8 non-varus (on right in figure) tibiae.

In the varus subgroup, BV/TV in the medial condyle was consistently high (range 42-50%, regions 1-10) in all regions but the most posterior aspect, which was significantly lower (region 11). In the non-varus subgroup, medially, the BV/TV distribution was more heterogeneous than for varus knees, with BV/TV higher central-anteriorly (range 38-40%, regions 1-4, 6) than posteriorly (range 16-29%) and significantly higher centrally (regions 6 and 7), than posteriorly (8, 9 and 11). In the varus knees, lateral condyle, the BV/TV was significantly highest internally (29%, 31%, regions 7, 10) than all other regions (range 15-23%), with BV/TV decreasing towards the peripheral ROIs (regions 1, 2, 5, 8). Similarly, non-varus knees in the lateral condyle exhibited higher BV/TV internally (43%, 44%, regions 7, 10), with a non-significant trend for decreasing BV/TV from inner towards peripheral regions. Correspondingly, within-condyle regional differences in the other STB morphometric parameters were found: in the medial condyle, Tb.Th, Tb.N was higher whereas SMI and Tb.Sp lower anteriorly compared with more posterior regions (significances reported in Tables 4.1 and 4.2); whereas in the lateral condyle, these were inner-posteriorly compared to externally.

For the overlaying SBP, the Pl.Th and Pl.Po revealed significant within-condylar differences,

in particular in the lateral condyles of varus knees. In both subgroups, in the medial condyle, anteriorly the Pl.Th was higher and Pl.Po lower than external-posteriorly (see Tables 4.1 and 4.2 for significances). In the lateral condyle, internal-posteriorly, the Pl.Th was higher and Pl.Po lower than external-anteriorly.

Taken together, regions with higher Pl.Th also had lower Pl.Po, and were co-located with regions of higher BV/TV in the underlying STB (Fig. 4.5 and 4.6(a)), while regions with lower Pl.Th had higher Pl.Po and had lower BV/TV in the underlying STB (Fig. 4.6(b)). Interestingly, in the varus subgroup, the within-condylar distribution for all STB and SBP microarchitectural parameters was more heterogeneous in the lateral condyle, showing more statistically significant differences among regions, than in the medial condyle.

4.3.2 Between-condylar (medial-to-lateral) differences in STB and SBP morphometric parameters

In the varus subgroup, almost all ROIs exhibited consistently significantly higher BV/TV (up to +194% higher), Tb.Th and Tb.N and lower SMI and Tb.Sp in the medial condyle compared to lateral (Table 4.1, Fig. 4.7). Similarly, in the overlaying SBP, the Pl.Th was significantly higher in the medial compared to the lateral condyle, particularly in anterior and more external ROIs (up to +145%, regions 1-6, 8, 9). The Pl.Po showed fewer significant differences (5 of 11 ROIs) between condyles and with signs depending on the region, being significantly lower anterior-externally in the medial condyle compared to lateral and higher internal-anteriorly and posteriorly compared to lateral. Meanwhile, in the non-varus subgroup (Table 4.2, Fig. 4.7), the between-condylar differences in bone microarchitecture were of lower magnitude than in varus (e.g. BV/TV differences of up to +96%, with BV/TV higher laterally than medially in the posterior regions), significant in much fewer regions and only for the parameters Tb.N (in most posterior region 11, medially lower than laterally), Pl.Th (up to +107%, in anterior region 1, medially lower than laterally, in posterior regions 10 and 11 medially higher than laterally) and Pl.Po (in anterior-external region 2, medially lower than laterally).

4.3.3 Associations between STB and SBP morphometric parameters

Region-specific associations of variable strength and significance among microarchitectural parameters were detected in both varus and non-varus aligned knees (Table 4.3, Fig 4.8). In varus-aligned knees, more regions with significant associations were found than in non-varus and these were more in the medial condyle than in the lateral. The associations 'STB BV/TV vs. Pl.Th' were stronger in non-varus than varus knees (r-values up to 0.85 and

0.75, respectively; Table 4.3). Where significant, the STB BV/TV associated positively with Pl.Th (Fig. 4.7(a,b)) and negatively with Pl.Po (Fig. 4.8(c)) in both subgroups. In one lateral region (internal-anterior, region 4) of non-varus knees the 'BV/TV vs. Pl.Po' showed a positive association ($r = 0.78$, $p < 0.05$, Fig. 4.8(d)) whereas it was negative in the posterior region of the same condyle ($r = -0.76$, $p < 0.05$). Within the SBP itself, the region-specific associations 'Pl.Th vs. Pl.Po' were negative (Fig. 4.8(e,f)) in both subgroups, with varus knees showing stronger associations medially than non-varus (r-value up to -0.86 and -0.81, respectively), whereas laterally these were stronger in more regions in non-varus than in varus knees (r-value up to -0.84 and -0.70, respectively). Region-specific associations were also found among remaining STB parameters (SMI, Tb.Th, Tb.N and Tb.Sp) with Pl.Th and Pl.Po. However, when the morphometric parameters were averaged across all 11 subregions per condyle, none of the aforementioned associations between STB BV/TV and SBP parameters were significant in either subgroup, except for 'Pl.Th vs. Pl.Po' in the medial condyles of varus knees ($r = -0.79$, $p < 0.01$, Table 4.4).

Table 4.1: Varus aligned knee joints (n = 17): 3D bone morphometric parameters in the 11 regions of interest (ROIs) in the medial and lateral condyle

ROI	BV/TV (%)	Sig. diff. to ROI	SMI	Sig. diff. to ROI	Tb.Th (μm)	Sig. diff. to ROI	Tb.N (1/mm)	Sig. diff. to ROI
Medial Condyle								
R1	44.0 ± 9.8 [24.3, 65.4]	*,11	0.24 ± 0.95 [-2.05, 1.88]	*	210 ± 44 [142, 316]	*	2.1 ± 0.4 [1.4, 2.9]	*,11
R2	45.3 ± 9.1 [34.7, 64.3]	*,11	0.34 ± 0.82 [-1.19, 1.33]	*,11	219 ± 44 [141, 320]	*	2.1 ± 0.3 [1.5, 2.6]	*,11
R3	47.3 ± 11.4 [21.3, 69.3]	*,11	-0.05 ± 1.12 [-2.52, 2.01]	*,11	209 ± 37 [141, 272]	*	2.3 ± 0.4 [1.5, 3.1]	*,11
R4	42.2 ± 8.6 [23.5, 59.9]	*,11	0.43 ± 0.79 [-1.58, 1.94]	*,11	198 ± 26 [163, 257]	*	2.1 ± 0.3 [1.4, 2.6]	*,11
R5	44.5 ± 10.3 [29.3, 62.4]	*,11	0.39 ± 0.93 [-1.56, 1.73]	*,11	217 ± 41 [153, 299]	*	2.1 ± 0.3 [1.5, 2.6]	*,6,11
R6	50.0 ± 11.8 [28.3, 71.2]	*,11	-0.29 ± 1.42 [-3.58, 1.75]	*,11	214 ± 30 [146, 280]	*	2.3 ± 0.3 [1.9, 3.0]	*,5,7,9-11
R7	43.6 ± 9.3 [29.8, 60.7]	*,11	0.21 ± 0.98 [-1.70, 1.59]	*,11	206 ± 27 [171, 267]	*	2.1 ± 0.3 [1.7, 2.8]	*,6,11
R8	42.1 ± 14.3 [19.0, 64.8]	*,11	0.52 ± 1.14 [-2.33, 2.04]		217 ± 44 [136, 314]	*,11	1.9 ± 0.5 [1.2, 2.9]	*,11
R9	43.9 ± 14.7 [23.1, 74.9]	*,11	0.02 ± 1.71 [-4.00, 1.74]	*,11	214 ± 45 [154, 339]	*,11	2.0 ± 0.3 [1.5, 2.7]	*,11
R10	42.4 ± 10.2 [29.3, 59.9]	*,11	0.17 ± 1.00 [-1.63, 1.54]	*,11	212 ± 28 [178, 290]	*,11	2.0 ± 0.3 [1.5, 2.6]	*,6,11
R11	28.6 ± 12.0 [13.4, 50.8]	*,1-10	1.29 ± 0.75 [-0.03, 2.21]	2-7,9,10	177 ± 45 [113, 286]	*,8-10	1.6 ± 0.4 [1.1, 2.3]	*,1-10
Lateral Condyle								
R1	17.7 ± 5.5 [7.2, 28.7]	7,9,10	1.89 ± 0.40 [0.91, 2.64]	7,10	144 ± 19 [108, 182]	7,10	1.2 ± 0.3 [0.7, 1.7]	2,3,6,7,9,10
R2	15.4 ± 4.4 [8.9, 22.6]	4,6,7,9-11	1.99 ± 0.30 [1.49, 2.54]	7,9,10	142 ± 14 [117, 163]	6,7,10	1.1 ± 0.2 [0.8, 1.5]	1,3,4,6,7,9-11
R3	19.8 ± 6.5 [10.2, 32.7]	7,10	1.84 ± 0.44 [0.74, 2.63]	7,10	150 ± 26 [111, 195]	6,7,10	1.3 ± 0.3 [0.8, 1.8]	1,2,5-8,10
R4	21.1 ± 5.8 [12.0, 33.6]	2,5,7,8,10	1.77 ± 0.42 [0.89, 2.61]	7	159 ± 24 [122, 205]	7	1.3 ± 0.3 [0.8, 1.8]	2,7,10
R5	15.9 ± 5.1 [10.0, 24.8]	4,6,7,9-11	1.94 ± 0.42 [1.08, 2.42]	6,7,9,10	142 ± 16 [119, 166]	6,7,10	1.1 ± 0.3 [0.8, 1.6]	3,6,7,9-11
R6	22.5 ± 7.5 [10.1, 36.6]	2,5,7,8,10	1.67 ± 0.50 [0.38, 2.41]	5,7,10	163 ± 26 [118, 207]	2,3,5,7,8	1.4 ± 0.3 [0.9, 1.9]	1-3,5,8
R7	28.7 ± 8.2 [16.6, 46.9]	1-6,8,9,11	1.35 ± 0.61 [0.17, 2.13]	1-6,8,9,11	187 ± 31 [136, 235]	1-6,8,9,11	1.5 ± 0.3 [1.2, 2.2]	1-5,8
R8	15.9 ± 5.1 [7.6, 25.1]	4,6,7,9-11	1.82 ± 0.36 [1.13, 2.50]	7,10	140 ± 17 [105, 168]	6,7,9,10	1.1 ± 0.3 [0.7, 1.5]	3,6,7,9-11
R9	22.3 ± 6.7 [12.8, 35.2]	1,2,5,7,8,10	1.66 ± 0.46 [0.44, 2.28]	2,5,7,10	157 ± 25 [119, 208]	7,8,10	1.4 ± 0.3 [1.0, 1.8]	1,2,5,8,10
R10	30.6 ± 10.9 [14.1, 51.3]	1-6,8,9,11	1.18 ± 0.74 [-0.29, 2.16]	1-3,5,6,8,9,11	185 ± 33 [130, 246]	1-3,5,8,9,11	1.6 ± 0.4 [1.1, 2.4]	1-5,8,9,11
R11	20.2 ± 6.5 [10.0, 32.0]	2,5,7,8,10	1.74 ± 0.41 [0.77, 2.27]	7,10	149 ± 23 [101, 190]	7,10	1.3 ± 0.3 [0.9, 1.8]	2,5,8,10

Subchondral Trabecular Bone: BV/TV: bone volume fraction, SMI: structure model index, Tb.Th: trabecular thickness, Tb.N: trabecular number

The indicated values are: average ± standard deviation [minimum, maximum]. 'Sig.diff to ROI' indicates the ROIs within the same condyle showing statistically significant differences to the ROI considered (paired t-test with Bonferroni adjustment, $p < 0.05$). *: significant difference between corresponding regions in the medial and lateral condyles

Table 4.1: Continued ...

ROI	Tb.Sp (μm)	Sig. diff. to ROI	Pl.Th (μm)	Sig. diff. to ROI	Pl.Po (%)	Sig. diff. to ROI
Medial Condyle						
R1	337 ± 86 [225, 502]	*	701 ± 150 [498, 986]	*,11	9.6 ± 4.3 [3.9, 18.8]	*
R2	327 ± 73 [244, 503]	*,11	651 ± 165 [460, 1178]	*	11.5 ± 4.6 [4.8, 21.1]	*
R3	296 ± 68 [204, 432]	*,11	696 ± 176 [379, 995]	*,11	12.3 ± 5.7 [5.5, 23.4]	
R4	340 ± 73 [232, 488]	*,11	647 ± 161 [413, 1072]	*	12.0 ± 4.1 [5.4, 19.5]	*
R5	353 ± 114 [258, 654]	*	567 ± 206 [248, 978]	*	15.1 ± 7.6 [7.0, 29.8]	
R6	282 ± 60 [169, 373]	*,7-11	654 ± 234 [245, 1045]	*	13.6 ± 6.9 [3.8, 31.7]	
R7	332 ± 66 [233, 437]	*,6,11	609 ± 180 [291, 945]		13.0 ± 5.7 [6.5, 29.9]	*
R8	362 ± 87 [229, 481]	*,6	517 ± 224 [228, 894]	*	16.1 ± 8.8 [4.8, 28.9]	
R9	342 ± 70 [183, 453]	*,6,11	647 ± 224 [310, 1076]	*	12.1 ± 6.6 [5.1, 27.9]	
R10	353 ± 76 [225, 479]	*,6,11	599 ± 109 [378, 843]		10.7 ± 3.0 [6.9, 16.4]	
R11	425 ± 70 [291, 551]	*,2-4,6,7,9,10	422 ± 172 [228, 842]	1,3	17.7 ± 8.5 [8.0, 33.3]	*
Lateral Condyle						
R1	494 ± 75 [372, 605]	2	305 ± 91 [182, 508]	3,4,6,7,10	13.9 ± 5.8 [6.0, 26.3]	4
R2	545 ± 80 [384, 661]	1,3,6,7,9-11	267 ± 98 [163, 574]	3,4,6,7,9,10	16.5 ± 6.2 [7.0, 28.7]	3,4,6,7
R3	469 ± 63 [355, 572]	2,5,8	413 ± 120 [257, 742]	1,2,4,5,7,8	11.1 ± 4.0 [5.6, 21.4]	2,5,8
R4	481 ± 74 [314, 569]	7	479 ± 89 [323, 684]	1-3,5,8,11	9.5 ± 2.2 [4.2, 12.2]	2,5,8
R5	530 ± 75 [379, 642]	3,6,7,9,10	263 ± 81 [183, 536]	3,4,6,7,9,10	16.7 ± 5.2 [9.3, 27.5]	3,4,6,7,9,10
R6	447 ± 67 [305, 534]	2,5,8	450 ± 113 [298, 656]	1,2,5,7,8	10.4 ± 3.5 [3.9, 18.3]	2,5,8
R7	441 ± 71 [274, 530]	2,4,5,8	591 ± 163 [373, 909]	1-3,5,6,8,9,11	8.8 ± 2.7 [5.3, 13.3]	2,5,8
R8	540 ± 81 [404, 674]	3,6,7,9-11	254 ± 57 [175, 407]	3,4,6,7,9-11	16.4 ± 4.2 [7.9, 23.0]	3,4,6,7,9,10
R9	450 ± 74 [315, 563]	2,5,8	416 ± 109 [292, 633]	2,5,7,8	11.8 ± 4.2 [5.0, 18.5]	5,8
R10	423 ± 88 [231, 538]	2,5,8,11	536 ± 159 [313, 791]	1,2,5,8,11	10.1 ± 3.5 [5.6, 15.3]	5,8
R11	478 ± 76 [345, 573]	2,8,10	343 ± 81 [225, 584]	4,7,8,10	12.1 ± 6.3 [4.5, 28.9]	

Subchondral Trabecular Bone: Tb.Sp: trabecular separation, Subchondral Bone Plate: Pl.Th: plate thickness, Pl.Po: plate porosity
The indicated values are: average ± standard deviation [minimum, maximum]. 'Sig.diff to ROI' indicates the ROIs within the same condyle showing statistically significant differences to the ROI considered (paired t-test with Bonferroni adjustment, $p < 0.05$).
*: significant difference between corresponding regions in the medial and lateral condyles

Table 4.2: Non-varus aligned knee joints (n = 8): 3D bone morphometric parameters in the 11 regions of interest (ROIs) in the medial and lateral condyle

ROI	BV/TV (%)	Sig. diff. to ROI	SMI	Sig. diff. to ROI	Tb.Th (μm)	Sig. diff. to ROI	Tb.N (1/mm)	Sig. diff. to ROI
Medial Condyle								
R1	32.7 ± 10.5 [23.0, 52.1]	3	0.97 ± 0.53 [-0.01, 1.46]		187 ± 29 [162, 238]		1.7 ± 0.4 [1.3, 2.2]	3,4
R2	34.5 ± 13.4 [19.2, 50.9]		0.68 ± 0.90 [-0.83, 1.45]		205 ± 27 [175, 246]		1.6 ± 0.4 [1.1, 2.2]	3
R3	40.9 ± 8.4 [32.7, 55.1]	1,8	0.51 ± 0.51 [-0.22, 1.17]		200 ± 19 [174, 227]		2.0 ± 0.4 [1.6, 2.5]	1,2,5,8
R4	38.3 ± 5.7 [31.1, 47.2]		0.80 ± 0.31 [0.51, 1.33]		196 ± 8 [183, 206]		2.0 ± 0.3 [1.5, 2.4]	1,8
R5	29.0 ± 10.3 [18.7, 42.7]		1.30 ± 0.57 [0.23, 1.73]		181 ± 15 [167, 206]		1.6 ± 0.4 [1.1, 2.3]	3,6
R6	40.2 ± 8.5 [32.7, 53.6]	8,9,11	0.77 ± 0.77 [-0.68, 1.52]		203 ± 16 [185, 217]	11	2.0 ± 0.5 [1.5, 2.8]	5,8,9
R7	38.3 ± 5.7 [28.2, 45.1]	8,9,11	0.87 ± 0.32 [0.61, 1.50]		197 ± 8 [185, 205]	11	1.9 ± 0.3 [1.5, 2.2]	8,11
R8	19.7 ± 7.2 [12.6, 32.1]	3,6,7	1.88 ± 0.39 [1.11, 2.17]		155 ± 19 [138, 191]		1.2 ± 0.3 [0.9, 1.7]	3,4,6,7
R9	26.1 ± 10.9 [13.8, 44.0]	6,7	1.55 ± 0.64 [0.34, 2.23]		174 ± 22 [145, 202]		1.5 ± 0.4 [1.1, 2.2]	6
R10	28.9 ± 6.4 [19.8, 34.6]		1.39 ± 0.31 [1.01, 1.75]		181 ± 19 [161, 215]		1.6 ± 0.3 [1.2, 2.0]	
R11	16.4 ± 2.8 [12.2, 19.7]	6,7	2.08 ± 0.27 [1.70, 2.47]		149 ± 13 [133, 164]		1.1 ± 0.2 [0.9, 1.4]	*,7
Lateral Condyle								
R1	25.8 ± 8.1 [17.7, 37.3]		1.50 ± 0.48 [0.92, 2.08]		169 ± 29 [132, 220]		1.5 ± 0.4 [1.1, 2.2]	
R2	25.3 ± 12.4 [10.9, 49.3]		1.43 ± 0.79 [-0.08, 2.32]		181 ± 45 [112, 226]		1.3 ± 0.4 [1.0, 2.2]	
R3	33.6 ± 11.0 [17.1, 48.1]		1.02 ± 0.85 [-0.29, 2.15]		191 ± 35 [136, 230]		1.7 ± 0.4 [1.3, 2.3]	
R4	34.4 ± 11.6 [20.6, 52.8]		0.94 ± 0.88 [-0.57, 2.05]		194 ± 23 [160, 231]		1.8 ± 0.5 [1.2, 2.5]	
R5	28.4 ± 12.2 [14.6, 50.3]		1.36 ± 0.74 [-0.18, 2.01]		186 ± 46 [130, 250]		1.5 ± 0.3 [1.1, 2.0]	
R6	39.1 ± 12.1 [17.9, 55.2]		0.79 ± 0.93 [-0.78, 2.08]		198 ± 34 [145, 237]		2.0 ± 0.5 [1.2, 2.4]	
R7	43.1 ± 11.8 [29.6, 64.3]		0.40 ± 1.23 [-2.09, 1.52]		220 ± 32 [181, 273]		1.9 ± 0.4 [1.5, 2.4]	
R8	27.2 ± 11.7 [12.0, 43.6]		1.42 ± 0.65 [0.43, 2.22]		184 ± 48 [121, 248]		1.4 ± 0.3 [1.0, 1.8]	
R9	38.5 ± 12.3 [18.4, 55.2]		0.97 ± 0.85 [-0.51, 2.16]		203 ± 45 [144, 256]		1.9 ± 0.3 [1.3, 2.2]	
R10	44.1 ± 11.7 [29.1, 65.7]		0.45 ± 1.10 [-1.87, 1.65]		221 ± 43 [165, 291]		2.0 ± 0.3 [1.5, 2.3]	
R11	32.2 ± 11.8 [13.7, 47.5]		1.37 ± 0.55 [0.77, 2.19]		199 ± 46 [132, 253]		1.6 ± 0.3 [1.0, 1.9]	

Subchondral Trabecular Bone: BV/TV: bone volume fraction, SMI: structure model index, Tb.Th: trabecular thickness, Tb.N: trabecular number

The indicated values are: average ± standard deviation [minimum, maximum]. 'Sig.diff to ROI' indicates the ROIs within the same condyle showing statistically significant differences to the ROI considered (paired t-test with Bonferroni adjustment, $p < 0.05$). *: significant difference between corresponding regions in the medial and lateral condyles

Table 4.2: Continued ...

ROI	Tb.Sp (μm)	Sig. diff. to ROI	Pl.Th (μm)	Sig. diff. to ROI	Pl.Po (%)	Sig. diff. to ROI
Medial Condyle						
R1	416 ± 90 [285, 530]	3	472 ± 102 [338, 593]	*	10.1 ± 2.9 [6.9, 13.6]	
R2	454 ± 120 [305, 612]		540 ± 219 [364, 904]		8.1 ± 1.9 [5.6, 10.4]	*
R3	354 ± 86 [240, 459]	1,8	484 ± 59 [411, 565]	11	12.2 ± 2.7 [8.3, 14.8]	
R4	367 ± 85 [249, 481]		574 ± 150 [406, 793]		10.5 ± 3.8 [5.9, 15.7]	
R5	436 ± 114 [291, 565]		439 ± 246 [266, 926]		11.7 ± 3.6 [7.6, 16.9]	
R6	340 ± 93 [218, 448]	8,9,11	518 ± 168 [359, 754]		11.2 ± 3.4 [8.1, 17.6]	
R7	360 ± 79 [269, 485]	8,11	503 ± 114 [362, 687]	11	11.8 ± 4.7 [7.9, 20.6]	
R8	483 ± 85 [377, 602]	3,6,7	297 ± 146 [162, 579]		17.2 ± 8.4 [7.6, 30.4]	
R9	427 ± 92 [302, 550]	6,7	412 ± 218 [229, 839]		14.6 ± 7.3 [6.6, 26.1]	
R10	424 ± 84 [339, 551]		434 ± 66 [347, 535]	*	11.5 ± 3.5 [8.6, 17.8]	
R11	510 ± 53 [450, 599]	6,7	290 ± 61 [221, 381]	*,3,7	13.6 ± 7.1 [7.2, 25.0]	
Lateral Condyle						
R1	444 ± 88 [300, 592]		339 ± 104 [196, 460]	7,10	14.4 ± 9.2 [5.2, 31.7]	
R2	497 ± 98 [304, 599]		441 ± 272 [178, 1016]		13.7 ± 6.6 [5.3, 24.3]	
R3	403 ± 79 [305, 550]		526 ± 173 [323, 773]		11.3 ± 5.2 [5.9, 21.6]	
R4	405 ± 104 [275, 577]		507 ± 121 [365, 698]		11.0 ± 4.5 [5.7, 19.9]	
R5	445 ± 61 [318, 494]		509 ± 296 [268, 1139]		11.1 ± 4.6 [4.6, 19.2]	
R6	349 ± 76 [258, 438]		564 ± 195 [419, 900]		11.9 ± 3.3 [5.6, 16.4]	
R7	356 ± 68 [280, 451]		597 ± 112 [412, 741]		9.1 ± 2.4 [6.9, 13.7]	
R8	466 ± 40 [403, 527]	9	479 ± 242 [243, 944]	1,11	10.0 ± 6.3 [5.4, 23.6]	
R9	354 ± 41 [291, 410]	8	624 ± 229 [384, 1005]		9.3 ± 2.6 [5.0, 13.9]	
R10	332 ± 50 [252, 410]		633 ± 134 [466, 871]	1	8.5 ± 1.5 [6.3, 10.4]	
R11	414 ± 59 [341, 490]		600 ± 235 [385, 1021]	8	7.9 ± 3.0 [5.1, 13.9]	

Subchondral Trabecular Bone: Tb.Sp: trabecular separation, Subchondral Bone Plate: Pl.Th: plate thickness, Pl.Po: plate porosity
The indicated values are: average ± standard deviation [minimum, maximum]. 'Sig.diff to ROI' indicates the ROIs within the same condyle showing statistically significant differences to the ROI considered (paired t-test with Bonferroni adjustment, $p < 0.05$).
*: significant difference between corresponding regions in the medial and lateral condyles

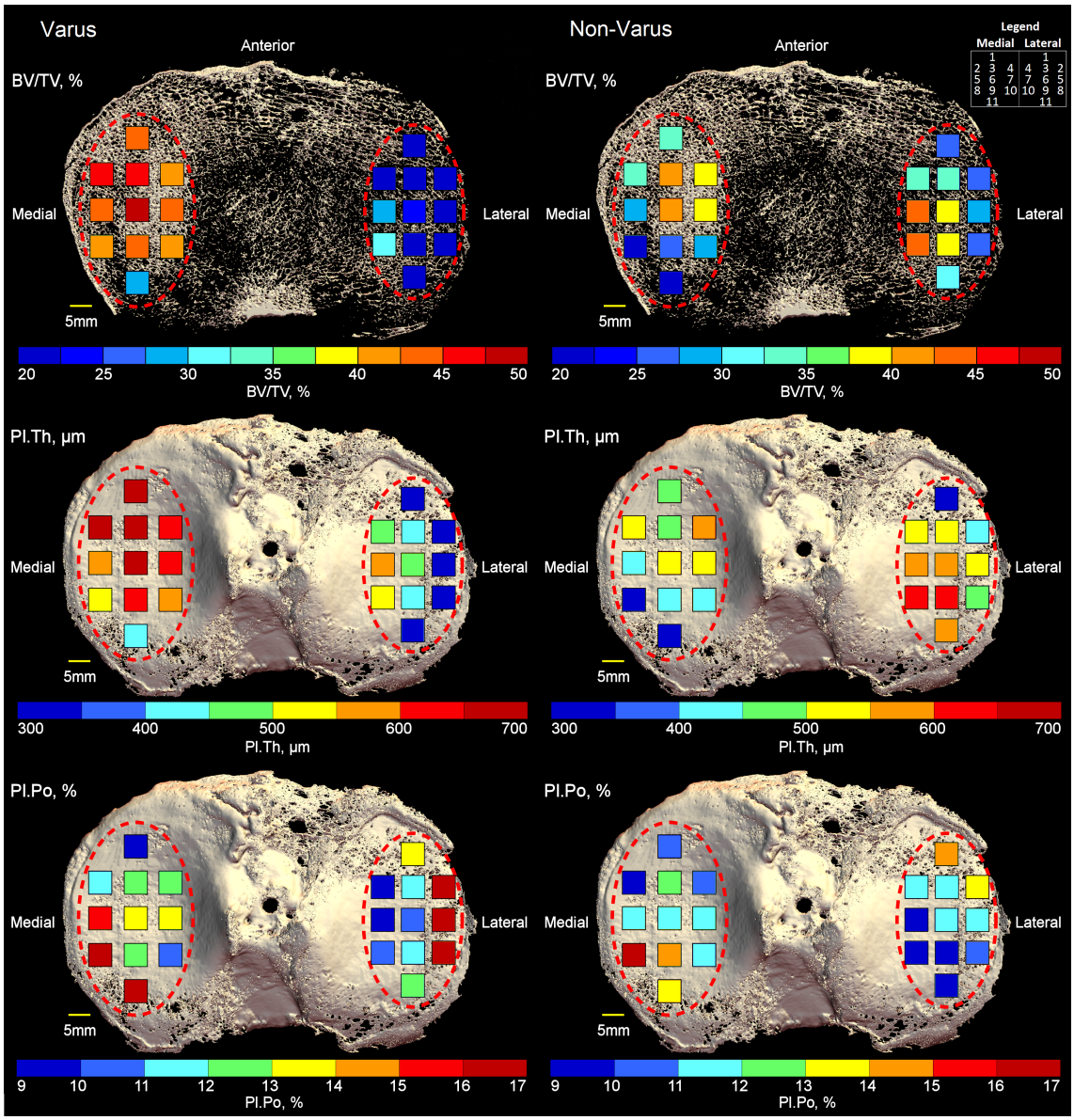

Figure 4.5: 3D micro-CT images of a right human tibial plateau. The colour heat map (11 regions per condyle) shows, within (left images) varus and (right images) non-varus knees, the regional distribution in the medial and lateral condyle of: (top image) subchondral trabecular bone volume fraction (BV/TV, in %), (middle image) subchondral bone plate thickness (Pl.Th, in μm) and (bottom) subchondral plate porosity (Pl.Po, in %). The values are averaged over the 17 varus and 8 non-varus tibial plateaus investigated.

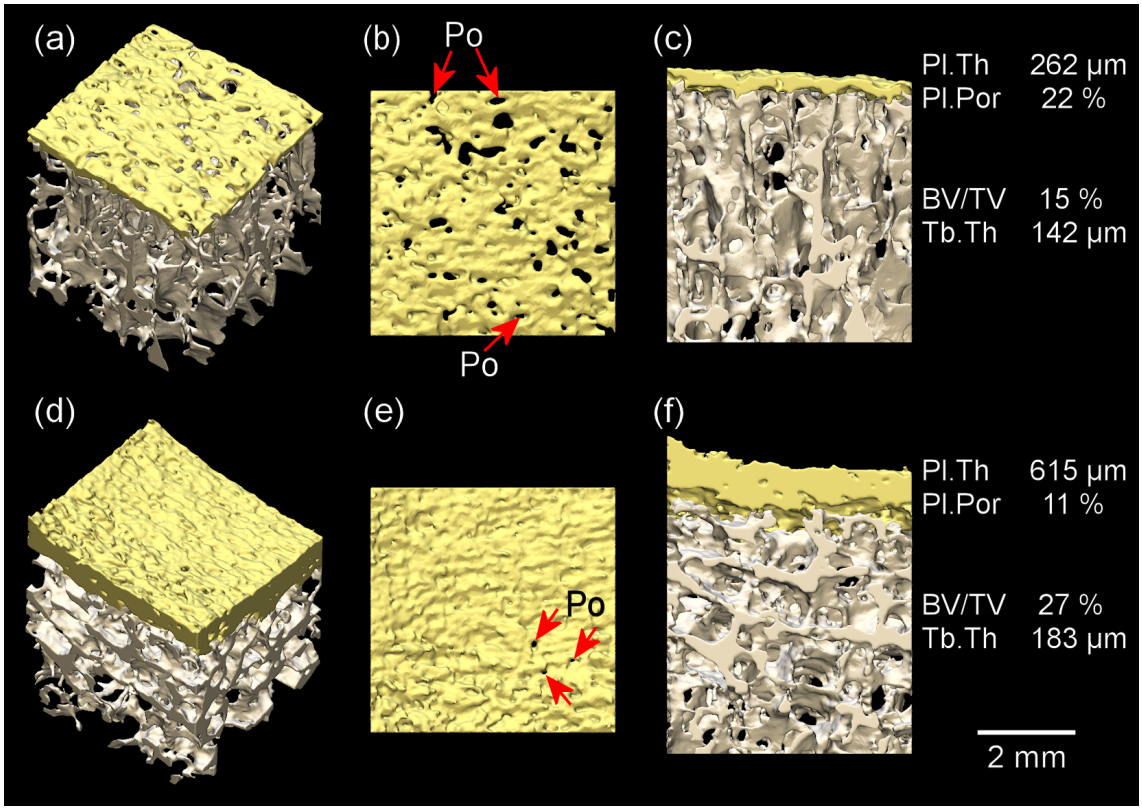

Figure 4.6: 3D micro-CT renderings of two subregions in the lateral condyle (subregion 8 in top row, subregion 10 in bottom row) of the subchondral bone plate (yellow colour) and underlying subchondral trabecular bone (white, volume of 5 x 5 x 5 mm^3). (a-c) subregion 8 (external-posterior condyle), with lower BV/TV (15%), Tb.Th (142 μm), Pl.Th (262 μm) and higher Pl.Po (22%), compared to (d-f) subregion 10 (inner-posterior condyle), with higher BV/TV (27%), Tb.Th (183 μm), Pl.Th (615 μm) and lower Pl.Po (11%). (b,e) Superior view of the subchondral bone plate; (c,f) coronal view of subchondral bone plate and subchondral trabecular bone. Note that in (b), a number of pores (Po) traversing the thin plate from the articular surface to the marrow space are clearly visible.

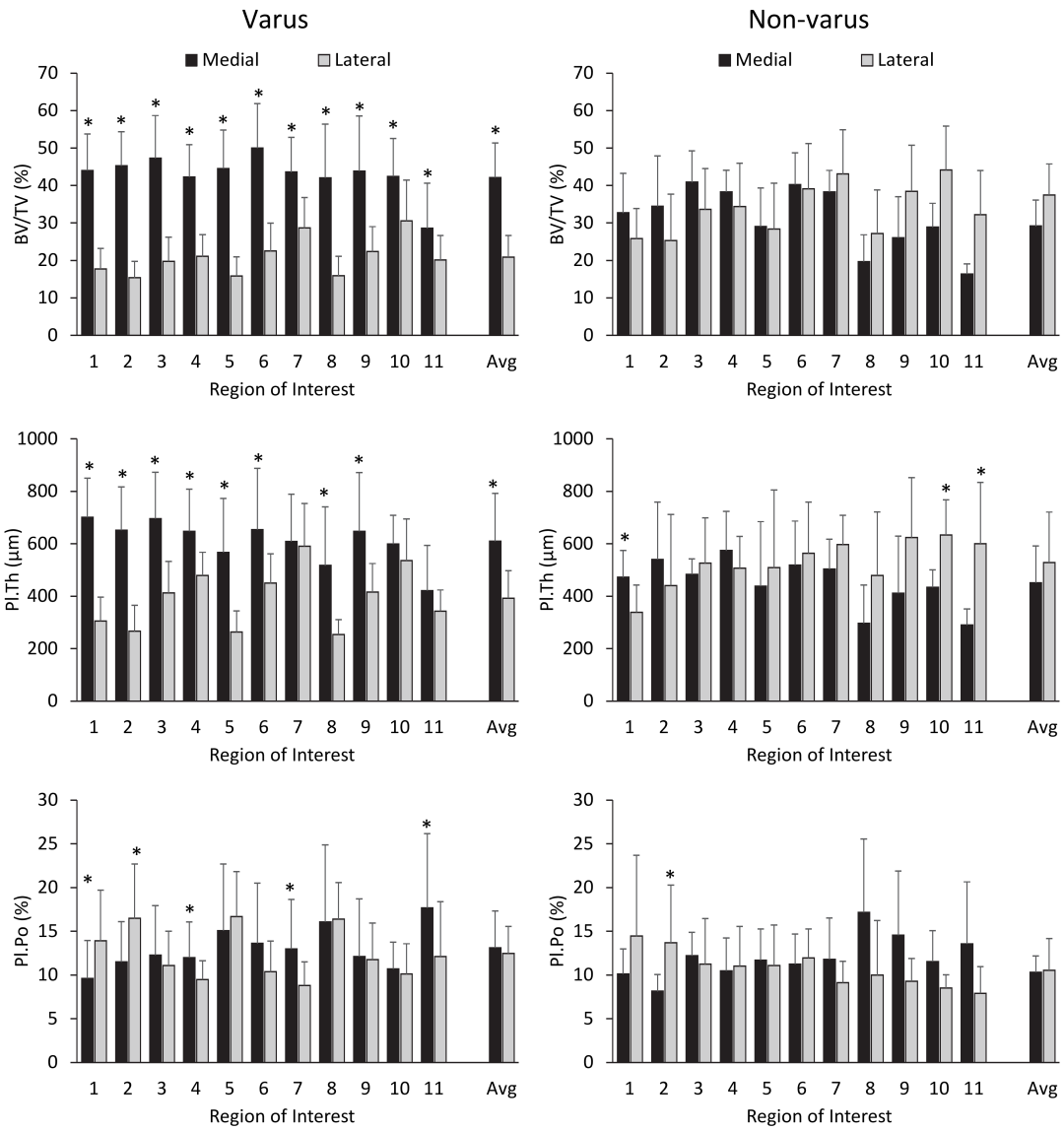

Figure 4.7: Bar graphs reporting average values and standard deviations (error bars) of subchondral trabecular bone volume fraction (BV/TV), and subchondral bone plate thickness (Pl.Th) and porosity (Pl.Po) in the 11 subregions of interest within the medial and lateral tibial condyles of (left) varus and (right) non-varus knees. *: Significant difference between corresponding medial and lateral region (paired t-test with Bonferroni adjustment, $p < 0.05$).

Table 4.3: r-values for region-specific correlations between STB BV/TV and SBP Pl.Th and Pl.Po

Varus (n = 17)

BV/TV vs Pl.Th

Medial			Lateral		
	0.317			-0.315	
0.194	0.508*	0.114	-0.298	-0.145	0.027
0.498*	0.530*	0.371	0.593*	-0.102	-0.202
0.752**	0.333	0.053	0.586*	0.117	-0.345
	0.730**			0.043	

BV/TV vs Pl.Po

Medial			Lateral		
	-0.394			0.357	
-0.108	-0.380	-0.165	0.387	0.191	0.221
-0.462	-0.602*	-0.337	-0.386	0.130	0.428
-0.624**	-0.337	-0.032	-0.372	0.090	0.037
	-0.491*			-0.124	

Pl.Th vs Pl.Po

Medial			Lateral		
	-0.786**			-0.605*	
-0.723**	-0.842**	-0.718**	-0.175	-0.499*	-0.552*
-0.675**	-0.825**	-0.776**	-0.644**	-0.165	-0.305
-0.857**	-0.820**	-0.483*	-0.702**	-0.437	0.092
	-0.747**			-0.386	

Non-varus (n = 8)

BV/TV vs Pl.Th

Medial			Lateral		
	0.758			-0.092	
0.680	0.644	-0.445	-0.231	0.307	0.310
0.774	0.514	-0.454	0.091	0.309	0.386
0.848*	0.719	-0.321	0.696	0.737	0.692
	0.021			0.642	

BV/TV vs Pl.Po

Medial			Lateral		
	-0.674			0.171	
-0.560	-0.248	0.138	0.776*	0.414	0.272
-0.404	0.185	0.541	0.574	0.180	-0.404
-0.147	-0.108	0.773	0.745	-0.688	-0.540
	-0.509			-0.762*	

Pl.Th vs Pl.Po

Medial			Lateral		
	-0.809			-0.843*	
-0.639	-0.144	-0.747	-0.505	-0.637	-0.537
-0.573	-0.438	-0.754	-0.517	-0.814*	-0.717
-0.641	-0.661	-0.254	0.139	-0.705	-0.576
	-0.603			-0.713	

Legend - Regions of interest

Medial			Lateral		
	1			1	
2	3	4	4	3	2
5	6	7	7	6	5
8	9	10	10	9	8
	11			11	

Statistically significant linear correlations ($p < 0.05$) are indicated: *: $p < 0.05$, **: $p < 0.01$; the three strongest region-specific correlations (based on their r-value are highlighted from strongest (lightest grey), to second strongest (lighter grey), to third strongest (dark grey).

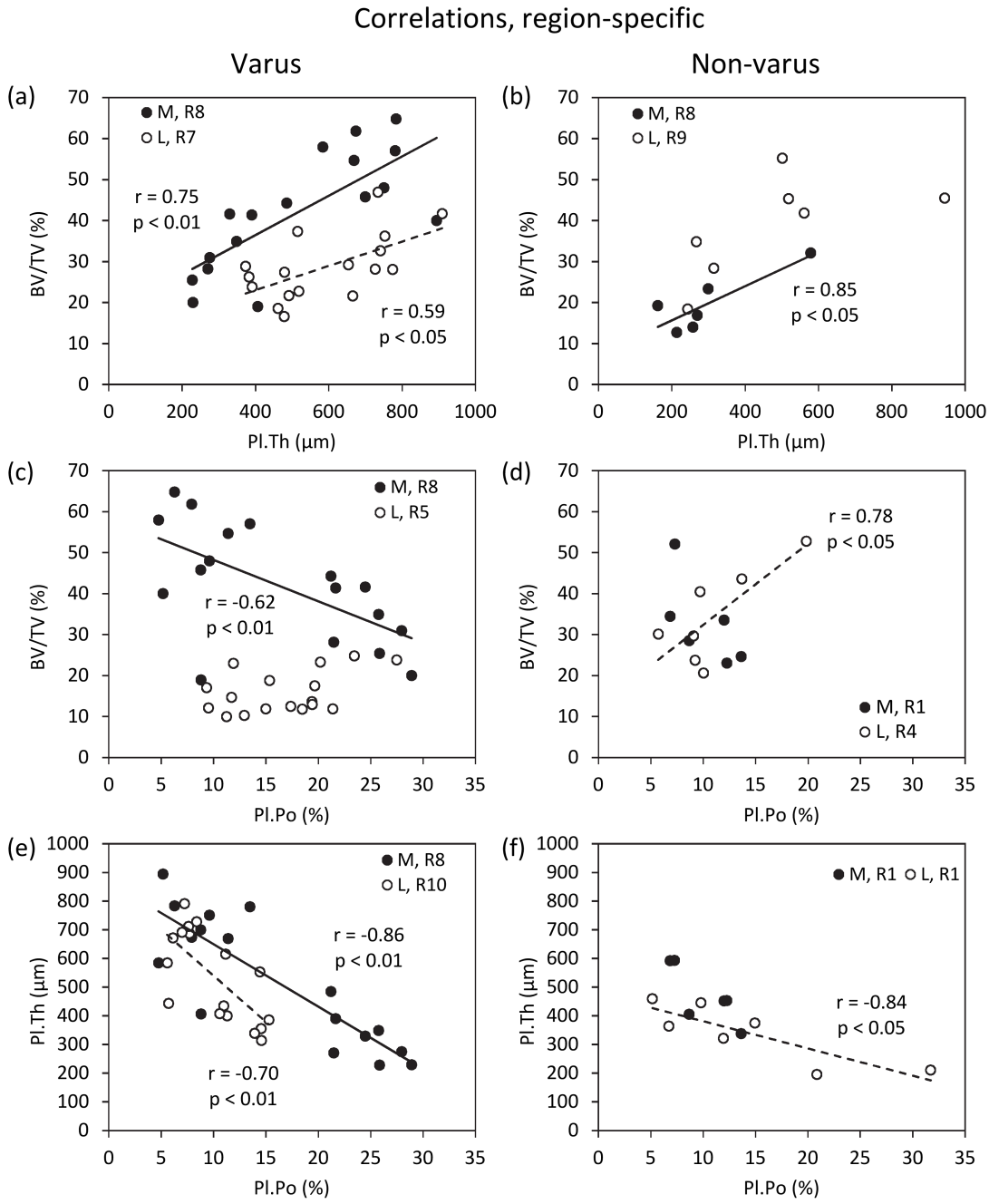

Figure 4.8: Scatter plots with best-fit line for regions of interest with strongest correlations (based on r-value) between morphometric parameters considered within each condyle of the 17 varus and 8 non-varus tibial plateaus; (a,b) 'subchondral trabecular bone volume fraction (BV/TV) vs. subchondral plate thickness (Pl.Th)'; (c,d) 'BV/TV vs. subchondral plate porosity (Pl.Po)' and (e,f) 'Pl.Th vs. subchondral plate porosity (Pl.Po)'. Solid line: best fit line for medial condyle; dashed line: best fit line for lateral condyle. M, medial; L, lateral.

Table 4.4: r-values for correlations between subchondral trabecular bone (BV/TV, SMI, Tb.Th, Tb.SP, Pl.Th) and subchondral bone plate morphometric parameters (Pl.Th, Pl.Po) for values averaged over the 11 subregions of interest within each condyle

	Varus (n = 17)				Non-varus (n = 8)			
	Medial		Lateral		Medial		Lateral	
Parameters	Pl.Th	Pl.Po	Pl.Th	Pl.Po	Pl.Th	Pl.Po	Pl.Th	Pl.Po
Bone volume fraction (BV/TV)	0.293	−0.386	0.025	0.238	0.442	0.200	0.562	−0.028
Structure model index (SMI)	−0.408	0.455	0.141	−0.208	−0.692	0.028	−0.586	−0.033
Trabecular thickness (Tb.Th)	−0.119	−0.133	0.108	0.255	0.245	0.261	0.758*	−0.353
Trabecular number (Tb.N)	0.493*	−0.366	0.003	0.159	0.485	0.166	0.199	0.237
Trabecular separation (Tb.Sp)	−0.403	0.374	−0.143	0.013	−0.331	−0.246	0.115	−0.571
Plate Thickness (Pl.Th)		−0.794***		−0.231		−0.502		−0.611

Statistically significant linear correlations are indicated: *$p < 0.05$, ***$p < 0.001$

4.4 Discussion

In this study, a systematic mapping of the human tibia condylar subchondral bone microarchitecture was performed using micro-CT on entire tibial plateaus retrieved from 25 OA patients, categorised as exhibiting either varus or non-varus joint alignment. A dense grid of 22 subvolumes for each tibia (11 per condyle) was examined, in which the SBP and underlying STB 3D microarchitecture was successfully quantified and compared, at 17 μm pixel size. Overall, heterogeneous distribution patterns of subchondral bone microarchitecture within the OA tibial condyles of both varus and non-varus specimens were revealed. Subchondral bone microarchitecture differed between the medial and lateral condyles, with more regions showing significant between-condylar differences in the varus than in the non-varus subgroup. Significant region-specific associations between the subchondral plate thickness, plate porosity and the underlying subchondral trabecular bone microarchitecture were detected.

4.4.1 Within-condylar differences in STB and SBP morphometric parameters

In varus knees, medially, BV/TV was significantly and consistently high throughout the entire condyle compared to the most posterior tibial region (10 regions out of 11), while in the non-varus subgroup, medially, it was more heterogeneously distributed, with more regions showing statistically significant differences among each other, with significantly higher BV/TV centrally (2 regions) than posteriorly (3 regions). In both varus and non-varus knees, laterally, BV/TV was highest in the inner-posterior subregions, decreasing towards the anterior and peripheral regions, although significantly so only for varus. These results are in agreement with previous OA-reports that however used 2D histology on 3-4 subregions per condyle, although these did not consider variations in joint alignment (Bobinac et al., 2003; Matsui et al., 1997). Moreover, regions of higher STB BV/TV tended to be co-located with regions of higher overlaying Pl.Th (Fig. 4.7 and 4.8), supporting earlier reports that however were on normal subjects, using 2D techniques (Milz & Putz, 1994; Noble & Alexander, 1985). As bone adaptation occurs in response to the mechanical environment (Turner, 1998), these regional variations in bone microarchitecture within the tibial condyles of OA knees likely reflect the joint's loading history. Anatomically, regions exhibiting higher BV/TV and Pl.Th compared to others within the tibial plateau reported here correspond with tibiofemoral joint contact regions and maxima of joint contact pressures, which have previously been shown to vary within the condyles during the gait cycle (Adouni & Shirazi-Adl, 2014a; Liu et al., 2010). The differing regional distribution of within-condylar bone microarchitecture in varus and non-varus knees suggests that also the within-condylar stress distribution patterns may differ between these two subgroups. In varus, the more homogenous distribution of high BV/TV and Pl.Th medially compared to a

more heterogeneous distribution laterally (with more regions showing statistically significant differences among each other) could be due to a more homogenous stress distribution medially compared to a more localised tibiofemoral joint contact region laterally in this cohort (Liu et al., 2010), generating a spatially more uniform response (adaptation) of the bone in the former or localised response in the latter, respectively. Conversely, in non-varus, there was higher heterogeneity (more regions showing significant within-condylar differences) medially than laterally, with laterally showing no significant within-condylar differences. This could correspond to a more localised contact region in the medial condyle in this cohort compared to lateral. Furthermore, it has to be recognised that OA is a multifactorial disease, characterised by differences in subchondral bone changes during development of the disease (e.g. SBP thinning in early OA, followed by subchondral bone sclerosis in the end stages (Botter et al., 2011; Burr & Gallant, 2012; Li et al., 2013)). The samples examined are from end-stage OA; other factors, apart from loading, including age, genetics, or the local biochemical environment, in the presence of subchondral bone sclerosis, can effect subchondral bone metabolism (Li et al., 2013). These factors may, in combination with loading, exacerbate structural changes in the joint, leading to the observed variations in subchondral bone microarchitecture.

4.4.2 Between-condylar difference in STB and SBP morphometric parameters

In the varus subgroup, medial condyle STB BV/TV was significantly higher with values often more than doubled in all subregions compared with the lateral condyle. The medial condyle (varus) also had significantly higher values of Tb.Th and Tb.N and lower SMI and Tb.Sp compared to the lateral condyle, supporting previous studies in human OA on excised bone cores examining fewer ROIs (Bobinac et al., 2003; Ding et al., 2003; Patel et al., 2003). The overlaying SBP Pl.Th was also higher in the anterior medial condyle compared with the same regions lateral, consistent with previous 2D reports although on normal subjects (Milz & Putz, 1994). Meanwhile, in the non-varus subgroup, between-condylar differences in STB microarchitecture, SBP thickness or porosity were detected only for few subregions and mainly in the posterior ROIs. Knee joint malalignment has previously been linked to altered medial-to-lateral distribution of loads (Adouni & Shirazi-Adl, 2014b). Greater varus alignment, indicating higher medial condyle joint forces compared to lateral, has been associated with greater medial-to-lateral tibial condyle bone mineral density (BMD) differences (Christensen et al., 1982; Hulet et al., 2002). However, in non-varus aligned joints these differences are reduced and some studies even reported higher BMD laterally (Hulet et al., 2002). The absence of significant medial-to-lateral differences in subchondral bone microarchitecture of non-varus joints detected in this study could reflect an adaptation of the bone to a more balanced medial-to-lateral distribution of forces across these tibiae. Taken together, these results in OA tibiae

may suggest that joint alignment 1) not only influences the medial-to-lateral ratios of force across the tibial plateau, as of the between-condylar (medial-to lateral) microarchitectural bone differences; but 2) also influences the within-condylar stress distribution patterns, as suggested by the differing within-condylar regional heterogeneity in BV/TV (and other parameters) when comparing varus and non-varus subgroups.

4.4.3 Associations between STB and SBP morphometric parameters

The BV/TV showed region-specific positive associations with Pl.Th and negative with SBP Pl.Po, whereas Pl.Th and Pl.Po were negatively associated. These regional findings numerically support those from OA-induced mice and qualitative reports on non-OA humans (Botter et al., 2011; Clark & Huber, 1990; Duncan et al., 1987). However, whereas STB microarchitecture showed significant region-specific associations with SBP Pl.Th and Pl.Po, no significant associations were detected for the values averaged over each condyle. That is, whereas for certain regions a high (or low) BV/TV corresponded with high (or low) Pl.Th, the same cannot be generalised for the entire tibia; tibial condyles with overall high average Pl.Th did not necessarily also have overall high average BV/TV underneath. Similarly, region-specific, 'BV/TV vs SBP Pl.Po' (apart from one lateral condyle region of non-varus knees) and 'Pl.Th vs Pl.Po' was negatively associated. Pores in the SBP may provide communication pathways between the STB and overlying cartilage by increased vascular invasion across the bone-cartilage interface (Burr & Gallant, 2012). Region-specific changes (including sign) in Pl.Po with STB BV/TV, if confirmed, could be linked to differences in vascular density within the underlying trabecular region. Moreover, 'Pl.Po vs. Pl.Th' was the only association being significant also for average values, only in the medial compartment of varus knees; this means that in this cohort in OA, tibiae which on average have a thicker subchondral bone plate in the medial condyle also have lower plate porosity in that condyle. The SBP and STB are adjacent bone compartments; however, they are architecturally different and animal models of post-traumatic OA show that the time sequence of architectural changes occurring may differ between compartments from early- to late-stage OA (Burr & Gallant, 2012; Florea et al., 2015; Li et al., 2013). Thus, if linked to the disease, the region-specific variations in the strength (and perhaps sign) of the aforementioned associations could reflect spatial differences in the stage of OA and/or regional differences in the local mechanical and biochemical environments. Further work is required to understand how bone microarchitecture responds due to differences in local environmental factors and if the aforementioned associations in OA differ in a non-pathological joint.

The micro-CT method described is currently restricted to excised bone retrieved from TKR surgery or from cadavers and impractical for in vivo application on humans, due to the high radiation dose associated with high resolution scanning (Müller et al., 1996). The regional

BV/TV measures reported in this study show similar distribution patterns as revealed for proximal tibial BMD using clinical CT, in vivo on OA patients (Johnston et al., 2011). However, in vivo measures of BMD alone cannot reveal localised microarchitectural changes in the subchondral plate and subchondral trabecular compartment. Recent high-resolution peripheral quantitative CT (HR-pQCT) imaging systems, which permit in vivo scanning of the proximal tibia at up to 61 μm voxel size (Kroker et al., 2016), may in future be employed by adapting the here described method for investigating regional subchondral bone microarchitectural changes in knee OA.

There were limitations to this study. The cross-sectional study design meant that we could not directly determine whether the observed regional heterogeneity in the tibial plateau is characteristic only within the late-stage OA joint, or whether similar variations are present also in non-diseased joints. Future work in our laboratory will apply this method to specimens without OA, to investigate this question. Furthermore, as patient data was limited, we were unable to delineate between patients with or without history of ligament injuries within the examined joints. Ligament injuries have been linked with altered contact mechanics within the tibial condyles (Andriacchi et al., 2009) and thus distribution of bone microarchitecture may differ between patients whom have developed idiopathic or post-traumatic OA. Finally, we had a limited sample size, particularly within the non-varus subgroup (n = 8) compared to varus (n = 17). Some differences in the non-varus subgroup could be non-significant due to limited statistical power in that cohort; to test for differences with alpha = 0.05 and power = 80%, for a sought effect size of 1 standard deviation, n = 17 specimens would have been needed in that cohort (Lieber, 1990). However, the ratio of varus to non-varus aligned joints examined (17:8) is representative of the distribution in OA patients reported in literature (Burnett et al., 2015; Niu et al., 2009) and despite the sample size significant differences were found for this subgroup. A strength of this study was the examination of the entire intact tibial plateau, from joints of known mechanical alignment, with micro-CT at high spatial resolution (17 μm pixel size). This permitted, for the first time reported in the published literature, a systematic mapping of subchondral bone microarchitecture in the SBP and STB regions of the human tibial plateau in OA, achieved by examining multiple subregions within a dense grid within each condyle without physically coring it, whilst preserving the intact specimen for further examination (Zysset et al., 1994).

Concluding, we performed a systematic mapping of the bone microarchitecture in the cortical subchondral bone plate and underlying trabecular bone, in entire human tibial plateaus from 25 end-stage knee OA patients with and without varus joint alignment. By examining each medial and lateral condyle in 11 subregions, significant microarchitectural differences in the plate and the subchondral trabecular bone were revealed, within and between condyles, which were affected by the mechanical axis. Moreover, region-specific significant associations

between the subchondral plate thickness and plate porosity and the underlying subchondral trabecular bone microarchitecture were detected, which in general were not captured when considering only the values averaged for each condyle. As subchondral bone changes reflect responses to local mechanical and biochemical factors within the joint, our results suggest that joint alignment influences both the medial-to-lateral as well as the within-condyle distribution of force across the tibia, generating corresponding local responses in terms of adaptation of both the subchondral bone plate and subchondral trabecular bone microarchitecture. A systematic mapping of the 3D microarchitecture in the subchondral bone plate and the underlying subchondral trabecular bone, and of the relationships between them, contributes to better understanding the bone changes occurring in pathologies affecting the human knee joint, such as OA.

Chapter 5

Study 2: Relationships between *in vivo* dynamic knee joint loading, static alignment and tibial subchondral bone microarchitecture in end-stage knee osteoarthritis

The previous chapter (**Chapter 4**, Study 1) characterised, in 25 end-stage knee OA patients, the spatial distribution of proximal tibia subchondral bone plate and subchondral trabecular bone 3D microarchitecture. That study considered the influence of knee alignment, a static marker of tibiofemoral joint forces, on subchondral bone microarchitecture, by comparing varus and non-varus patient subgroups. The present chapter (Study 2) extends upon that work, examining relationships between dynamic joint load measures during gait (knee moments, joint reaction forces), static alignment and subregional tibial subchondral trabecular bone microarchitecture. For exploring these relationships, four subchondral trabecular bone subregions of interest have been considered within each tibial plateau (two each in the medial and lateral tibial condyles). Analysis has been conducted in 25 end-stage knee osteoarthritis patients (including a subset of 20 patients whom were investigated in Study 1).

The study presented in this chapter is the subject of the following paper:

Roberts BC, Solomon LB, Mercer G, Reynolds KJ, Thewlis D and Perilli E. Relationships between *in vivo* dynamic knee joint loading, static alignment and tibial subchondral bone microarchitecture in end-stage knee osteoarthritis, Osteoarthritis and Cartilage. *In revision*. May 2017.

Abstract:

Objective: To study, on end-stage knee osteoarthritis (OA) patients, relationships between *in vivo* dynamic knee joint loads measured pre-operatively using gait analysis, static alignment, and the proximal tibial subchondral trabecular bone (STB) microarchitecture of their excised knees quantified with 3D micro-CT.

Design: Twenty-five knee OA patients scheduled for total knee arthroplasty underwent pre-operative gait analysis. Static alignment was determined radiographically. Following surgery, excised tibial plateaus were micro-CT scanned and STB microarchitecture analysed in four anatomical subregions of interest within the tibial condyles (anterior-medial, posterior-medial, anterior-lateral, posterior-lateral). Regional differences in microarchitecture (repeated measures ANOVA and Bonferroni-adjusted paired t-tests) and relationships between joint loading and microarchitecture (Pearson's correlations with Benjamini-Hochberg correction; forward stepwise regression) were explored.

Results: STB microarchitecture differed significantly among the four anatomical subregions ($p < 0.001$), anterior-medially exhibiting highest bone volume fraction (BV/TV) and lowest structure model index (SMI). Anterior-medial BV/TV and SMI correlated strongest with the peak external rotation moment during early stance (ERM) ($r = -0.74$, $r = 0.67$, $p < 0.01$); medial-to-lateral BV/TV ratios correlated most strongly with ERM (negatively) and mechanical axis deviation (MAD, positively) ($|r|$ range 0.57 – 0.74, $p < 0.001$). When controlling for the walking speed, knee adduction moment and MAD, ERM explained an additional 30% and 16% of the variation in AM BV/TV and medial-to-lateral BV/TV ratio (final model, adjusted $R^2 = 0.59$, $R^2 = 0.65$, $p < 0.01$).

Conclusions: Subregional STB microarchitecture was associated with dynamic knee joint loads and static alignment; particularly, anterior-medial BV/TV with ERM. Reductions in ERM may indicate increased stresses in the anterior-medial condyle, resulting in greater BV/TV and more plate-like microarchitecture in this subregion.

5.1 Introduction

Knee osteoarthritis (OA) is a debilitating disease affecting all tissues within the joint, including bone. The subchondral bone is a mechanical shock absorber and protects the overlying articular cartilage from excessive joint loads (Madry et al., 2010). The compromised integrity of subchondral bone plays an important role in the onset and progression of the disease (Madry et al., 2010; Radin & Rose, 1986). In prospective studies, abnormal joint biomechanics that are common in patients with knee OA (Astephen et al., 2008; Baliunas et al., 2002; Mündermann et al., 2005), have previously been associated with rate of radiographic progression of the disease (Miyazaki et al., 2002; Sharma et al., 2001), and in cross-sectional studies have been linked with pathological variations to joint structures (e.g. presence of cartilage defects (Creaby et al., 2010) bone marrow lesions (Bennell et al., 2010), variations in subchondral bone area (Creaby et al., 2010; Vanwanseele et al., 2010) and cartilage thickness (Andriacchi et al., 2009)).

Abnormal *in vivo* joint loading, as indicated by the frontal plane knee adduction moment (KAM) measured during gait, has been associated with local variations in bone mineral density (BMD) and mineral content (BMC) in the proximal tibia measured by dual X-ray absorptiometry (DXA) (Hurwitz et al., 1998; Thorp et al., 2006b; Wada et al., 2001). Also the static knee alignment has been associated with the tibial subchondral BMD medial-to-lateral ratio acquired with DXA (Thorp et al., 2006b; Wada et al., 2001). DXA, however, is a two-dimensional technique which has limited spatial resolution and cannot differentiate between cortical and trabecular bone, or among different subregions within the same condyle. Furthermore, it cannot quantify the bone microarchitecture, which has been shown to vary within the tibia, in both healthy and pathological joints (Bobinac et al., 2003; Ding et al., 2003; Patel et al., 2003).

To understand the degeneration of the subchondral bone in OA it is necessary to study its micro-architecture. However, previous studies examining subchondral bone microarchitecture on humans were restricted to thin histological slices or excised bone cores (Bobinac et al., 2003; Ding et al., 2003; Patel et al., 2003). Nowadays, X-ray micro-computed tomography (micro-CT) allows three-dimensional (3D) structural characterization of entire bone segments including the tibial plateau, non-destructively and at high resolution (Ab-Lazid et al., 2014; Perilli et al., 2012; Roberts et al., 2016). Moreover, to the best of our knowledge, those studies exploring the bone microarchitecture did not examine gait or *in vivo* joint biomechanics data from the same patients, to investigate possible relationships between these measures. Thus, the associations between knee joint biomechanics and tibial subchondral trabecular bone (STB) microarchitecture in OA, in the same patient, have not yet been explored. Through a better

understanding of how joint loading is related to local changes in subchondral bone microarchitecture in knee OA, it may be possible to better describe the role of both of these factors in the disease.

The aim of this exploratory study was to examine, on end-stage OA patients undergoing total knee arthroplasty, the relationships between *in vivo* dynamic knee joint loads measured preoperatively using 3D gait analysis (knee moments and peak tibiofemoral joint reaction forces), static alignment (mechanical axis deviation, medial proximal tibial angle) and regional proximal tibia subchondral bone microarchitecture of their excised knees quantified with 3D micro-CT. While to date, much research has focused on relationships between static alignment, KAM indices, and structural variations in the OA knee joint (Thorp et al., 2006b; Wada et al., 2001), significant differences in rotational moments have been observed between OA patients and controls (Astephen et al., 2008; Gök et al., 2002; Landry et al., 2007; Weidow et al., 2006). We thus hypothesise that measures of static alignment and KAM indices, as well as the peak rotation moments, will be significantly associated with subregional STB bone microarchitecture in the examined end-stage knee OA joints.

5.2 Methods

5.2.1 Participants

Twenty-five (n = 25) adult patients with end-stage knee OA, scheduled for total knee arthroplasty, were recruited from the orthopaedics departments at the Royal Adelaide Hospital, Repatriation General Hospital and Burnside War Memorial Hospital in Adelaide, Australia (Table 5.1). The examined patient cohort included a subset of 20 patients whom were part of Study 1 (See Appendix A for further patient recruitment and study allocation details). In all patients, indication for surgery was painful and symptomatic knee OA. Patients were excluded from this study if: they were unable to walk unaided for 10 m; had a history of inflammatory arthritis; had neurological disorders that would affect walking; had severe cardiovascular or pulmonary disease; had isolated patellofemoral knee OA; or were unable to understand English. This study received ethics approval from the Southern Adelaide Clinical and Royal Adelaide Hospital Human Research Ethics Committees. All patients provided written informed consent prior to their involvement.

Table 5.1: Physical characteristics of total knee arthroplasty patients

	All OA (n = 25)	Neutral-varus (n = 18)	Valgus (n = 7)
Age (years)	68 ± 7	67 ± 8	70 ± 6
Gender (male:females)	11:14	10:8	1:6
Affected limb (right:left)	13:12	9:9	4:3
Height (m)	1.66 ± 0.09	1.67 ± 0.10	1.64 ± 0.07
Body mass (kg)	91.6 ± 18.0	93.8 ± 18.2	86.0 ± 17.7
BMI (kg/m^2)	32.9 ± 4.4	33.4 ± 4.2	31.8 ± 5.1
WOMAC (total)	56 ± 13	55 ± 13	59.5 ± 13.8
Pain	12 ± 2	12 ± 2	11 ± 2
Stiffness	6 ± 1	6 ± 1	6 ± 2
Function	39 ± 12	38 ± 12	42 ± 10
Kellgren-Lawrence (II:III:IV)	4:7:14	2:5:11	2:2:3
Walking speed (m/s)	0.70 ± 0.25	0.74 ± 0.23	0.60 ± 0.29
Knee moments (Nm/kg)			
Knee flexion moment	0.35 ± 0.23	0.41 ± 0.22	0.18 ± 0.15
Knee extension moment	-0.11 ± 0.29	-0.07 ± 0.27	-0.21 ± 0.34
First peak knee adduction	-0.40 ± 0.23	-0.49 ± 0.18	-0.17 ± 0.20
Second peak knee adduction	-0.39 ± 0.22	-0.45 ± 0.20	-0.23 ± 0.19
Knee adduction moment impulse	27.0 ± 14.2	31.7 ± 13.6	14.6 ± 6.4
External rotation moment	0.022 ± 0.023	0.010 ± 0.013	0.051 ± 0.012
Internal rotation moment	-0.085 ± 0.079	-0.111 ± 0.074	-0.019 ± 0.039
Joint reaction force (BW)	3.02 ± 0.96	3.20 ± 0.93	2.57 ± 0.95
Static alignment			
Mechanical axis deviation (mm)	9.2 ± 34.8	29.4 ± 18.7	-34.1 ± 14.9
Medial proximal tibia angle (°)	90.1 ± 2.7	91.0 ± 2.2	88.1 ± 2.7

Average ± standard deviation

5.2.2 Gait Analysis

Patients underwent pre-operative gait analysis within one week prior to surgery. Three successful walking trials were collected with the patient walking at a self-selected speed and without footwear along a 10 m walkway. 3D kinematics and ground reaction force data were collected using 12 VICON MX-F20 cameras (Vicon Metrics, Oxford, UK) and four floor-embedded force platforms (2 × 9281B, Kistler Instrument Corporation, Switzerland; 2 × AMTI BP400600,

Advanced Mechanical Technology Inc., USA) at 100 Hz and 400 Hz, respectively. A lower-limb marker set was used consisting of 40 retro-reflective markers placed on the subject's pelvis and lower limbs. Markers were placed over palpable anatomical landmarks to define the joints of the lower limbs, and rigid clusters of four non-collinear markers were attached to the thighs and shanks (Cappozzo et al., 1995). Marker trajectories and ground reaction forces were low-pass filtered, using a zero-lag 4th order Butterworth filter with cut off frequency of 6 and 25 Hz, respectively (Winter, 2009). The pose of the body segments was reconstructed using global optimisation (Lu & O'Connor, 1999). The kinematic model (details in Thewlis et al. (2015)) consisted of a pelvis, two thighs, two shanks and two feet connected by six joints with 3, 2 and 2 degrees of freedom, respectively.

Walking velocity was calculated from kinematic data. The external joint moments were computed using inverse dynamics following a recursive Newton-Euler method (Doriot & Chèze, 2004) in Visual3D (V5, C-Motion Inc., USA). The knee joint moments were expressed in the shank coordinate system. The moments were normalised to body mass (Nm/kg) and reported as the mean of the three successful trials per participant. Data were time normalised to 101 points representing 0 to 100% of the stance phase. The knee moments included the peak knee flexion (KFM), peak knee extension during terminal stance (KEM), peak knee adduction (KAM, first (KAM_1) and second (KAM_2) peaks), external (ERM) and internal rotation (ERM) moments (Zabala et al., 2013). The KAM impulse, representing the area under the adduction moment curve, was computed using the trapezoidal method across the entire stance phase. The tibiofemoral total joint reaction force (JRF) was also computed using a musculoskeletal model based on the geometry of Delp et al. (1990) and as described in detail previously (Thewlis et al., 2015). All JRF measures were computed using MATLAB and normalised to body weights (R2013a, Mathworks, Inc., Natick, MA, USA).

5.2.3 Clinical and radiographic data

The Western Ontario & McMaster Universities Osteoarthritis Index (WOMAC) (5 point Likert-type format) was completed by each participant during the biomechanics laboratory visit to assess the degree of self-reported knee pain and functional limitation (Bellamy et al., 1988). To quantify the mechanical alignment in the affected joint, the mechanical axis deviation (MAD) and medial proximal tibial angle (MPTA) were measured from full-length anterior-posterior weight-bearing radiographs by an experienced examiner (LBS). MAD is defined as the perpendicular distance (in mm) from the knee joint centre to the mechanical axis, where the mechanical axis is the line connecting the centre of the femoral head to the centre of the ankle joint. *Valgus alignment* was defined as $>$ 0 mm lateral deviation, *neutral alignment* between 0-15 mm medial deviation and *varus alignment* as $>$ 15 mm medial deviation (Paley,

2002). The MPTA is defined as the medial angle between the anatomical axis of the tibia (line from centre of the knee to centre of the ankle) and a line parallel to the tibial plateau surface.

5.2.4 Micro-computed tomography (micro-CT) imaging and morphometric analysis

Following TKA surgery, tibial plateaus were retrieved and fixed in 70% ethanol solution. Each tibial plateau was scanned with a desktop micro-CT system (Skyscan 1076, Skyscan-Bruker, Kontich, Belgium) at 17.4 μm isotropic pixel size, source voltage 100 kVp, current 90 μA, rotation step 0.4°over 180°rotation, exposure time 590 ms, 4 frames averaging and 0.5 mm-thick aluminium filter for beam hardening reduction (Perilli et al., 2012; Roberts et al., 2016). Prior to scanning, specimens were removed from the ethanol solution and individually wrapped in cling-film. Scans were performed with the tibial plateau fixed on a carbon bed, with the medial-lateral axis of each specimen aligned with the system's rotation axis. For each specimen, 4997 consecutive cross-section images were reconstructed (86.9 mm length, slice thickness of one pixel i.e. 17.4 μm) using a filtered back-projection algorithm, each image 3936 x 3936 pixels (68.5 x 68.5 mm) in size and saved in 8-bit grayscale format (NRecon software, v1.6.9.8, Skyscan-Bruker, Kontich, Belgium). The cross-section images were then realigned such that the anatomical superior-inferior axis of each plateau was aligned with the z-axis of the image stack (DataViewer software, v 1.5.1.2, Skyscan-Bruker, Kontich, Belgium) (see **Chapter 4** and Roberts et al. (2016) for further details).

In each tibial plateau image dataset, four cylindrical STB volumes of interest (VOI) were selected within the load bearing regions of the tibial condyles; each VOI was centred within the anterior or posterior halves of the medial and lateral condyles, which were defined by elliptical regions (Fig. 6.1(a)): anterior-medial (AM), posterior-medial (PM), anterior-lateral (AL) posterior-lateral (PL) VOI (Khodadadyan-Klostermann et al., 2004). The cylindrical VOIs were of diameter 10 mm and minimum length 3 mm (to satisfy the continuum assumption of trabecular bone (Harrigan et al., 1988; Tassani & Perilli, 2013)), maximum 5 mm, depending on the specimen. The superior surface of each VOI was subjacent to the inferior surface of the subchondral bone plate, extending distally towards the growth plate (Fig. 6.1(b)). Only STB within the first 5 mm below the inferior subchondral bone plate was considered, as it has been reported that microarchitectural differences in tibial condyles are most prominent within this distance (Patel et al., 2003; Roberts et al., 2016). Each STB VOI was binarised with uniform thresholding (Perilli et al., 2007a,b) and the following morphometric parameters were calculated for each volume with software CT Analyser (v1.14.4.1): bone volume fraction (BV/TV, %), trabecular thickness (Tb.Th, μm), trabecular separation (Tb.Sp, μm), trabecular number (Tb.N, 1/mm) and structure model index (SMI) (Perilli et al., 2012; Roberts et al.,

2016). BV/TV was calculated as the voxels segmented as bone within the VOI, divided by the voxels constituting the examined VOI (Perilli et al., 2012). The Tb.Th, a 3D measure of the average thickness of the trabeculae, and the Tb.Sp, a 3D measure of the mean distance between the trabeculae, were both computed by using the local sphere fitting method (Hildebrand & Rüegsegger, 1997a; Perilli et al., 2006). The Tb.N, the number of trabecular plates per unit length (Parfitt et al., 1987), was calculated as is implemented in CT Analyser software (Tb.N = (BV/TV)/Tb.Th) (Perilli et al., 2012, 2015b). The SMI describes the ratio of rod- to plate-like trabecular structures, ranging in value from 0 (ideal plate-like structure) to 3 (ideal rod-like structure), with intermediate values indicating a mixed structure (Hildebrand & Rüegsegger, 1997b; Perilli et al., 2006).

The medial (M) and lateral (L) condyle BV/TV were computed as the average BV/TV of the anterior (A) and posterior (P) VOIs within each condyle. The BV/TV ratios between subregions within each condyle (anterior-to-posterior, A:P) and between the condyles (medial-to-lateral M:L) were also computed.

5.2.5 Statistics

A power analysis (software G*Power 3.1, Brunsbüttel, Germany (Faul et al., 2009)) indicated that for a power = 0.8 and alpha = 0.05, a minimum sample size of 17 patients would be necessary for detecting significant differences (effect size of 1 standard deviation) among STB subregions and significant associations (effect size r = 0.6) between knee loading and STB microarchitectural parameters.

Differences in morphometric parameters among the four regions (AM, PM, AL, PL) within the tibia were assessed by using repeated measures ANOVA followed by paired t-test with Bonferroni adjustment for multiple comparisons. Multiple ANOVAs were conducted, in place of a single MANOVA test, due to strong interrelationships among morphometric parameters ($r > 0.8$). Prior to ANOVA, all STB microarchitecture were tested for assumptions of multivariate normality and sphericity, with departures from sphericity corrected using the Greenhouse-Geisser method.

Correlations, exploring for linear relationships between the STB subregional microarchitecture parameters, BV/TV ratios, the dynamic joint loads and the knee alignment parameters were examined using Pearson's correlations. A Benjamini-Hochberg adjustment was then made (false discovery rate = 0.05) to control for multiple testing (Benjamini & Hochberg, 1995). To control for potentially confounding variables that influence the medial joint contact force, or medial-to-lateral load distribution, stepwise multiple linear regression was used for predicting

subregional BV/TV or M:L BV/TV ratio. Peak knee moments (KFM, KEM, KAM_2, ERM, IRM) were input as independent variables, and walking speed, MAD and KAM_1 were considered, separately and together, as covariates (Adouni & Shirazi-Adl, 2014b; Kutzner et al., 2013; Schipplein & Andriacchi, 1991). All STB microarchitecture and joint loading parameters were tested for assumptions of normality (Shapiro-Wilks test), homogeneity of variance (Levene's test), linearity and homoscedasticity (scatter plot of residuals).

The analysis was first performed on all OA specimens grouped together. Then a secondary analysis was performed subdividing the cohort in two subgroups: one presenting with neutrally to varus aligned joints (constituting the "neutral-varus" subgroup, MAD $>$ 0 mm) and one with valgus aligned joints. The patient cohort was subdivided into a neutral-varus and a valgus subgroup, rather than into a varus and non-varus subgroup (as per Study 1), because the neutral-varus subgroup, whose patients all presented with medial compartment OA, enables comparison with previous literature, as relationships between joint loading and proximal tibial BMD were exclusively explored in medial knee OA patients (Thorp et al., 2006b; Wada et al., 2001). Relationships for the valgus subgroup, to the best of our knowledge, are reported for the first time. The significance level was set to $p < 0.05$. All statistical analysis were performed using SPSS Statistics 22 (IBM Corp., Armonk, NY, USA).

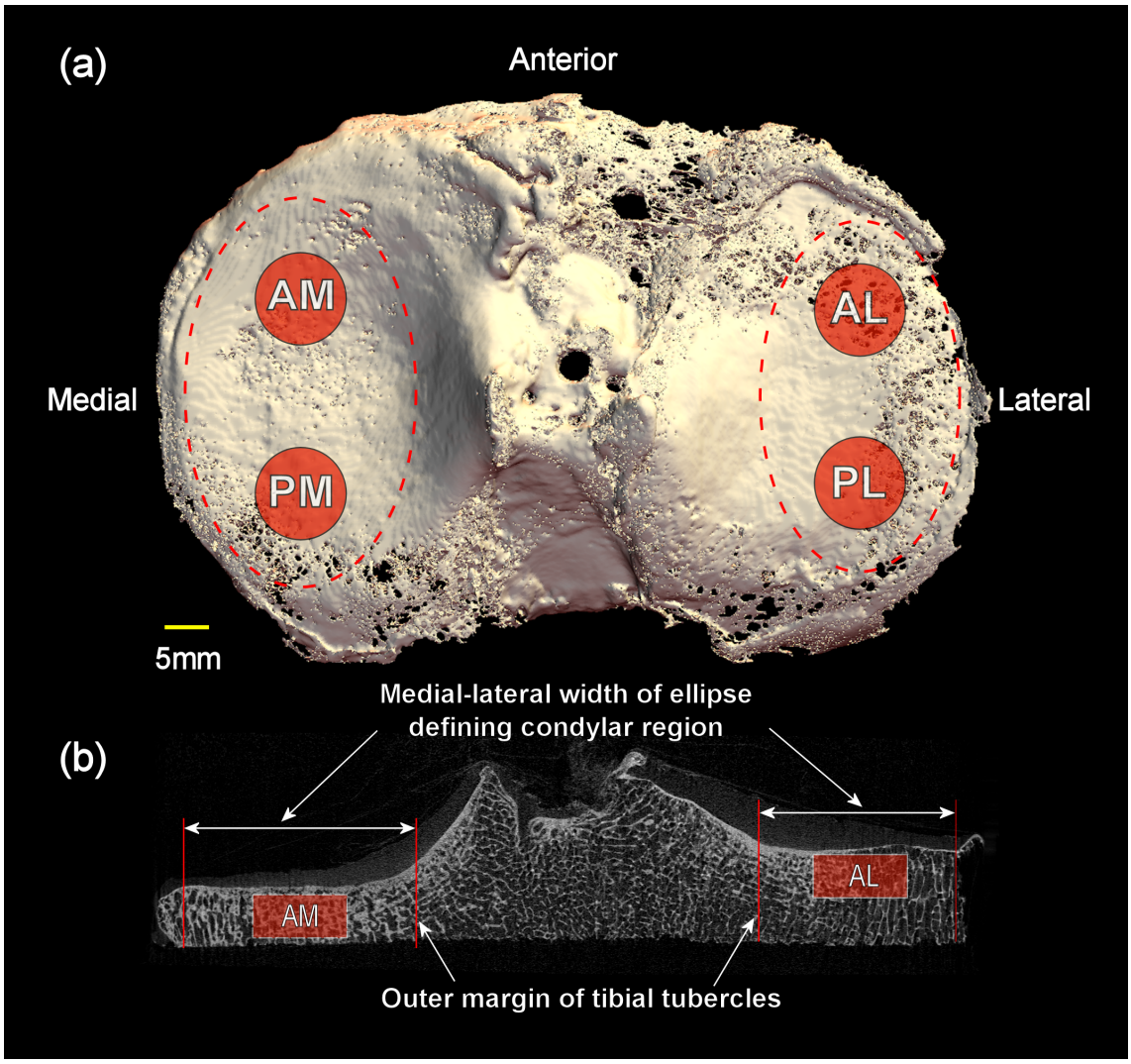

Figure 5.1: (a) 3D micro-CT image of an excised tibial plateau from a right knee (view from top). The ellipses defining the medial and lateral tibial condyles are shown (dashed lines), containing the location of the four subvolumes of interest (VOIs, two per condyle as indicated by red circles) in the anterior-medial (AM), anterior-lateral (AL), posterior-medial (PM) and posterior-lateral (PL) compartments; (b) 2D coronal micro-CT cross-section image of the tibial plateau with medial and lateral boundaries of the ellipses indicated by red lines. The location of the AM and AL VOIs, relevant to the subchondral bone plate, are indicated.

5.3 Results

Of the 25 patients recruited for this study, 15 patients exhibited varus, three neutral and seven valgus joint alignment. For the secondary analysis, the neutral and the varus patients whom all presented with medial knee OA were then merged, constituting the "neutral-varus" subgroup (Table 5.1, n = 18). Two VOIs, one PM and one PL VOI from separate patients were excluded from analysis, as these VOIs were too thin (height of VOI $<$ 3 mm). Patient characteristics and gait data are reported in Table 5.1 and Figure 5.2.

5.3.1 Subchondral trabecular bone microarchitecture

All OA specimens: When considering all specimens together, significant differences (ANOVA, $p < 0.001$) in bone morphometric parameters were found among the four anatomical VOIs (Fig. 5.3). The AM VOI had the highest BV/TV and Tb.N (up to +75% [45%, 104%] (mean difference [95% confidence interval]) and +41% [22%, 59%]), respectively) and lowest SMI (up to -69% [-36%, -68%]) compared with the other regions, with largest differences to the AL VOI (Fig. 5.4). AM Tb.Th was higher (up to +26% [16%, 36%]) and AM Tb.Sp lower (up to -25% [-15%, -35%]) compared with the AL and PL VOIs. On the other hand, the AL and PL VOIs showed no significant differences among each other, in any morphometric parameter.

Subgroups: In the neutral-varus subgroup, the AM and PM VOIs compared with AL and PL had significantly higher BV/TV (up to +124% [102%, 145%], almost double the difference compared to all the specimens taken together), whereas in the valgus subgroup BV/TV did not differ significantly. Similar observations were made for SMI and trabecular indices (Fig. 5.3).

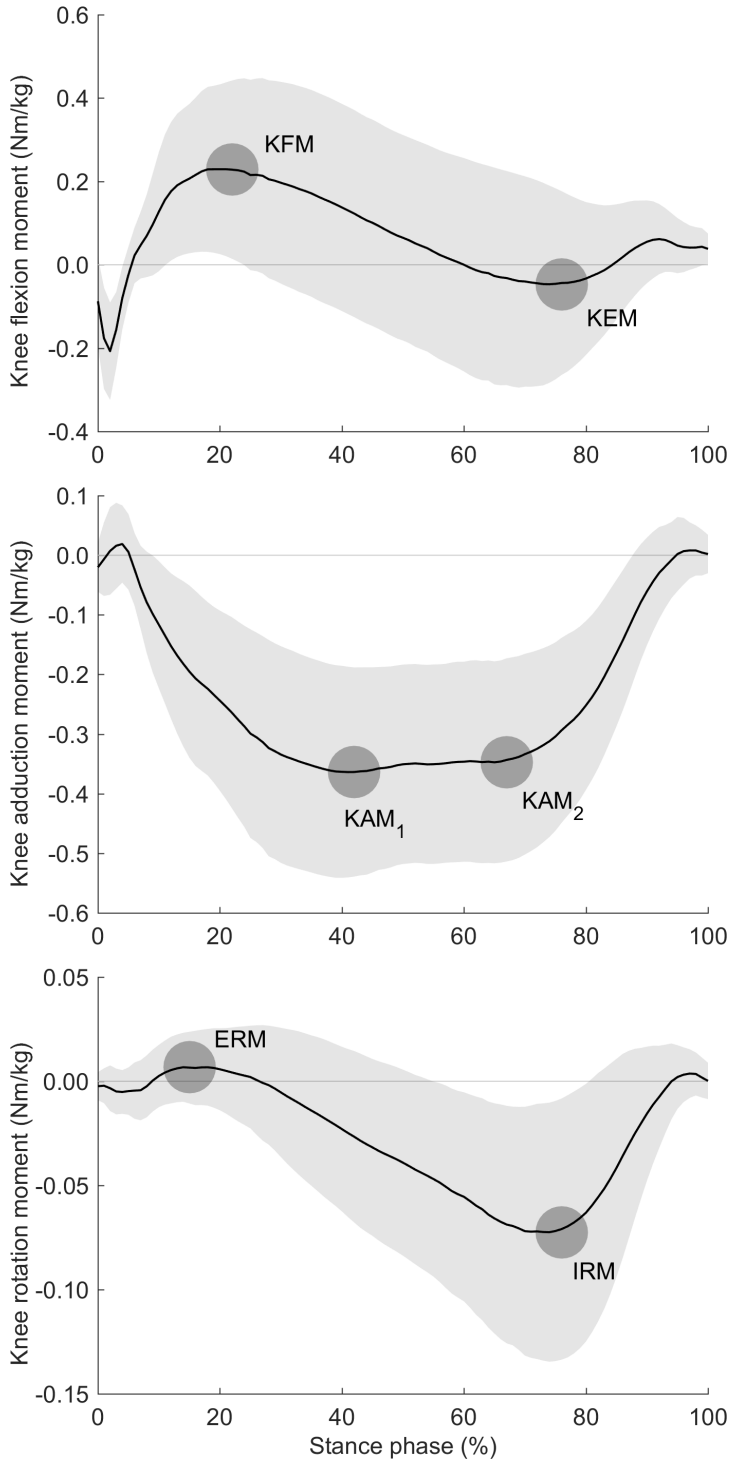

Figure 5.2: Average external knee moment curves and standard deviation (shaded area) over the stance phase of the gait cycle for all knee OA patients (n = 25). Reported peak knee moments are highlighted: KFM: knee flexion moment, KEM: knee extension moment, KAM_1, KAM_2: first and second peak knee adduction moments, ERM: external rotation moment, IRM: internal rotation moment

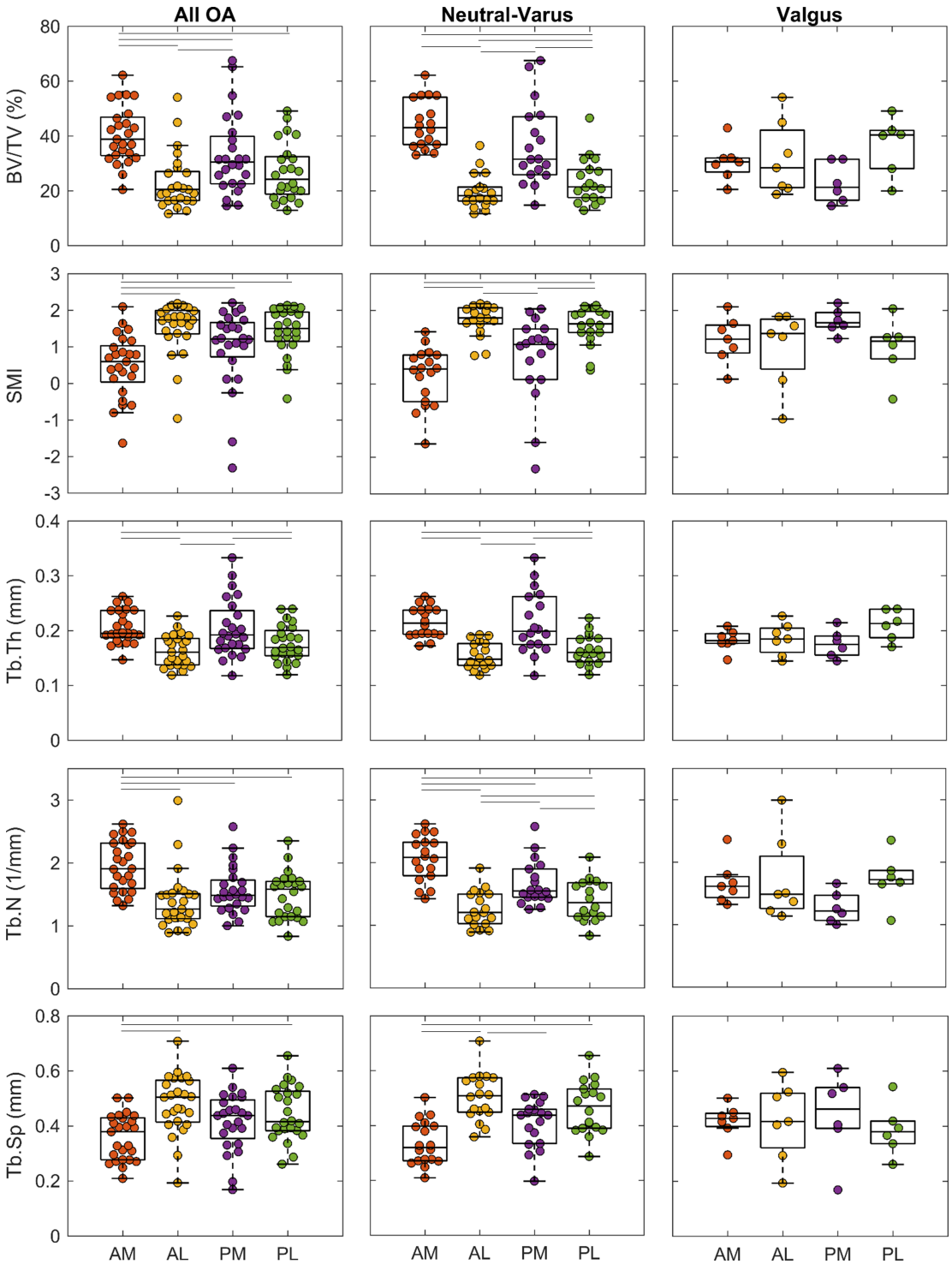

Figure 5.3: Univariate scatter and box and whisker plots reporting values of 3D subchondral trabecular bone morphometric parameters in the four subregions of interest within the proximal tibial plateau, for All OA, for the neutral-varus and valgus subgroups. Boxplots report median and interquartile range (IQR, first and third quartiles). Whiskers represent minimum and maximum datum within 1.5 x IQR. AM: anterior-medial, AL: anterior-lateral, PM: posterior-medial, PL: posterior-lateral. Significant differences among the regions are indicated by lines ($p < 0.05$, paired t-test with Bonferroni adjustment).

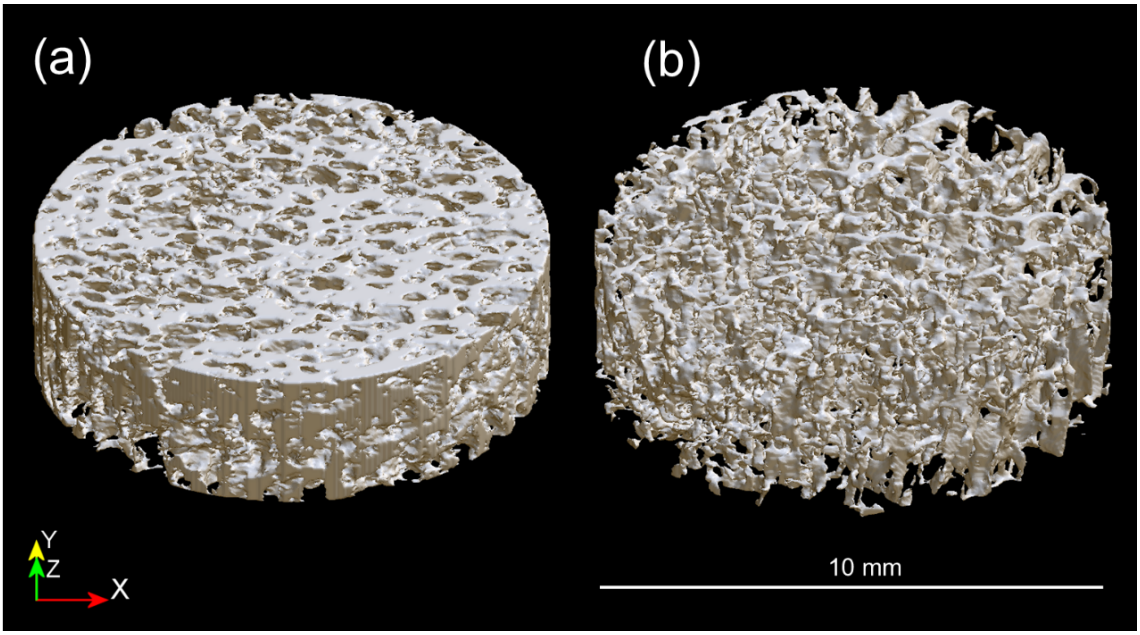

Figure 5.4: 3D micro-CT images of the cylindrical subchondral bone volumes examined (10 mm diameter, 3 mm length), (a) specimen from the AM subregion showing high BV/TV and plate-like structure (BV/TV = 42%, SMI = 0.4); (b) specimen from the AL subregion showing low BV/TV and mainly rod-like structure (BV/TV = 13%, SMI = 2.2).

5.3.2 Relationships between joint loading and tibial subchondral trabecular bone microarchitecture

All OA specimens: On the entire OA cohort, measures of joint loading were significantly ($p < 0.05$) correlated with regional tibial 3D microarchitectural parameters (Fig. 5.5). Among these, the ERM was most strongly correlated with medial STB microarchitecture, in particular negatively with AM BV/TV (r = -0.74 [-0.48, -0.88], Fig. 5.8(a)), M BV/TV (r = -0.69 [-0.40, -0.85]) and positively with the AM SMI (r = 0.67 [0.38, 0.84]). The MAD correlated significantly with STB microarchitecture in the lateral VOIs, most strongly with BV/TV (PL, r = -0.71 [-0.40, -0.87], Fig. 5.8(c); L, r = -0.71 [-0.41, -0.87]; AL, r = -0.68 [-0.36, -0.85]). Remaining loading indices were not significantly associated with any microarchitectural parameter, except for KEM which strongly correlated with AL Tb.Sp and Tb.N (r = 0.72 [0.45, 0.87], and r = -0.57 [-0.22, -0.78], respectively).

Subgroups: For both the neutral-varus and valgus subgroups, associations between joint loading and subregional microarchitectural parameters were in general weaker than those for all OA patients, and all were non-significant (n.s.) statistically (Fig. 5.6 and Fig. 5.7). For neutral-varus, although non-significant, ERM was the parameter with highest r-value for associations with subregional BV/TV ("AM BV/TV vs. ERM", r = -0.54 [-0.10, -0.81], n.s.; Fig.

5.8(b)). In valgus, r-value was highest for MAD with PL SMI (r = 0.93 [0.80, 0.98], n.s.) and L BV/TV (r = -0.87 [-0.65, -0.96], n.s.).

5.3.3 Relationships between knee joint loading and tibial condyle BV/TV ratios among subregions

All OA specimens: For the entire cohort, measures of knee joint loading significantly correlated with BV/TV ratios among subregions (Fig. 5.5). Medial-to-lateral BV/TV ratios (M:L, AM:PL, PM:AL and PM:PL ratios) were most strongly associated, negatively with ERM and positively with MAD. The strongest correlations were "M:L BV/TV vs. ERM" and "M:L BV/TV vs. MAD" (r= -0.74 [-0.48, -0.88] and 0.74 [0.45, 0.88], Fig. 5.8(e) and 5.8(g)); for all other ratios, |r| range: 0.57 to 0.71, $p < 0.05$ for all). The M:L BV/TV ratio was also significantly associated with, in order of descending strength, the KAM_1, KAM, KAM_2, IRM and the KAM impulse (|r| range: 0.54 to 0.60). No significant associations were observed between measures of joint loading and AM:PM BV/TV or AL:PL BV/TV subregional ratios.

Subgroups: All associations between joint loading and subregional bone volume ratios, in OA subgroups, were non-significant statistically (Fig. 5.5). Notably, in neutral-varus, associations between M:L BV/TV and ERM, MAD and KAM indices (KAM, KAM_1, KAM_2, KAM impulse) were weak ("M:L BV/TV vs. ERM", r = -0.31 [-0.68, 0.17], Fig. 5.8(f); "M:L B/TV ratio vs. MAD", r = 0.12 [-0.42, 0.59] Fig. 5.8(h); "M:L BV/TV ratio vs. KAM_1, r = -0.30 [-0.67, 0.19], all n.s.); in valgus, r-values for these associations were of moderate strength, and non-significant statistically (|r| range 0.35 – 0.68, n.s.). In valgus, the r-value was highest for association "ERM vs. PM:PL" (r = -0.95 [-0.86, -0.98], n.s.).

5.3.4 Multiple regression analysis

ERM was the only loading parameter to enter regression models, for prediction of AM BV/TV or M:L BV/TV ratio, when controlling for walking speed, MAD and KAM_1 or a combination of these variables (Table 5.2). After controlling for confounding variables, ERM explained an additional 28% to 50% of the variance in AM BV/TV (final model, adjusted $R^2 = 0.59$, $p = 0.001$), and between 16% to 24% of the variance in M:L BV/TV ratio (final model, adjusted $R^2 = 0.65$, $p < 0.0005$).

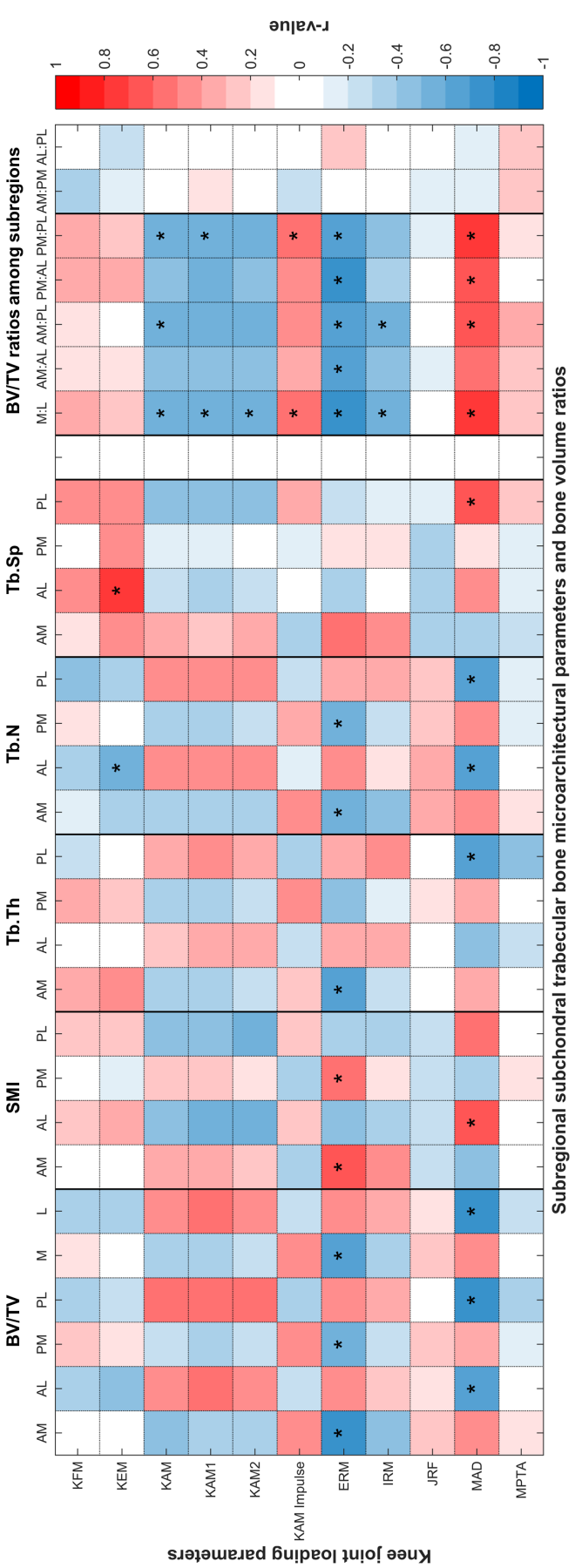

Figure 5.5: Heatmap of Pearson's correlations "knee joint loads vs. subregional subchondral trabecular bone microarchitecture parameters and subregional bone volume ratios" for all OA patients ($n = 25$). Significant correlations (Benjamini-Hochberg adjusted, false discovery rate $= 0.05$) indicated: *$p < 0.05$. BV/TV: bone volume fraction, SMI: structure model index, Tb.Th: trabecular thickness, Tb.Sp: trabecular separation, Tb.N: trabecular number, AM: anterior-medial, AL: anterior-lateral, PM: posterior-medial, PL: posterior-lateral.

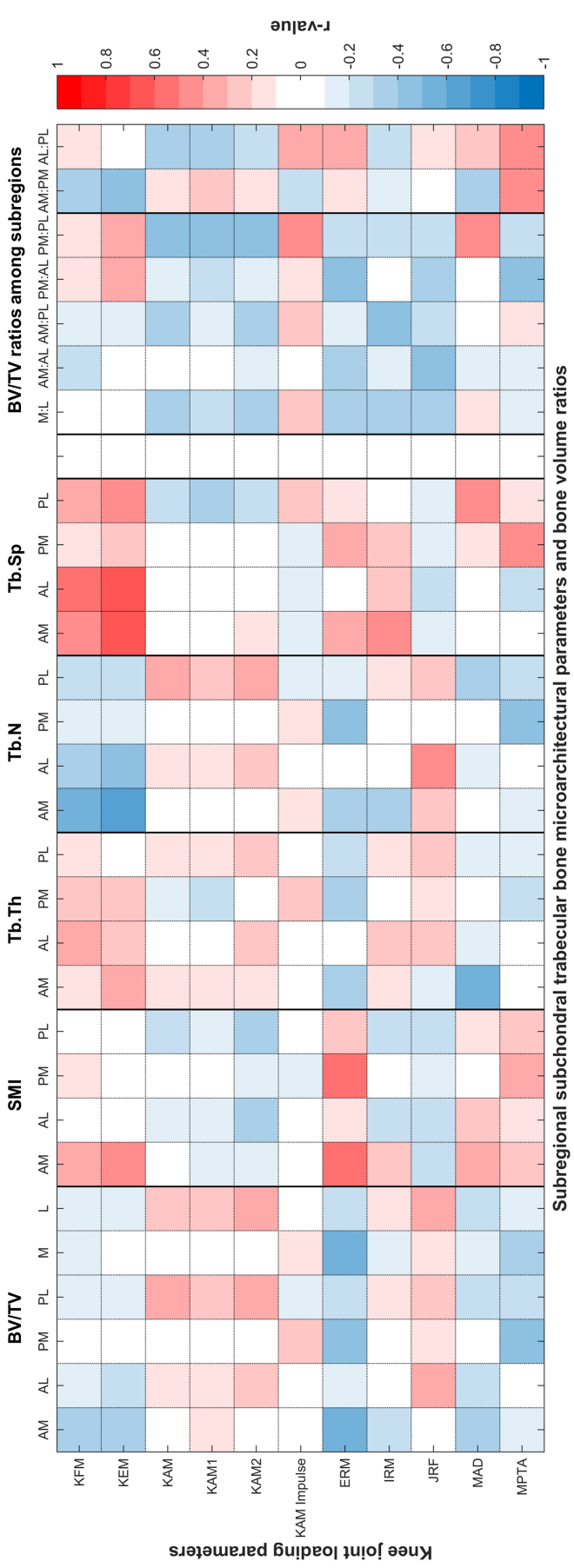

Figure 5.6: Heatmap of Pearson's correlations 'knee joint loads vs. subregional subchondral trabecular bone microarchitecture parameters and subregional bone volume ratios' for neutral-varus OA patients ($n = 18$). Significant correlations (Benjamini-Hochberg adjusted, false discovery rate $= 0.05$) indicated: *$p < 0.05$. BV/TV: bone volume fraction, SMI: structure model index, Tb.Th: trabecular thickness, Tb.Sp: trabecular separation, Tb.N: trabecular number, AM: anterior-medial, AL: anterior-lateral, PM: posterior-medial, PL: posterior-lateral.

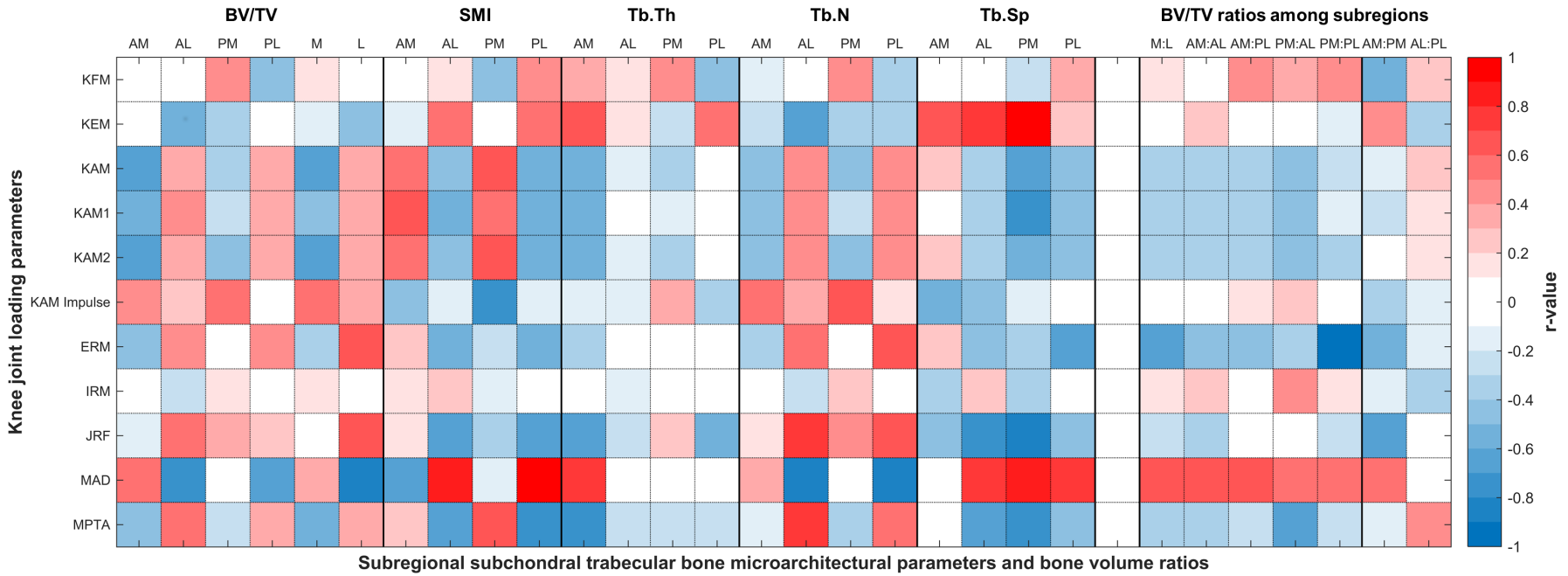

Figure 5.7: Heatmap of Pearson's correlations "knee joint loads vs. subregional subchondral trabecular bone microarchitecture parameters and subregional bone volume ratios" for valgus OA patients (n = 7). Significant correlations (Benjamini-Hochberg adjusted, false discovery rate = 0.05) indicated: *p $<$ 0.05. BV/TV: bone volume fraction, SMI: structure model index, Tb.Th: trabecular thickness, Tb.Sp: trabecular separation, Tb.N: trabecular number, AM: anterior-medial, AL: anterior-lateral, PM: posterior-medial, PL: posterior-lateral.

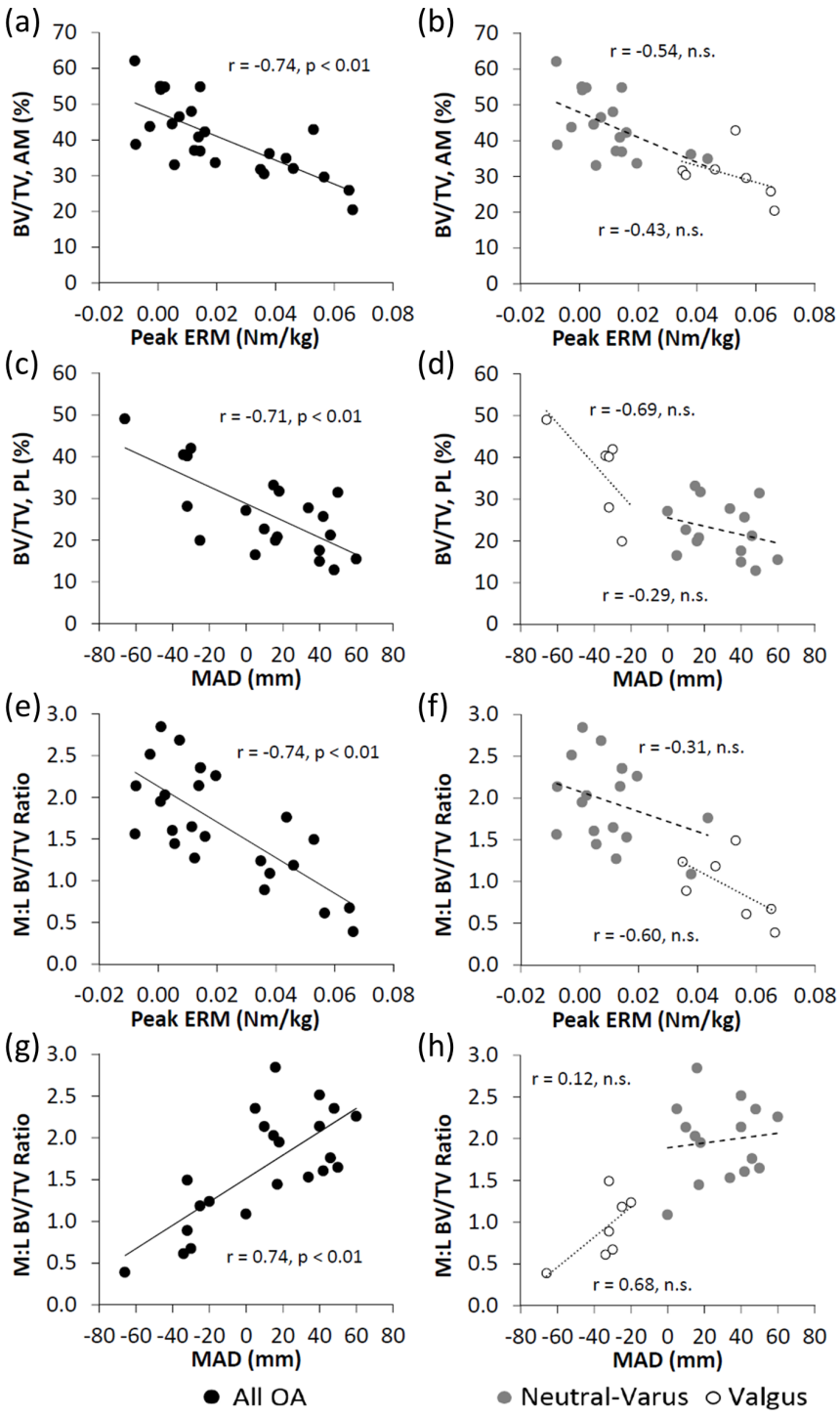

Figure 5.8: Scatter plot and best fit line for Pearson's correlations: (a,b) "AM BV/TV vs. ERM", (c,d) "PL BV/TV vs. MAD", (e,f) "M:L BV/TV vs. ERM", (g, h) "M:L BV/TV vs. MAD", for (graphs on left) all OA, (graphs on right) subdivided into neutral-varus and valgus subgroups.

Table 5.2: Summary of stepwise multiple linear regression analysis, for prediction of AM BV/TV and M:L BV/TV ratio, considering covariates that influence medial condyle joint forces (walking speed, mechanical axis deviation (MAD) and first peak knee adduction moment (KAM_1) (Kutzner et al., 2013)) and medial-to-lateral load distribution (KAM_1, MAD (Adouni & Shirazi-Adl, 2014b; Schipplein & Andriacchi, 1991))

Dependent Variable	Model	R^2 change	Sig. F-change	Unadjusted R^2	Adjusted R^2	p-value
AM BV/TV	1) *WS*			0.112	0.074	0.102
	ERM	**0.495**	< 0.0005	0.607	0.571	< 0.0005
	2) *MAD*			0.242	0.204	0.020
	ERM	**0.275**	0.004	0.518	0.467	0.001
	3) *KAM_1*			0.152	0.115	0.054
	ERM	**0.393**	< 0.0005	0.545	0.503	< 0.0005
	4) *WS, MAD*			0.356	0.288	0.015
	ERM	**0.297**	0.001	0.653	0.595	< 0.0005
	5) *WS, MAD, KAM_1*			0.371	0.266	0.036
	ERM	**0.297**	0.001	0.668	0.590	0.001
M:L BV/TV ratio	1) *KAM_1*			0.356	0.328	0.002
	ERM	**0.243**	0.001	0.600	0.563	< 0.0005
	2) *MAD*			0.541	0.518	< 0.0005
	ERM	**0.157**	0.005	0.697	0.666	< 0.0005
	3) *KAM_1, MAD*			0.545	0.497	0.001
	ERM	**0.156**	0.007	0.701	0.652	< 0.0005

Covariates are in italics. Significant contributions of additional loading parameters are indicated in bold. BV/TV: bone volume fraction, AM: anterior-medial, M:L: medial-to-lateral ratio, WS: walking speed, ERM: external rotation moment. Peak knee moments (knee flexion, knee extension, second peak knee adduction, knee external and internal rotation moments) were input as independent variables.

5.4 Discussion

This study performed, on the same patient, a combination of 3D gait analysis and micro-CT imaging to investigate relationships between knee joint loading and regional measurements of proximal tibial subchondral trabecular bone microarchitecture in end-stage knee OA. The STB microarchitecture differed significantly among condylar regions, with highest BV/TV and more plate-like structure anterior-medially; it was significantly associated with *in vivo* measures of dynamic knee loading during early stance, as well as with static joint alignment. When considering the entire cohort, the STB microarchitecture in the medial condyle, particularly in the AM compartment, was most strongly associated with ERM. Laterally it was most strongly associated with MAD. The M:L BV/TV subregional ratios were also significantly and most strongly associated with ERM and MAD. Moreover, the ERM explained a significant amount of variation in AM BV/TV and M:L BV/TV ratio, also after controlling for the potentially confounding variables, such as walking speed, MAD and KAM_1.

The overall strongest associations between loading and STB microarchitecture were found for "ERM vs. AM (and M) BV/TV" and "ERM vs. AM SMI", with a positive and negative sign, respectively, supporting our hypothesis to detect significant associations between the rotation moments and subregional STB microarchitecture. This finding means that a lower ERM corresponds with higher bone volume fraction and more plate-like architecture in the AM condyle, which is also the anatomical location where BV/TV was highest and SMI lowest in the present OA series (Fig. 5.3). Moreover, ERM was the only loading parameter to enter a regression model, to predict AM BV/TV, when controlling for loading indices that may influence medial joint load (Kutzner et al., 2013). Previous studies reported either significantly lower ERM in OA patients (Landry et al., 2007) or no significant differences compared with controls (Kaufman et al., 2001). However, these did not investigate the bone microarchitecture. Other studies documented higher medial condyle BV/TV in OA subjects compared with a control group, however, no gait analysis was performed (Ding et al., 2003; Patel et al., 2003). Hence, to the best of the authors' knowledge, this study is the first to explore associations between peak rotation moments and regional variations in joint bone microarchitecture in the same patient. Taken together, reductions in ERM may be indicative of increased stress concentrations in the anterior-medial condyle that, in part, explain higher BV/TV and more plate like microarchitecture in this region, as an adaptation of the bone to increased compartmental mechanical loads (Turner, 1998).

The overall strongest associations between joint loading parameters and BV/TV ratios among subregions were found for "ERM vs M:L BV/TV" and "MAD vs. M:L BV/TV", followed by associations with the knee adduction moments (KAM, KAM_1 and KAM_2) and the KAM

impulse. These findings for the MAD and KAM are consistent with previous reports on associations with proximal tibia BMD ratios (analogous with the BV/TV ratios reported here) (Thorp et al., 2006b; Wada et al., 2001), while the stronger associations "MAD vs. BV/TV subregional ratios" compared with "KAM vs. BV/TV subregional ratios" are consistent with previous findings using BMD (Thorp et al., 2006b). As the MAD and KAM indices may reflect the medial-to-lateral distribution of joint load across the tibial condyles during the stance phase of gait (Adouni & Shirazi-Adl, 2014b; Schipplein & Andriacchi, 1991), the variation in subchondral trabecular BV/TV subregional ratios with differences in joint alignment likely demonstrates an adaptation of the subchondral bone in response to variations in partitioning of joint loads. The MAD was also the parameter most strongly correlated with lateral STB microarchitecture, particularly with PL BV/TV, Tb.Th and Tb.N. A higher MAD, indicator of a higher M:L distribution of joint loads, may at least in part, be a result of decreased joint loads upon the lateral tibial condyle with a shift towards the medial condyle; this consequently may result in lower bone volume in the lateral region, characterised by thinner and fewer trabeculae, as shown here.

When subsequently examining either the neutral-varus or the valgus subgroup, associations between joint loading and BV/TV ratios were generally weaker, and were non-significant statistically compared with the entire OA cohort, likely as a consequence of limited sample size. Notably, in neutral-varus, associations between frontal plane loading indices (KAM and MAD) with M:L BV/TV ratios were all weak. This finding suggesting that the associations between these loading parameters and subregional BV/TV ratios detected in the entire OA cohort are driven by large variations in mechanical alignment from varus to valgus within the examined joints.

The link between reduced ERM and higher medial BV/TV, possibly indicating increased medial joint stresses, is unclear. Knee moments and joint kinematics are closely related (Andriacchi & Dyrby, 2005), thus variations in ERM may reflect altered rotation mechanics that result in shifts in joint contact regions to areas of unconditioned cartilage (Andriacchi et al., 2009). This shift in joint loads may lead to degenerative changes within the articular cartilage and to increased load transfer to the underlying STB structure. Alternatively, the ERM may be a surrogate measure for peak AM compartment stresses, as the ERM during early to midstance is potentially coincident with peak contact stresses in the AM subregion during this period (Adouni & Shirazi-Adl, 2014a; Liu et al., 2010). Moreover, a reduced ERM could be related to an increased muscle co-contraction in knee OA during the load-bearing period of stance, resulting in increased compressive forces upon the tibial condyle (Childs et al., 2004; Zeni et al., 2010). Regardless of what exactly ERM might represent, it was the loading parameter most strongly associated with variations in medial compartment STB microarchitecture and only loading parameter that explained significantly greater variations in AM BV/TV and M:L

BV/TV ratio, when controlling for KAM_1 and/or MAD. Thus, further exploration is warranted for understanding the contribution of the full 3D knee moments, including the ERM, in the progression of knee OA.

Finally, the JRF was not significantly associated neither with subregional measures of STB microarchitecture, nor with BV/TV subregional ratios. One reason for this absence of significant associations may be due to the used musculoskeletal model computing the overall JRF, rather than medial or lateral condyle-specific JRF, hence not giving a measure of the M:L load distribution. Furthermore, the model assumes non-pathological muscle activation patterns, thus not accounting for differences in loading that may be due to variations in muscle activity in knee OA (Heiden et al., 2009). We don't exclude that by using models computing a condyle-specific JRF and that are driven with patient-specific EMG data, different relationships between JRF and subregional bone microarchitecture could be found.

Interestingly, in the present OA series, females accounted for 6 of 7 valgus-aligned joints. This supports results from a large multicentre study documenting higher incidences of valgus-joint alignment in females than in males (Wise et al., 2012). These gender-related differences are suggested to be a consequence of anatomical differences in the pelvis and lower limb, resulting in altered knee loading (Wise et al., 2012). Given potential differences in knee joint biomechanics between men and women, whom were pooled in this study, it cannot be excluded that gender may have influenced the relationships observed herein. Further exploration on the effect of gender, considering appropriate sample size, in future is thus warranted.

There were limitations to this study. Importantly, it is unclear whether joint loading indices reported are reflective of knee loads that occur during earlier stages of the disease, and that may have influenced resultant bone microarchitecture observed within this study. Moreover, examined bone are from end-stage OA where other factors, apart from loading, including age, genetics, or the local biochemical environment in the presence of bone sclerosis, can effect subchondral bone metabolism (Li et al., 2013). Furthermore, due to the cross-sectional study design, we could not determine whether the revealed relationships between joint loading and STB microarchitecture are characteristic only within the end-stage OA joints examined, or whether these are present in the earlier stages of the disease, or within non-pathological joints. Micro-CT cannot currently be applied *in vivo* on human knees for characterisation of STB microarchitecture, thus this study was restricted to patients with end-stage knee OA who underwent total knee arthroplasty. However, recent high-resolution peripheral quantitative CT (HR-pQCT) imaging systems, permitting *in vivo* examination of proximal tibial STB microarchitecture with 61 μm voxel size (Kroker et al., 2016), may in future be employed to examine the above relationships, in early OA and non-pathological joints. HR-pQCT may also be useful for examining whether longitudinal changes in STB microarchitecture can be explained by

baseline measures of joint loading. Moreover, we did not study articular cartilage morphology, for example cartilage thickness, which is important in load transfer across the tibiofemoral joint. Finally, we suggest that these results, in particular for ERM, be interpreted with some caution as poor measurement reliability has been documented for the rotation moment during the early stance phase of gait (Robbins et al., 2013). A strength of this study is the combination of micro-CT and gait analysis, on the same patient. This permits examination of the subchondral trabecular bone microarchitecture in specific subregions of the proximal tibial plateau, where microarchitectural changes in the STB are most evident in OA, combining them with measures of joint loading, moments and static alignment of the same subject. Moreover, as the micro-CT examination was performed on entire tibial plateaus without coring them, these are preserved intact for further examination (Roberts et al., 2016).

Concluding, this study demonstrates that dynamic and static markers of knee joint loading are significantly associated with regional variations in 3D subchondral trabecular bone microarchitecture in end-stage knee OA. Medial condyle STB microarchitecture, in particular in the anterior-medial compartment, the region with highest BV/TV and more plate like micro-architecture, was most strongly correlated with the ERM; while laterally, STB microarchitecture was most strongly associated with static alignment (MAD). Furthermore, in all OA, the ERM and MAD were strongly associated with the medial-to-lateral BV/TV ratios. Future work is required to establish possible causal relationship between the 3D knee moments and knee alignment with subregional changes in the proximal tibia STB microarchitecture. Overall, these results suggest that the ERM may thus be useful as a surrogate measure of peak anterior-medial compartmental stresses that occur in this region during early to midstance, or of the medial-to-lateral distribution of joint loads, as indicated by the bony response.

Chapter 6

Study 3: Joint loading and proximal tibia subchondral trabecular bone microarchitecture differ with walking gait patterns in end-stage knee osteoarthritis

6 STUDY 3: TIBIAL MICROARCHITECTURE WITH VARIABLE GAIT PATTERNS

The previous chapter (**Chapter 5, Study 2**) determined, in end-stage knee OA patients, the relationships between *in vivo* dynamic knee joint loads during gait, static alignment, and proximal tibia STB microarchitecture in the affected joint. Analysis was performed in all knee OA patients recruited and then separately in patient subgroups whom were stratified by degree of static alignment ("neutral-to-varus" and "valgus"-aligned patient subgroups). The present chapter (Study 3) extends upon that work, stratifying all OA patients into subgroups as determined from the peak knee moments representing dynamic markers of joint load during walking. Joint loads and subchondral trabecular bone microarchitecture have then been compared among identified subgroups.

The study presented in this chapter is the subject of the following paper:

Roberts BC, Solomon LB, Mercer G, Reynolds KJ, Thewlis D and Perilli, E 2017 Joint loading and proximal tibia subchondral trabecular bone microarchitecture differs with walking gait patterns in end-stage knee osteoarthritis. Osteoarthritis and Cartilage. doi: 10.1016/j.joca.2017.06.001. In press.

Abstract:

Objectives: (1) To identify subgroups with distinct walking gait patterns in end-stage knee osteoarthritis (OA) patients; (2) to compare measures of joint loading and proximal tibia subchondral trabecular bone (STB) microarchitecture among them.

Design: Twenty-five knee OA patients scheduled for total knee arthroplasty underwent gait analysis. Following surgery, excised tibial plateaus were micro-CT scanned and STB microarchitecture analysed in four tibial condylar regions of interest. Peak knee moments were input to k-means cluster analysis, to identify subgroups with homogeneous gait patterns. Joint loading and STB microarchitecture parameters were compared among subgroups (Kruskal-Wallis and Bonferroni-corrected Mann-Whitney U-tests).

Results: Three gait subgroups were revealed: biphasics ($n = 7$), flexors ($n = 9$), counter-rotators ($n = 9$). Peak knee adduction moment (KAM) and KAM impulse were significantly higher ($p < 0.05$) in biphasics than in flexors and counter-rotators (KAM = -0.65, -0.40 and -0.21 Nm/kg, respectively), suggesting a higher medial-to-lateral tibiofemoral load ratio in biphasics. Interestingly, STB medial-to-lateral bone volume fraction ratio was also significantly higher in biphasics and flexors than in counter-rotators (2.15, 1.92 and 1.04, respectively); however, it was not significantly different between biphasics and flexors.

Conclusions: Despite higher indices of KAM in biphasics, subregional subchondral bone microarchitecture did not differ among OA patients with flexor and biphasic gait patterns; suggesting that, between these subgroups, there may be different mechanisms for generating comparable (non-differing) loads upon the tibial plateau, indicated by corresponding bony response. Future work may explore the utility of identifying distinct walking gait patterns for identifying, and improving management of, persons at risk for developing knee OA.

6.1 Introduction

Knee osteoarthritis (OA) is a multifactorial disease in which the local mechanical environment is implicit in the initiation and development of the pathology (Griffin & Guilak, 2005). OA is commonly associated with cartilage breakdown; however, OA also affects the underlying bone, altering the subchondral bone structure (Loeser et al., 2012). The subchondral bone plays an important role as a mechanical shock absorber of the joint (Imhof et al., 1999).

Peak joint loads during gait are associated with progression of knee OA (Miyazaki et al., 2002). Conservative treatments attempt to delay progression of knee OA by aiming at reducing the external knee adduction moment (KAM) or KAM impulse, surrogate markers for compartment-specific (medial-to-lateral) joint loads, during walking gait. However, the inter-individual responses to conservative treatments are highly variable, and in some patients the use of these treatments, for example prescription of lateral wedge insoles, have resulted in a paradoxical increase in the KAM (Chapman et al., 2015; Hinman et al., 2012). Moreover, to date, these interventions do not appear to attenuate disease related changes in joint structures (Bennell et al., 2011; Pham et al., 2004). Such undesirable outcomes, it is suggested, may be a consequence of heterogeneity within the knee OA cohort to whom the intervention has been applied (Arnold et al., 2015). A stratification of the knee OA population into more homogeneous subgroups may enable identification of individuals likely to exhibit a desirable treatment response. A subgrouping based on biomechanical features could also aid in the development of novel treatments or early identification of populations susceptible to knee OA.

Previous research has identified distinct walking gait patterns in knee OA patients (Levinger et al., 2012; Smith et al., 2004). However, whether joint loading indices (KAM, KAM impulse and static alignment) also vary among different walking gait patterns in knee OA has not yet been explored. Moreover, structural bone changes in the affected joint, including variations in bone mass, have been associated with variations in joint loads (Creaby et al., 2010; Thorp et al., 2006b). Whether the subchondral trabecular bone (STB) microarchitecture varies among gait patterns in OA, however, is still unknown. Subchondral bone adapts to its local mechanical environment (Turner, 1998). Hence, comparing proximal tibia STB microarchitecture among gait subgroups may provide insights into the loading history of the corresponding joints.

The aims of this study, in end-stage knee OA patients undergoing TKA, were (1) to identify patient subgroups with distinct walking gait patterns; and (2) to examine whether in vivo knee joint loading indices and STB microarchitecture of their excised tibial plateau differ among these gait subgroups. We hypothesised that those knee OA gait subgroups exhibiting higher KAM measures and greater varus knee alignment will also exhibit higher medial-to-lateral STB volume fraction (BV/TV) ratios.

6.2 Methods

6.2.1 Participants, gait analysis, clinical and radiographic data, and micro-CT and morphometric analysis

The analysis conducted in this study (Study 3) is a continuation upon the research conducted in Study 2 (Chapter 5). Methods for patient recruitment, gait analysis, collection of clinical and radiographic patient data, micro-CT imaging and morphometric analysis of the excised tibial plateaus are described in detail in **Chapter 5, Sections 5.2.1 to 5.2.4.**

The same cohort of 25 end-stage knee OA patients recruited for Study 2 were used in the present study (age 68 $\pm$ 7 years, BMI 32.9 $\pm$ 4.4 kg/m^2), with patient characteristics and gait parameters for all patients reported in Table 5.1. The examined patient cohort included a subset of 20 patients whom were part of Study 1 (See Appendix A for further patient recruitment and study allocation details).

Knee loading indices of interest include the peak knee moments and joint reaction force (JRF), from 3D gait analysis, and measures of static alignment, from full-length anterior-posterior pre-operative radiographs (Table 5.1). The knee moments included the peak knee flexion (KFM), peak knee extension during terminal stance (KEM), peak knee adduction (KAM, first (KAM_1) and second (KAM_2) peaks), internal (IRM) and external rotation (ERM) moments (Zabala et al., 2013) and the KAM impulse, representing the area under the adduction moment curve. Measures of static alignment included the mechanical axis deviation (MAD) and medial proximal tibia angle (MPTA).

The following morphometric parameters were calculated for each of four volumes of interest within the condyles of each tibial plateau specimen (Fig. 6.1): bone volume fraction (BV/TV, %), structure model index (SMI, unitless), trabecular thickness (Tb.Th, μm), trabecular separation (Tb.Sp, μm) and trabecular number (Tb.N, 1/mm). Details for explanation of these morphometric parameters are given in **Chapters 2, 4 and 5**.

6.2.2 Cluster Analysis

Principal component analysis (PCA) followed by k-means cluster analysis was performed (Kulmala et al., 2013), to stratify the knee OA subjects into relatively homogeneous subgroups, based on their walking gait knee kinetic parameters. The parameters selected as input for PCA included the full 3D knee moments: KFM, KEM, peak KAM (KAM_1 or KAM_2), ERM and IRM. Prior to PCA, all variables were uniformly normalized into the range [0, 1]. The first three

principal components that described more than 85% of the data variance were then taken as input for cluster analysis. K-means cluster analysis was performed for sorting participants into between two and four subgroups. To determine the appropriate number of clusters for further analysis, silhouette plots and mean silhouette values were evaluated (Rousseeuw, 1987). Subgroup classifications were defined by examination of the sagittal or transverse knee joint moment profiles in each subgroup. All PCA and cluster analyses were performed in MATLAB (2014b, Mathworks, Inc., Natick, MA, USA).

6.2.3 Statistical Analysis

Differences among the gait subgroups in subject characteristics, gait parameters and STB microarchitecture were tested with non-parametric Kruskal-Wallis tests, followed by a Bonferroni corrected Mann-Whitney U-test when significant. The significance level was set to $p < 0.05$. All statistical analysis were performed using SPSS Statistics 22 (IBM Corp., Armonk, NY, USA).

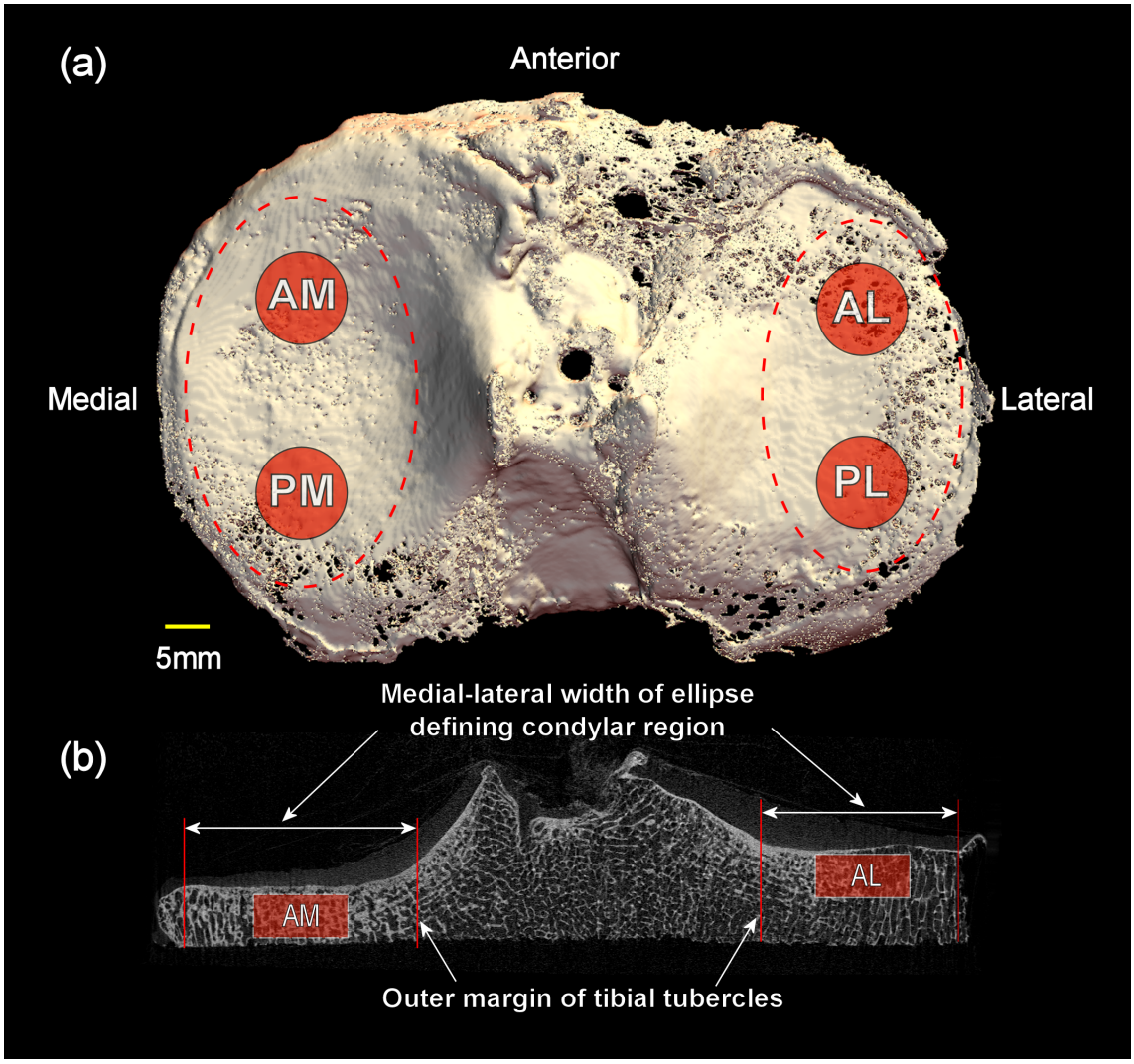

Figure 6.1: (a) 3D micro-CT image of an excised tibial plateau from a right knee (view from top). The ellipses defining the medial and lateral tibial condyles are shown (dashed lines), containing the location of the four subvolumes of interest (VOIs, two per condyle as indicated by red circles) in the anterior-medial (AM), anterior-lateral (AL), posterior-medial (PM) and posterior-lateral (PL) compartments; (b) 2D coronal micro-CT cross-section image of the tibial plateau with medial and lateral boundaries of the ellipses indicated by red lines. The location of the AM and AL VOIs, relevant to the subchondral trabecular bone, are indicated.

6.3 Results

K-means cluster analysis was completed for values of $k = [2, 3, 4]$. Mean silhouette values were 0.566, 0.561 and 0.565 for respective values of k. A model with three clusters was selected, as all silhouette values were positive and group sizes remained suitable for further analysis (n $>$ 6). Patients were clustered into a biphasic (7 patients), a flexor-dominant (9 patients) or

a counter-rotation gait pattern subgroup (9 patients) (Fig. 6.2). The patient characteristics for the subgroups are summarized in Table 6.1. The biphasic gait pattern exhibited large excursions of the sagittal plane knee moment curve, starting from extension into flexion and then returning to extension in terminal stance. In the flexor gait pattern, the moment curve traverses from extension during the loading response, into flexion, where it remains for the duration of stance. Biphasic and flexor gait patterns were consistent with definitions described previously (Kulmala et al., 2013; Smith et al., 2004). Counter-rotators, meanwhile, exhibited a biphasic flexor-extensor knee moment curve with a lower peak flexion moment, compared with the biphasic pattern. In addition, the transverse knee moment curve of counter-rotators remained in external rotation throughout stance. The overall load at the knee was lower for the counter-rotators relative to the other classifications.

6.3.1 Comparison in loading indices among gait subgroups

No statistically significant differences in patient characteristics (e.g. age, height, BMI) or in WOMAC data were found among subgroups (Table 6.1). Patients with valgus joint alignment (MAD $<$ 0 mm) were exclusively identified as counter-rotators (7 of 9 patients in that subgroup), while patients with varus alignment (MAD $>$ 15 mm (Paley, 2002; Roberts et al., 2016)) were predominantly in the biphasic and flexor subgroups. Loading indices differed significantly among subgroups ($p < 0.05$, Table 6.2). The KAM_1, KAM_2, KAM impulse and IRM were significantly higher in biphasic than in flexor and counter-rotator patients (KAM_1 = -0.65, -0.40 and -0.21 Nm/kg; KAM impulse = 43.8, 25.6 and 15.2 Nm.s/kg, respectively; Fig. 6.3). Flexor patients also exhibited higher KAM_1, KAM impulse and IRM than counter-rotators. Biphasic and flexor subgroups exhibited significantly lower ERM and higher MAD (indicating greater varus alignment) compared with counter-rotators (MAD = 40.8, 21.4 and -21.4 mm, respectively; Fig. 6.3). MAD also tended to be higher in biphasic compared with the flexor subgroup ($p = 0.16$). Knee excursion during the loading response was significantly lower in counter-rotators than in biphasics (Fig. 6.4). Flexors also exhibited lower knee excursion, though not significantly so, compared with biphasics ($p = 0.15$). No significant differences in peak KFM or KEM were detected among the gait subgroups, despite the unique sagittal plane moment curves that were identified. Also, no significant differences in JRF were detected, though there was a trend for higher forces in the biphasic subgroup compared with the counter-rotators ($p = 0.07$).

6.3.2 Comparison in morphometric parameters among gait subgroups

The STB microarchitectural parameters differed significantly among gait subgroups (Table 6.3). Whereas biphasic and flexor subgroups had significantly (up to +48%) higher medial (AM and M) BV/TV compared with counter-rotators, counter-rotators had (up to +29%) higher lateral (AL and PL) BV/TV than the biphasic subgroup and a similar trend compared to the flexor subgroup (Fig. 6.5). Similarly, differences in regional measures of SMI were also found among subgroups (Table 6.3), with the biphasic and flexor group, medially, showing smaller SMI values (more plate-like structure) and a trend towards higher Tb.Th (thicker trabeculae) compared to the counter-rotators; laterally, it was the counter-rotator having smaller SMI values and a higher Tb.Th.

Biphasic and flexor subgroups also had significantly greater medial-to-lateral BV/TV ratios (M:L, AM:AL, AM:PL and PM:AL, range 1.88-2.51) compared with counter-rotators, which had ratios closer to unity (range 0.95–1.27, Table 6.3, Fig. 6.5). PM:PL BV/TV ratio was significantly higher (more than double) in biphasic subjects with a similar trend in flexor, compared with counter-rotators. No significant differences were detected for A:P BV/TV ratios among subgroups. Interestingly, between biphasic and flexor subgroups, no significant differences were detected, neither in STB microarchitecture nor in BV/TV ratios.

Table 6.1: Summary of patient characteristics and WOMAC data for the gait subgroups in knee osteoarthritis (OA)

	OA gait subgroups		
Parameters	Biphasic (n = 7)	Flexor (n = 9)	Counter-Rot. (n = 9)
Patient characteristics			
Age (years)	67.7 ± 6.9	66.0 ± 9.5	69.3 ± 5.2
Height (m)	1.70 ± 0.08	1.64 ± 0.11	1.65 ± 0.07
Body mass (kg)	98.8 ± 12.5	87.8 ± 22.5	90.1 ± 16.9
BMI (kg/m^2)	34.1 ± 3.9	32.0 ± 4.1	33.1 ± 5.4
Male:Female	5:2	4:5	2:7
Varus:Neutral:Valgus$^+$	5:1:0	5:2:0	1:1:7
Kellgren-Lawrence (II:III:IV)	0:0:7	2:5:2	2:3:4
WOMAC			
Pain	11.6 ± 3.4	11.6 ± 1.8	11.5 ± 2.2
Stiffness	5.4 ± 0.9	5.6 ± 0.9	6.0 ± 1.0
Function	39.4 ± 14.6	34.8 ± 11.9	44.0 ± 11.8
Total	56.4 ± 18.5	52.0 ± 11.0	61.5 ± 13.2

Data presented as average $\pm$ standard deviation. BMI: body mass index; $^+$Mechanical alignment data was available for only 22 of 25 knee OA subjects, its subdivision was performed according to the mechanical axis deviation (MAD, see Table 2), into varus (MAD $>$ 15 mm), neutral (0 – 15 mm), valgus ($<$ 0 mm) alignment.

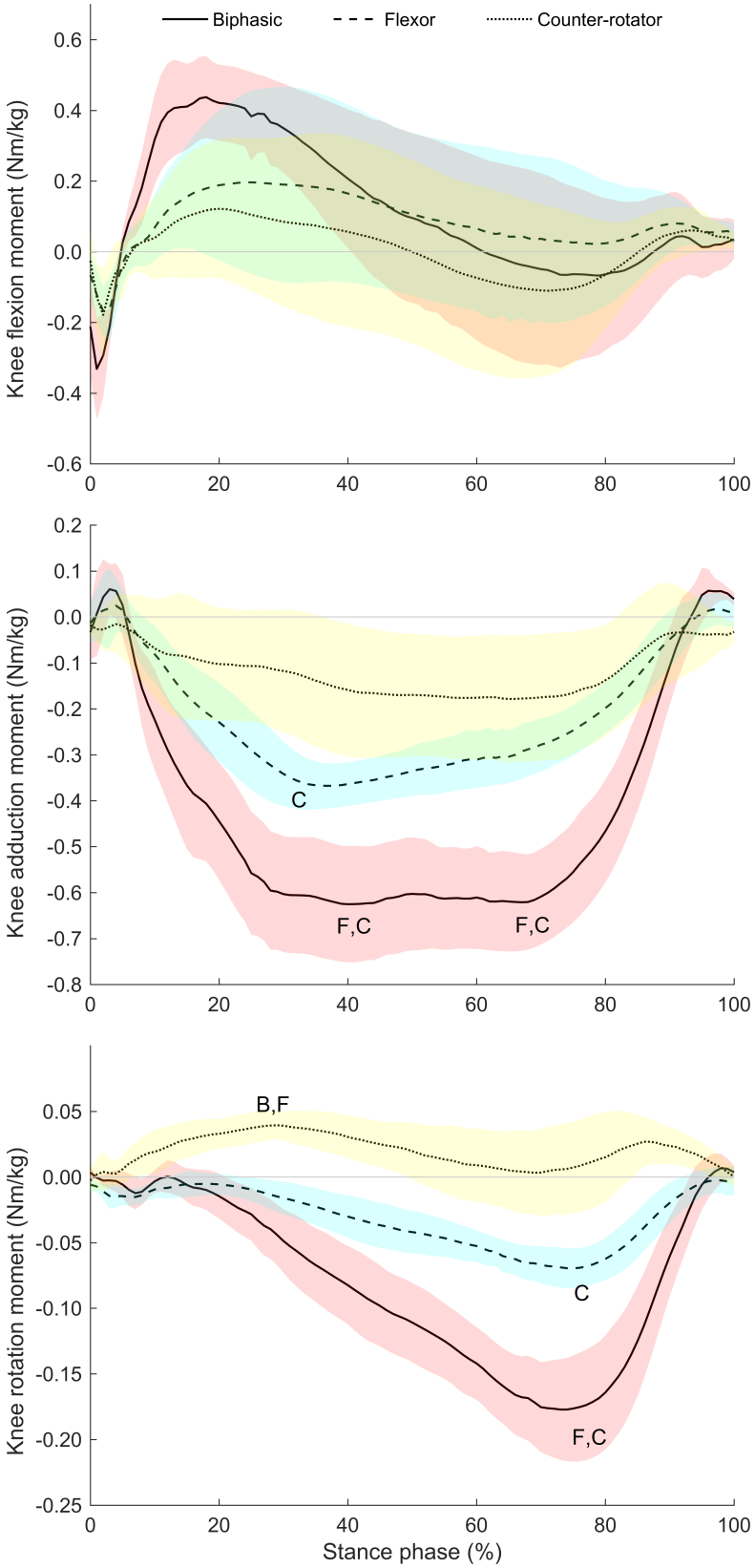

Figure 6.2: Average 3D knee moment curves and standard deviation (shaded area, pink: biphasic, blue: flexor, yellow: counter-rotators) for each gait subgroup in knee osteoarthritis (OA). Statistically significant differences in peak knee moments among subgroups are indicated ($p < 0.05$): B – compared with biphasic, F – compared with flexors, C – compared with counter rotators.

Table 6.2: Summary of kinematic and joint loading parameters for the gait subgroups in knee osteoarthritis (OA)

	OA gait subgroups		
Parameters	Biphasic (n = 7)	Flexor (n = 9)	Counter-Rot. (n = 9)
Knee excursion, LR (°)	9.55 ± 2.67^{C}	6.74 ± 3.93	4.15 ± 2.02
Knee moments (Nm/kg)			
Knee flexion moment, KFM	0.50 ± 0.16	0.29 ± 0.30	0.18 ± 0.30
Knee extension moment, KEM	-0.16 ± 0.29	-0.03 ± 0.28	-0.16 ± 0.31
Knee adduction moment 1st peak, KAM_1	$-0.65 \pm 0.17^{F,C}$	-0.40 ± 0.08^{C}	-0.21 ± 0.19
Knee adduction moment 2nd peak, KAM_2	$-0.67 \pm 0.13^{F,C}$	-0.34 ± 0.08	-0.24 ± 0.17
External rotation moment, ERM	0.012 ± 0.005^{C}	0.002 ± 0.008^{C}	0.049 ± 0.012
Internal rotation moment, IRM	$-0.188 \pm 0.053^{F,C}$	-0.076 ± 0.019^{C}	-0.015 ± 0.036
KAM impulse (Nm.s/kg)	$43.8 \pm 11.9^{F,C}$	25.6 ± 8.0^{C}	15.2 ± 5.9
Joint Reaction Force, JRF (BW)	3.62 ± 1.06	3.03 ± 0.83	2.55 ± 0.83
Static alignment			
Mechanical axis deviation, MAD (mm)	40.8 ± 18.9^{C}	21.4 ± 11.1^{C}	-21.4 ± 30.5
Medial proximal tibial angle, MPTA (°)	91.7 ± 2.7	90.0 ± 1.6	89.1 ± 3.1

Data presented as average $\pm$ standard deviation. Superscript letters indicate statistically significant difference ($p < 0.05$, Bonferroni-corrected Mann-Whitney U-test) between subgroups (e.g., comparing biphasics with flexors): F – compared with flexors, C – compared with counter-rotators.

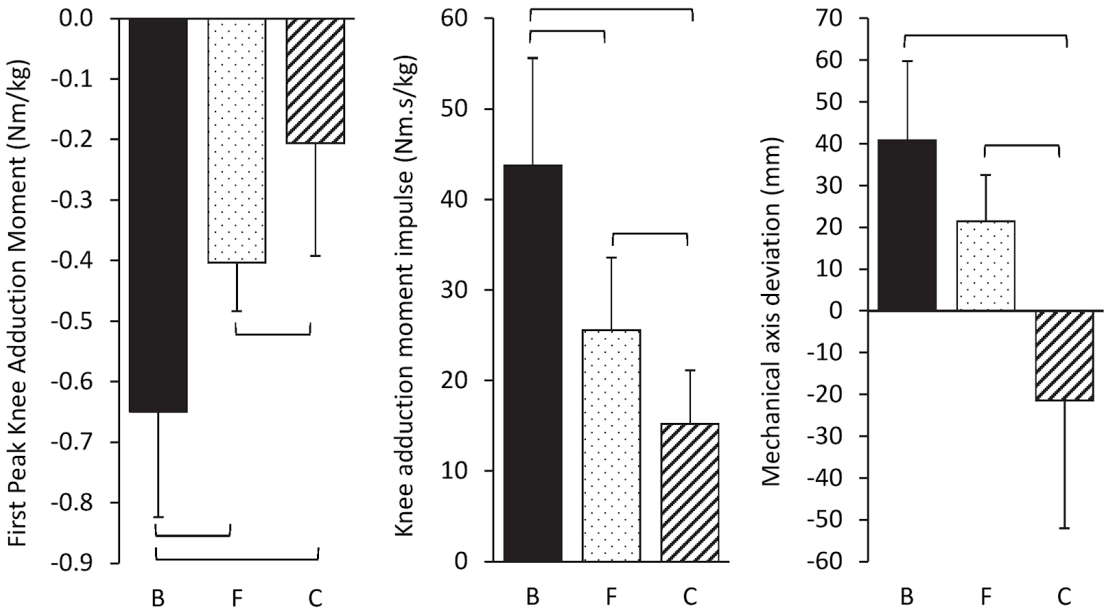

Figure 6.3: Bar graphs reporting average values and standard deviations (error bars) of loading indices for each gait subgroup in OA: (left) first peak knee adduction moment, (centre) knee adduction moment impulse and (right) mechanical axis deviation. Significant differences ($p < 0.05$, Bonferroni-corrected Mann-Whitney U-test) between groups are indicated by brackets. B, biphasic; F, flexor; and C, counter-rotator knee OA subgroup.

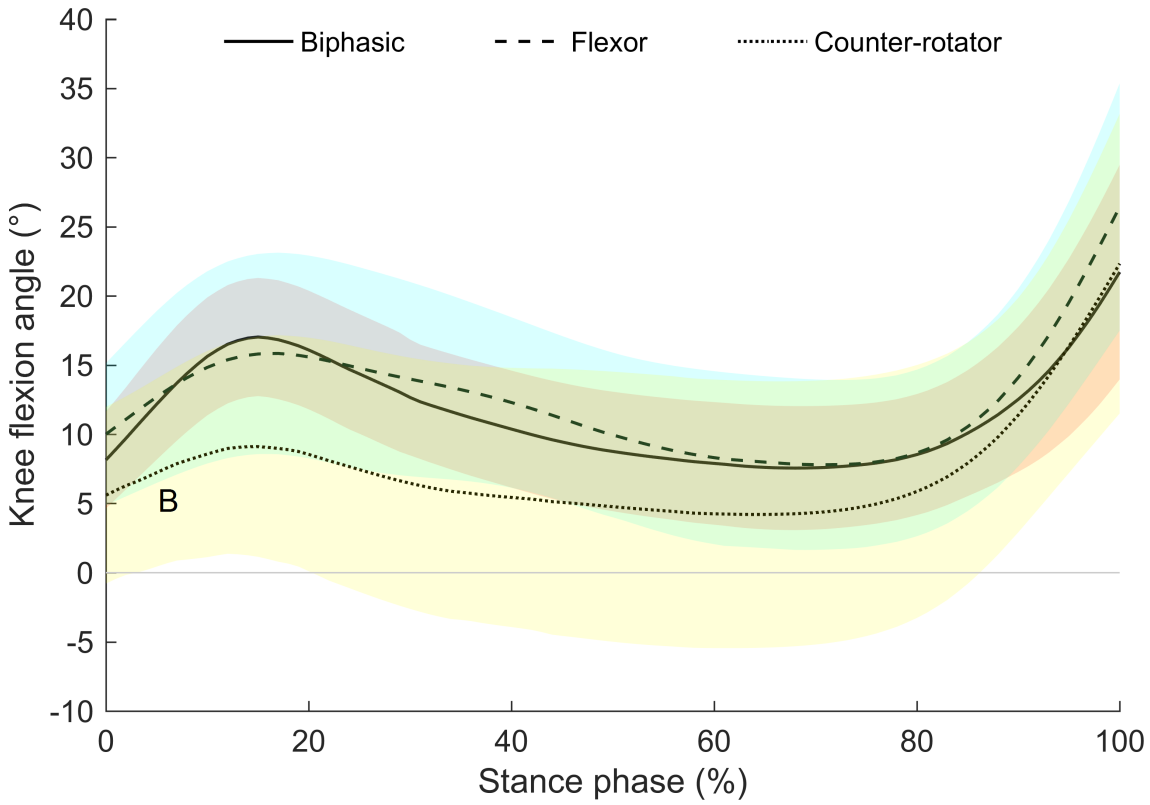

Figure 6.4: Average knee flexion angle curves and standard deviation (shaded area, pink: biphasic, blue: flexor, yellow: counter-rotators) for each gait subgroups in knee osteoarthritis (OA). Statistically significant differences ($p < 0.05$, Bonferroni-corrected Mann-Whitney U-test) in knee excursion (loading response) among subgroups are indicated: B – compared with biphasic

Table 6.3: Summary of subchondral trabecular bone microarchitectural parameters (average ± SD) for the gait subgroups in knee osteoarthritis (OA)

Parameters		OA gait subgroups		
		Biphasic (n = 7)	Flexor (n = 9)	Counter-Rot. (n = 9)
BV/TV (%)	AM	43.6 ± 7.1^{C}	46.8 ± 10.0^{C}	31.6 ± 6.3
	AL	18.2 ± 4.2^{C}	20.7 ± 8.1	29.5 ± 12.7
	PM	34.6 ± 10.0	40.2 ± 18.5	23.8 ± 7.0
	PL	19.6 ± 6.6^{C}	26.5 ± 9.5	33.5 ± 10.8
	M	39.1 ± 6.0^{C}	43.5 ± 13.6^{C}	28.0 ± 5.8
	L	18.9 ± 5.3	23.6 ± 8.5	30.7 ± 10.8
SMI	AM	0.33 ± 0.71	-0.07 ± 0.82^{C}	1.14 ± 0.57
	AL	1.92 ± 0.30^{C}	1.63 ± 0.52	1.13 ± 0.94
	PM	1.00 ± 0.71	0.33 ± 1.44^{C}	1.66 ± 0.33
	PL	1.83 ± 0.36	1.38 ± 0.62	1.11 ± 0.73
Tb.Th (μm)	AM	211 ± 34	223 ± 34	187 ± 301
	AL	150 ± 30	157 ± 30	180 ± 623
	PM	215 ± 65	221 ± 65	176 ± 239
	PL	157 ± 32^{C}	172 ± 32	198 ± 382
Tb.N (1/mm)	AM	2.08 ± 0.35	2.12 ± 0.40	1.69 ± 0.30
	AL	1.21 ± 0.23	1.30 ± 0.35	1.62 ± 0.62
	PM	1.61 ± 0.27	1.75 ± 0.44	1.33 ± 0.24
	PL	1.24 ± 0.31	1.52 ± 0.32	1.67 ± 0.38
Tb.Sp (μm)	AM	324 ± 70	333 ± 95	411 ± 57
	AL	492 ± 68	512 ± 106	440 ± 131
	PM	411 ± 63	395 ± 111	441 ± 132
	PL	498 ± 92	441 ± 98	405 ± 95
BV/TV ratio among subregions	M:L	2.15 ± 0.39^{C}	1.92 ± 0.52^{C}	1.04 ± 0.44
	AM:AL	2.46 ± 0.51^{C}	2.51 ± 1.00^{C}	1.27 ± 0.58
	AM:PL	2.37 ± 0.63^{C}	1.88 ± 0.55^{C}	1.08 ± 0.50
	PM:AL	1.92 ± 0.47^{C}	2.01 ± 0.74^{C}	0.95 ± 0.50
	PM:PL	1.86 ± 0.57^{C}	1.51 ± 0.43	0.91 ± 0.50
	AM:PM	1.37 ± 0.96	1.34 ± 0.53	1.40 ± 0.40
	AL:PL	0.96 ± 0.11	0.78 ± 0.15	0.95 ± 0.36

Data presented as average ± standard deviation. Superscript letters indicate significant difference ($p < 0.05$, Bonferroni-corrected Mann-Whitney U-test) between subgroups: F – compared with flexors, C – compared with counter-rotators. Subchondral trabecular bone parameters: BV/TV, bone volume fraction; SMI, structure model index; Tb.Th, trabecular thickness; Tb.N, trabecular number; Tb.Sp, trabecular separation.

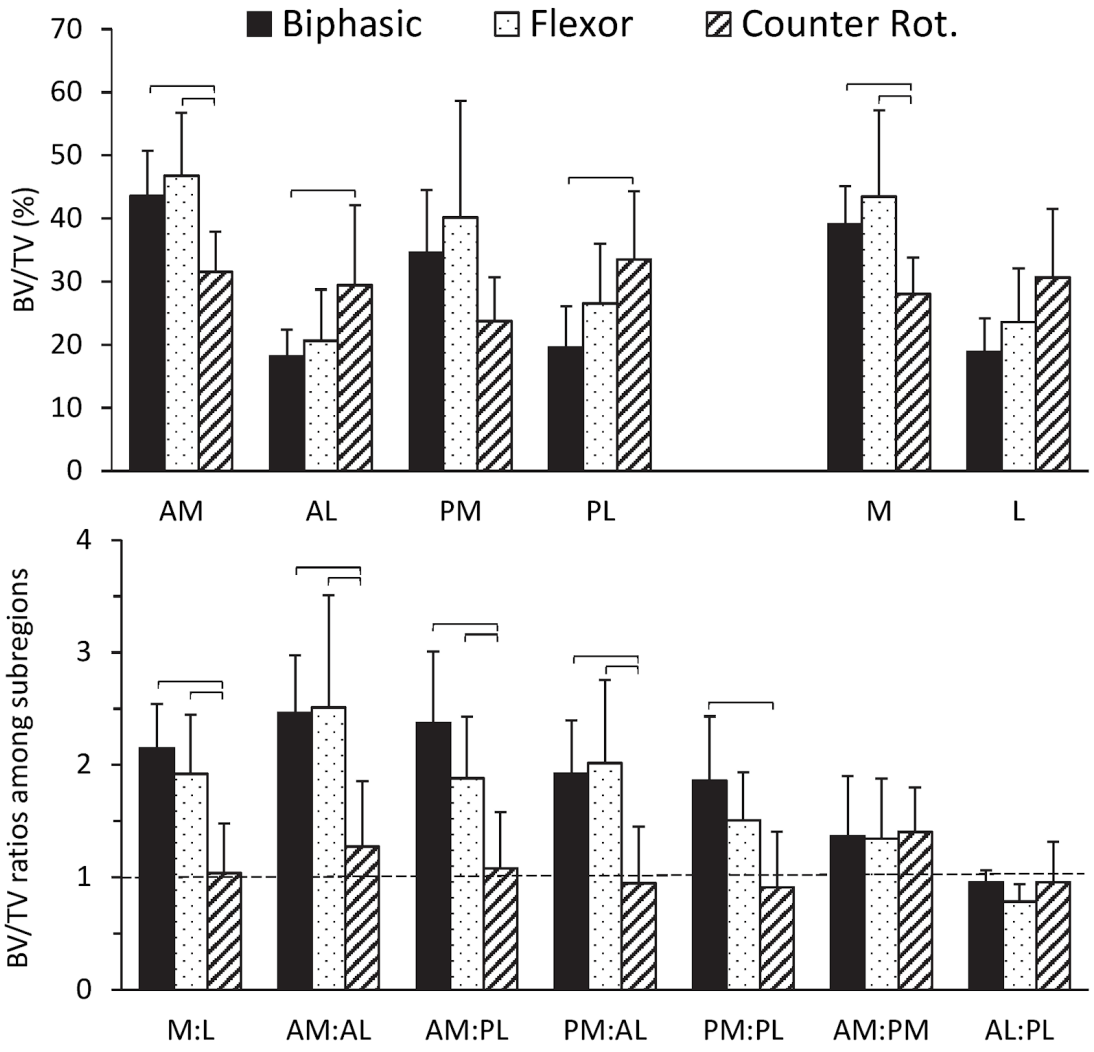

Figure 6.5: Bar graphs reporting average values and standard deviations (error bars) of (top) subregional bone volume fraction (BV/TV) and (bottom) BV/TV ratios among subregions for the gait subgroups in knee osteoarthritis. Statistically significant differences between gait subgroups are indicated by brackets ($p < 0.05$, Bonferroni-corrected Mann-Whitney U-test). The horizontal dashed line indicates unity in the BV/TV ratios among subregions.

6.4 Discussion

This study identified three distinct walking patterns in knee OA patients, characterised by either a biphasic, or a flexor-dominant sagittal plane moment curve, or an external rotation-dominant transverse plane moment curve (counter-rotator subgroup). Differences in knee excursion, knee moments and joint alignment were detected among these subgroups, as well as in STB microarchitecture. To the best of our knowledge, this is the first study to compare

loading indices and tibial subchondral trabecular bone microarchitecture among subgroups categorized by different walking gait patterns in knee OA.

6.4.1 Comparison in loading indices among gait subgroups

Biphasic and flexor-dominant gait patterns have previously been documented in both healthy and pathological subjects, including pre-operative TKA patients (Andriacchi et al., 1982; Chassin et al., 1996; Kulmala et al., 2013; Levinger et al., 2012; Simon et al., 1983; Simonsen & Alkjær, 2012; Smith et al., 2004; Winter, 1984). In this study, the biphasic OA subgroup exhibited significantly higher peak KAM_1, KAM_2 and IRM, compared with flexors. These findings differ from observations in the published literature, where a relatively young male cohort (40 $\pm$ 11 years) without evidence of musculoskeletal disease, showed higher moments in a flexor-dominant rather than in a biphasic subgroup (Kulmala et al., 2013). This discrepancy to that study may, in part, be attributed to gender- and age-related differences and/or pathological adaptations in the present knee OA cohort, including variations in joint structure, deficits in neuromuscular control and disease related symptoms (i.e. joint pain), that influence gait mechanics (Hall et al., 2017; Phinyomark et al., 2016; Wilson et al., 2011). Furthermore, our results in OA revealed a higher KAM_1, IRM, and lower ERM in both biphasic and flexor-dominant subgroups, compared with counter-rotators. For static alignment, MAD was significantly higher in both biphasics and flexors compared with counter-rotators, with a trend to be higher also in biphasics than in flexors; hence, OA patients with a biphasic gait pattern were more varus-aligned compared to flexors and counter-rotators. As KAM indices and static alignment are associated with the medial-to-lateral distribution of force across the tibial plateau (Kutzner et al., 2013; Schipplein & Andriacchi, 1991), the differences in these measures among OA subgroups suggest that 1) the biphasic patients exhibit higher M:L distribution of joint loads across the tibia compared with flexors and counter-rotators; and 2) the M:L load ratio is higher in flexors compared with counter-rotators during walking.

6.4.2 Comparison in morphometric parameters among gait subgroups

Micro-CT data revealed higher M:L BV/TV ratios and medially lower SMI values (more plate-like structure) in both biphasic and flexor OA patients, compared with counter-rotators. Bone adapts its structure to mechanical loads to which it is exposed to during daily life (Turner, 1998); hence, the higher M:L BV/TV ratios in biphasic and flexor-dominant OA subgroups could reflect a microarchitectural adaptation of the STB to increased M:L load ratio within these tibiae as indicated by higher moments or greater varus alignment (greater MAD values) compared to counter-rotators, supporting our hypothesis. Interestingly, STB microarchitecture

and M:L BV/TV ratios did not statistically differ between the flexor and biphasic subgroups, despite flexors exhibiting significantly lower KAM_1, KAM_2, KAM impulse and a trend for lower MAD, this finding being inconsistent with our hypothesis. The peak adduction moments and KAM impulse have previously been associated with the M:L distribution of proximal tibial bone mineral density (BMD) in a medial knee OA cohort (Thorp et al., 2006b; Wada et al., 2001). In the present end-stage knee OA cohort, however, relationships between KAM indices and M:L BV/TV ratio were weak and non-significant when examining only neutral-varus aligned patients (from whom biphasics and flexors were comprised) (see Study 2 ((Chapter 5, Section 5.3.3)). Thus, although this study was cross-sectional, and hence it is impossible to conclude direct cause-effect relationships, these findings potentially suggest that despite differences in KAM indices between biphasic and flexor subgroups there may be different mechanisms for generating comparable (non-differing) loads, as indicated by comparable M:L BV/TV ratios as a bony response.

Childs et al. (2004) postulate that knee joint stiffening could result in increased compressive forces upon more localized areas within the articulating surfaces of the tibial plateau. In the present study, although not statistically significant, a lower knee excursion during loading response was found in the flexor compared with the biphasic subgroup, which could be indicative of increased joint stiffness during this period of weight acceptance (Childs et al., 2004). The non-differing measures of subregional STB microarchitecture and BV/TV ratios among subregions observed between the flexors and biphasics could thus reflect a bony response to high stresses upon the tibial condyles that may be present in flexors – and – be comparable with those in biphasics, despite lower adduction moment (KAM) indices in flexors. However, we do not exclude that as the examined bones are from end-stage knee OA patients, other factors in addition to loading, including age, genetics, or the local biochemical environment in the presence of bone sclerosis, that effect subchondral bone metabolism, may in part explain observed variations in the STB microarchitecture among these subgroups (Li et al., 2013). Nevertheless, these results may suggest that in OA patients with a flexor gait pattern, conservative treatments (e.g. lateral wedge insoles, knee braces), designed to reduce knee adduction moment indices with the aim to delaying progression of OA, may not be appropriate. Moreover, whether a flexor-dominant gait pattern increases susceptibility to development and progression of OA, even in presence of lower peak adduction moments however, needs to be further explored.

There were several limitations to this study. Due to the cross-sectional study design, we cannot determine whether specific gait patterns increase an individual's susceptibility for development of knee OA. Future prospective cohort studies could consider stratification of OA patients according to gait mechanics to help elucidate these relationships. It is also unclear whether the present gait patterns exhibited by each individual are persistent over the lifespan, or are present within an age-matched population without OA. Future work in our laboratory will

apply these methods within a non-pathological cohort to address this question. Furthermore, the relatively small sample size limited the number of clusters that could be identified whilst remaining useful for subsequent analysis. To account for the small sample size, we used non-parametric statistics for comparisons among the subgroups. We do not exclude that additional walking gait phenotypes could be revealed with an increased sample size. Finally, micro-CT analysis is currently limited to *ex vivo* examination of the human tibial plateau; thus, only cadaveric tissue from donors with or without joint pathology, or specimens from OA patients who underwent TKA, as presented herein, may be examined. Recent high-resolution peripheral quantitative CT (HR-pQCT) imaging systems, permitting *in vivo* examination of proximal tibial STB microarchitecture with a 61 μm voxel size (Kroker et al., 2016), may in future be employed by adapting the here described method to examine the above relationships, in early OA and non-pathological joints. A strength of this study is the combination of micro-CT and gait analysis, on the same patient. This permitted examination of the subchondral trabecular bone microarchitecture in specific subregions of the proximal tibial plateau where changes are most evident in OA, combining them with *in vivo* measures of joint loading, thus providing insights into the loading history of the joint of the same patient. Moreover, as the micro-CT examination was performed on entire tibial plateaus without coring them, these are preserved intact for further examination (Chapter 4 and Roberts et al. (2016)).

In conclusion, three distinct walking gait patterns were revealed in knee OA patients undergoing TKA. Loading indices and subchondral bone microarchitecture differed among the gait subgroups. Compared with flexors and counter-rotators, patients with a biphasic pattern were more varus aligned and exhibited higher knee adduction moment indices (peak KAM, KAM impulse), suggesting a higher medial-to-lateral distribution of tibiofemoral joint loads during gait. Despite these higher indices of KAM, however, subregional BV/TV and M:L BV/TV ratios did not differ between the biphasic and flexor subgroup. Taken together, this could suggest that there are different mechanisms between these subgroups for generating comparable loads upon the tibial plateau and the corresponding bony response. As stratification of the knee OA population into more homogeneous subgroups may enable to identify individuals likely to benefit from specific treatments, our results could also suggest that in patients with a flexor gait pattern, conservative treatments (e.g. lateral wedge insoles, knee braces), designed to reduce adduction moment indices, may not be appropriate. Further study is warranted for testing this hypothesis. Understanding how joint loads vary among walking gait patterns and are related to variations in subchondral trabecular bone microarchitecture may be useful for identifying and improving the management of persons at risk for development of knee OA.

Chapter 7

Conclusions and Future Recommendations

The overall aims of the research conducted in this thesis were to describe, in end-stage knee OA patients who underwent total knee arthroplasty: (1) regional variations in subchondral bone microarchitecture; and (2) to explore associations between bone microarchitecture and joint loading parameters during walking gait.

More specifically, the aims were:

1. In the condyles of entire tibial plateaus retrieved from end-stage knee OA patients with varying joint alignment (varus or non-varus subgroups) (a) to characterise the spatial distribution of subchondral bone plate thickness, plate porosity and underlying subchondral trabecular bone microarchitecture, and (b) map region specific associations among these 3D microarchitectural parameters between these two compartments

2. To study, on end-stage knee OA patients undergoing total knee arthroplasty, the relationships between *in vivo* dynamic knee joint loads measured preoperatively using 3D gait analysis, static alignment and the proximal tibial subchondral trabecular bone microarchitecture of their excised knees quantified with 3D micro-CT

3. (a) To identify subgroups with distinct walking gait patterns in end-stage knee osteoarthritis (OA) patients; (b) to compare measures of joint loading and proximal tibia subchondral trabecular bone microarchitecture among them

7.1 Principal Findings

7.1.1 Regional heterogeneity of proximal tibia subchondral bone microarchitecture differs with variations in static knee joint alignment

In proximal tibia from 25 end-stage knee OA patients, significant differences in SBP and STB microarchitecture, within and between medial and lateral tibial condyles, were found, with changes dependent on joint alignment. In varus-aligned knees, STB bone volume fraction (BV/TV) was consistently high throughout the medial condyle, whereas in the non-varus aligned knees, medially, BV/TV was more heterogeneously distributed, highest in the anterior region of the condyle. Regions of high SBP thickness were co-located with regions of high STB BV/TV underneath. In varus-aligned knees, BV/TV was significantly higher medially than laterally, whereas in non-varus the medial-to-lateral (M:L) differences in BV/TV were smaller and in the posterior regions of the condyles favoured higher BV/TV laterally. These findings confirm, in 3D, previous findings for STB from 2D histological analysis (Bobinac et al., 2003; Matsui et al., 1997). Moreover, region-specific significant associations between SBP thickness, SBP porosity and the underlying STB microarchitecture were detected, which in general were not captured when considering the values averaged for each condyle. Overall, these results suggest that, in the OA knee, joint alignment influences not only the M:L distribution, but also the within condyle distribution of force across the tibia plateau, generating a corresponding bony response (adaptation) of both the subchondral bone plate and trabecular bone microarchitecture.

7.1.2 Knee joint loading is associated with proximal tibia subchondral trabecular bone microarchitecture

Relationships between knee loading indices measured *in vivo* and STB microarchitecture were examined, for the first time, in the same 25 end-stage knee OA patients. In all OA patients, whom had knee alignment ranging from varus to valgus, a strong relationship between the external rotation moment (ERM) and anterior-medial condyle (AM) STB microarchitecture was detected particularly with BV/TV, and this relationship remained when controlling for potentially confounding variables that influence medial condyle joint forces (walking speed, the mechanical axis deviation (MAD) and first peak knee adduction moment (KAM_1)). For neutral-varus, although non-significant, ERM remained the loading parameter with highest r-value for associations with AM BV/TV. Furthermore, in all OA patients, the M:L BV/TV ratios were most strongly associated with the ERM ($r = -0.74$) and static alignment (MAD) ($r = 0.74$), followed by KAM indices, including KAM impulse ($|r|$ range: 0.54 to 0.60). Notably,

relationships between M:L BV/TV ratios and MAD, as well as with KAM indices, were weak and not significant when examining patients with neutral-to-varus aligned joints, while in valgus OA these associations were of moderate strength, albeit non-significant statistically; this suggests that these associations, present in the entire OA cohort as a whole, were driven by large variations in static alignment, from varus to valgus. The findings for neutral-varus OA are in disagreement with significant relationships reported for mechanical alignment, KAM and M:L BMD ratios from DXA, observed in patients with medial knee OA (Thorp et al., 2006b; Wada et al., 2001). However, these relationships, reported in the scientific literature, were in patients presenting with mild to severe radiographic OA, whereas patients evaluated herein were all end-stage OA. Moreover, this thesis for the first time, examines and reports significant relationships between STB microarchitecture and peak rotation moments in the same OA patients, revealing significant associations with the ERM and subregional BV/TV and BV/TV subregional ratios. Overall, within the confines of the examined sample size (25 patients) these results suggest that the ERM may be useful as a surrogate measure of peak tibial stresses that occur in the anterior-medial compartment during early to midstance, or of the medial-to-lateral distribution of knee joint loads, as indicated by the AM BV/TV or M:L BV/TV ratio, taken as an indicator of bony response.

7.1.3 Knee joint loading and subchondral trabecular bone microarchitecture varies among end-stage knee OA patients with different walking gait patterns

Three subgroups with distinct walking gait patterns were identified in end-stage knee OA patients; biphasic, flexor and counter-rotator gait patterns. These results confirmed presence of biphasic and flexor dominant gait patterns previously reported in end-stage knee OA patients (Levinger et al., 2012; Smith et al., 2004). In this study, patients in the biphasic subgroup exhibited significantly higher KAM parameters and trend towards higher MAD (indicating greater varus alignment) than the flexor and counter-rotator subgroups, suggesting a higher M:L tibiofemoral load ratio in biphasics. These differences in knee moments between biphasics and flexors were inconsistent with findings previously reported in young males whom were free of musculoskeletal disease (Kulmala et al., 2013), which likely could be attributed to age-related, gender-related and pathological differences in the OA cohort, that affect gait mechanics. Interestingly in the present OA study, despite differences in joint loading indices, the subregional STB microarchitecture and BV/TV subregional ratios did not differ between biphasics and flexors. These findings suggesting that, between these subgroups, there may be different mechanisms for generating non-differing loads upon the tibial plateau, as indicated by comparable M:L BV/TV ratios as a bony response.

7.2 Significance to OA research

Structural adaptation of the subchondral bone occurs in response to the mechanical loads to which it is exposed during activities of daily living (Turner, 1998). Significant relationships between the peak KAM – a surrogate measure for peak loads during walking gait – and macroscopic variations in subchondral bone, have previously been observed in medial knee OA patients (Creaby et al., 2010; Thorp et al., 2006b; Wada et al., 2001). However, the research presented in this thesis is the first to explore in the same patient, relationships between joint loading and the subchondral trabecular bone microarchitecture as quantified using high-resolution 3D micro-CT.

Hitherto, only *in vivo* measures of the STB M:L BMD ratio measured by DXA and the tibial condylar subchondral bone articular surface area from MRI had been linked with knee loads from gait. These imaging techniques, however, are ill-suited for quantification of the important periarticular tibial STB microarchitecture *in vivo*. DXA, for example, is limited in spatial resolution and cannot differentiate between cortical and trabecular bone. MRI, although achieving a relatively high in-plane spatial resolution (130-190 μm), is restricted to large image slice thicknesses (greater than or equal to 500 μm), and although STB microarchitecture has been quantified from MR images, these studies were limited to examination of large regions of interest within the tibial plateau that often exclude the STB immediate to the articulating surfaces of the joint (Beuf et al., 2002; Bolbos et al., 2008).

From a basic science perspective, micro-CT image analysis of the entire excised (intact) tibial plateau is advantageous, as this permits examination of the STB microarchitecture in specific subregions where microarchitectural changes due to OA are most pronounced, albeit *ex vivo*. The findings in this thesis highlight a possible localized adaptation of the subchondral bone within the condyles of the tibial plateau as a response to joint loading (**Study 1** and **2**). Moreover, as highlighted in **Study 2**, loading indices were generally more strongly associated with subregional measures of STB microarchitecture within the tibial condyles, than for measures averaged among subregions. First, this reaffirms the importance of subchondral bone in knee OA; second, this may suggest that local variations in STB microarchitecture, as opposed to differences in average values among condylar subregions, are most sensitive to variations in joint loads during walking gait. In early OA, pathological changes in the subchondral bone may precede, in some disease phenotypes, clinically detectable alterations in all other joint tissues such as the articular cartilage (Goldring & Goldring, 2010). Moreover, STB changes can occur over a relatively short time in response to non-invasive treatments (between 6-12 weeks) (Callaghan et al., 2015). Hence, high-resolution quantitative *in vivo* imaging (and monitoring) of the tibial subchondral bone microarchitecture has the potential to (1) identify

persons at risk for disease development and progression; and (2) to evaluate the efficacy of load-modifying therapies, such as knee braces and shoe insoles.

The KAM and KAM impulse have previously been associated positively with M:L BMD and bone surface area ratios in medial knee OA. Results in **Study 2** of this thesis, however, could not confirm these relationships between KAM indices and the M:L BV/TV ratio in end-stage knee OA patients with neutral-to-varus aligned joints. Moreover, results in **Study 3** revealed that the M:L BV/TV ratio did not differ between OA patients with a biphasic or flexor gait pattern, despite differing KAM indices between these subgroups. Other studies using instrumented knee prosthesis suggest a moderate ability for KAM to predict load distribution across the tibial plateau. Together, this data may help in part to explain the unsatisfactory outcomes observed clinically in the prescription of load-modifying treatments that target KAM. Interestingly, results herein found that the ERM was a robust measure for predicting AM STB BV/TV and subregional ratios. These findings first, reinforce the importance of the local mechanical environment in knee OA, and second, suggest that rotational moments may play an important role in disease pathogenesis. Future work should thus evaluate the contribution of the full 3D knee moments, including the ERM, to the progression of the disease. Alternatively, machine-learning techniques, for example principal component analysis, may be useful for retaining the most salient parameters from gait waveform data, and thus, their use should be considered in future research.

7.3 Recommendations for future research

7.3.1 Characterising regional variations in the osteochondral unit in both osteoarthritic and non-pathological joints

Research in this thesis characterised the SBP and STB 3D microarchitecture in multiple subregions within the tibial condyles of OA knees. Subchondral bone is part of a functional structure, the osteochondral unit (OCU), which is important to the maintenance of joint health (see Chapter 2) (Mahjoub et al., 2012). The OCU is comprised of the overlaying articulating cartilage in addition to the subchondral bone; disruption of one structure has been shown to lead to abnormal remodelling of the other (Burr & Gallant, 2012).

Micro-CT is a well-established imaging modality for examination of bone microarchitecture. The capabilities of such systems to characterise soft tissue morphology, however, is less well known, though evidence is building for use of contrast-enhancement agents to evaluate the articular cartilage (Lin et al., 2015). Future work may thus consider adopting such techniques

for micro-CT imaging of the articular cartilage in the human tibial plateau. Studies may otherwise consider combining micro-CT with MR imaging, as applied previously to human humeral heads (Pawson et al., 2015), to evaluate regional variations in both compartments of the OCU. Moreover, use of *in vivo* MR imaging, combined with high-resolution *in vivo* CT imaging techniques, may permit a longitudinal evaluation of the OCU in subjects both with and without joint disease. As the image analysis techniques described in this thesis are non-destructive, they preserve the intact specimen for further examination, including mechanical testing or histological analysis. Finally, future work may also consider characterising variations in the OCU of the femoral condyles in addition to characterisation of the tibial plateau. A comprehensive investigation of both regional and temporal variations in all components of the OCU could be useful for better understanding the role of these structures in the development and progression of joint related pathologies, including knee OA.

7.3.2 Exploring a causal link between knee joint loading and knee osteoarthritis progression

The studies presented in this thesis were cross-sectional, exploring for relationships between knee joint loading and proximal tibia subchondral bone microarchitectural parameters in end-stage knee OA patients whom were scheduled for total knee arthroplasty. This limitation has important implications for this work. First, other factors, apart from loading, including age, genetics, or the local biochemical environment, that can affect subchondral bone metabolism, cannot be excluded for explaining variations in subchondral bone microarchitecture observed in this research. Second, it is unclear whether loading indices reported in this thesis are reflective of the knee loads that occur during earlier stages of the disease, and that may have influenced resultant bone microarchitecture observed at end-stages within these studies. Furthermore, whether similar subregional subchondral bone microarchitectural differences, and/or gait patterns, and relationships between subchondral bone and gait parameters, are present in a non-pathological cohort, is unclear. Finally, causal inferences between joint loading and subchondral bone microarchitecture could not be made. An increasing number of prospective cohort studies, combining 3D gait analysis with *in vivo* imaging modalities, have related baseline measures of joint loading with rate of structural knee OA progression over 12–72 month periods (Bennell et al., 2011; Chang et al., 2015; Chehab et al., 2014; Miyazaki et al., 2002). These studies, however, focused primarily on macroscopic changes in articular cartilage (e.g. cartilage thinning or cartilage volume loss), quantifiable using MRI *in vivo*. They consequently ignore changes that may occur in the important underlying subchondral bone.

Use of micro-CT as described in this thesis, currently remains impractical for *in vivo* applications on humans. This is due to the high radiation dose associated with high-resolution scanning

(Müller et al., 1996). High-resolution peripheral quantitative CT (HR-pQCT) systems that permit *in vivo* scanning of the human knee at voxel size as low as 61 μm, however, are becoming more readily available to both clinical and research institutions. Future research may adopt use of such imaging technologies, or may otherwise explore utility of DXA that is presently available clinically (and with aforementioned limitations, see Section 7.2), to elucidate any causal link between joint loading and the STB architectural changes observed in knee OA. Moreover, such techniques could be employed for examining differences in non-pathological subjects. Presently, work underway in our laboratory will apply micro-CT image analysis methods, described in this thesis, to non-pathological cadaveric tibiae to characterise the spatial distribution of subchondral bone microarchitecture in joints without OA. Furthermore, cluster analysis will be applied to gait data from age-matched non-pathological subjects, to elucidate whether the gait patterns described herein are related to the disease.

7.3.3 Elucidate the significance of the rotational moments to joint loading and structural variations in the knee joint

To date, much research has focused on the significance of the frontal and sagittal plane peak moments to describe loading at the knee joint. Meanwhile, the rotational moments are frequently overlooked, likely due to poor measurement reliability documented for these parameters (Robbins et al., 2013); thus their significance to joint loading remains poorly understood. However, in this thesis rotational moments, in particular the external rotation moment during early stance, were most strongly linked with subregional STB microarchitecture and STB BV/TV subregional ratios, warranting further exploration. In Study 2, it was hypothesised that the ERM could be closely related with tibiofemoral cartilage contact mechanics, with quadriceps and hamstrings muscle co-activity, and/or with anterior-medial tibiofemoral joint stresses during the load-bearing period of stance. To explore such hypotheses, future research could examine relationships between the transverse plane knee moments with (1) measures of cartilage contact from dual-plane fluoroscopic imaging; (2) electromyography derived measures of muscle co-contraction during the loading response phase of stance; or (3) compartmental joint reaction forces from instrumented knee prostheses. Furthermore, the ability for the ERM to predict structural progression of knee OA, as indicated by changes in bone or cartilage morphology, should be explored.

7.4 Concluding Statement

Findings from this thesis augment our understanding of the mechanics-structure relationship in knee OA, revealing, for the first time in the same end-stage knee OA patients, significant associations between subregional proximal tibia subchondral bone microarchitecture and dynamic knee joint loads during walking gait. These data further highlight the importance of biomechanical factors, including the full 3D knee moments and joint alignment, for explaining variations in subchondral bone microarchitecture in knee OA. On the basis of the findings presented within this thesis, future work is now required to elucidate whether or not there exist causative links between knee joint loading and microarchitectural changes in tibial subchondral bone. This may aid at identifying potential biomechanical factors that in future could be targeted using non-invasive therapies, to alleviate progression or symptoms of the disease.

References

Ab-Lazid, R, Perilli, E, Ryan, MK, Costi, JJ & Reynolds, KJ 2014, 'Does cancellous screw insertion torque depend on bone mineral density and/or microarchitecture?', *Journal of Biomechanics*, vol. 47, no. 2, pp. 347–353.

Adouni, M & Shirazi-Adl, A 2014a, 'Evaluation of knee joint muscle forces and tissue stresses-strains during gait in severe OA versus normal subjects', *Journal of Orthopaedic Research*, vol. 32, no. 1, pp. 69–78.

Adouni, M & Shirazi-Adl, A 2014b, 'Partitioning of knee joint internal forces in gait is dictated by the knee adduction angle and not by the knee adduction moment', *Journal of Biomechanics*, vol. 47, no. 7, pp. 1696–1703.

Akamatsu, Y, Mitsugi, N, Taki, N, Kobayashi, H & Saito, T 2012, 'Medial versus lateral condyle bone mineral density ratios in a cross-sectional study: A potential marker for medial knee osteoarthritis severity', *Arthritis Care and Research*, vol. 64, no. 7, pp. 1036–1045.

Al-Zahrani, KS & Bakheit, AMO 2002, 'A study of the gait characteristics of patients with chronic osteoarthritis of the knee', *Disability and Rehabilitation*, vol. 24, no. 5, pp. 275–280.

Andriacchi, TP 1990, 'Dynamics of pathological motion: applied to the anterior cruciate deficient knee', *Journal of Biomechanics*, vol. 23, pp. 99–105.

Andriacchi, TP & Dyrby, CO 2005, 'Interactions between kinematics and loading during walking for the normal and ACL deficient knee', *Journal of Biomechanics*, vol. 38, no. 2, pp. 293–298.

Andriacchi, TP, Galante, JO & Fermier, RW 1982, 'The influence of total knee-replacement design on walking and stair-climbing', *Journal of Bone and Joint Surgery American Volume*, vol. 64, no. 9, pp. 1328–1335.

Andriacchi, TP, Koo, S & Scanlan, SF 2009, 'Gait mechanics influence healthy cartilage morphology and osteoarthritis of the knee', *Journal of Bone and Joint Surgery American Volume*, vol. 91, no. Supplement 1, pp. 95–101.

Arnold, JB, Wong, DX, Jones, RK, Hill, CL & Thewlis, D 2015, 'Lateral wedge insoles for reducing biomechanical risk factors for medial knee osteoarthritis progression: A systematic review and meta-analysis', *Arthritis Care and Research*, vol. 68, no. 7, pp. 936–951.

Arthritis and Osteoporosis Victoria 2013, *A problem worth solving*, Arthritis and Osteoporosis Victoria, Elsternwick.

Astephen, JL, Deluzio, KJ, Caldwell, GE & Dunbar, MJ 2008, 'Biomechanical changes at the hip, knee, and ankle joints during gait are associated with knee osteoarthritis severity', *Journal of Orthopaedic Research*, vol. 26, no. 3, pp. 332–341.

Baliunas, AJ, Hurwitz, DE, Ryals, AB, Karrar, A, Case, JP, Block, JA & Andriacchi, TP 2002, 'Increased knee joint loads during walking are present in subjects with knee osteoarthritis', *Osteoarthritis and Cartilage*, vol. 10, no. 7, pp. 573–579.

Bassett, DR, Wyatt, HR, Thompson, H, Peters, JC & Hill, JO 2010, 'Pedometer-measured physical activity and health behaviors in United States adults', *Medicine and Science in Sports and Exercise*, vol. 42, no. 10, pp. 1819–1825.

Bellamy, N, Buchanan, WW, Goldsmith, CH, Campbell, J & Stitt, LW 1988, 'Validation study of WOMAC: a health status instrument for measuring clinically important patient relevant outcomes to antirheumatic drug therapy in patients with osteoarthritis of the hip or knee.', *Journal of Rheumatology*, vol. 15, no. 12, pp. 1833–1840.

Benjamini, Y & Hochberg, Y 1995, 'Controlling the false discovery rate: a practical and powerful approach to multiple testing', *Journal of the Royal Statistical Society Series B (Methodological)*, pp. 289–300.

Bennell, KL, Bowles, KA, Wang, Y, Cicuttini, F, Davies-Tuck, M & Hinman, RS 2011, 'Higher dynamic medial knee load predicts greater cartilage loss over 12 months in medial knee osteoarthritis', *Annals of the Rheumatic Diseases*, vol. 70, no. 10, pp. 1770–1774.

Bennell, KL, Creaby, MW, Wrigley, TV, Bowles, KA, Hinman, RS, Cicuttini, F & Hunter, DJ 2010, 'Bone marrow lesions are related to dynamic knee loading in medial knee osteoarthritis', *Annals of the Rheumatic Diseases*, vol. 69, no. 6, pp. 1151–1154.

Bennell, KL, Creaby, MW, Wrigley, TV & Hunter, DJ 2008, 'Tibial subchondral trabecular volumetric bone density in medial knee joint osteoarthritis using peripheral quantitative computed tomography technology', *Arthritis and Rheumatism*, vol. 58, no. 9, pp. 2776–2785.

Beuf, O, Ghosh, S, Newitt, DC, Link, TM, Steinbach, L, Ries, M, Lane, N & Majumdar, S 2002, 'Magnetic resonance imaging of normal and osteoarthritic trabecular bone structure in the human knee', *Arthritis and Rheumatism*, vol. 46, no. 2, pp. 385–393.

Bijlsma, JW, Berenbaum, F & Lafeber, FP 2011, 'Osteoarthritis: an update with relevance for clinical practice', *Lancet*, vol. 377, no. 9783, pp. 2115–2126.

Blackburn, TA & Craig, E 1980, 'Knee anatomy: a brief review', *Physical Therapy*, vol. 60, no. 12, pp. 1556–1560.

Bobinac, D, Spanjol, J, Zoricic, S & Maric, I 2003, 'Changes in articular cartilage and subchondral bone histomorphometry in osteoarthritic knee joints in humans', *Bone*, vol. 32, no. 3, pp. 284–290.

Bolbos, RI, Zuo, J, Banerjee, S, Link, TM, Ma, CB, Li, X & Majumdar, S 2008, 'Relationship between trabecular bone structure and articular cartilage morphology and relaxation times in early OA of the knee joint using parallel MRI at 3T', *Osteoarthritis and Cartilage*, vol. 16, no. 10, pp. 1150–1159.

Botter, SM, van Osch, GJ, Clockaerts, S, Waarsing, JH, Weinans, H & van Leeuwen, JP 2011, 'Osteoarthritis induction leads to early and temporal subchondral plate porosity in the tibial plateau of mice: an in vivo microfocal computed tomography study', *Arthritis and Rheumatism*, vol. 63, no. 9, pp. 2690–2699.

Briggs, AM, Perilli, E, Parkinson, IH, Wrigley, TV, Fazzalari, NL, Kantor, S & Wark, JD 2010, 'Novel assessment of subregional bone mineral density using DXA and pQCT and subregional microarchitecture using micro-CT in whole human vertebrae: applications, methods, and correspondence between technologies', *Journal of Clinical Densitometry*, vol. 13, no. 2, pp. 161–174.

Brindle, T, Nyland, J & Johnson, DL 2001, 'The meniscus: review of basic principles with application to surgery and rehabilitation', *Journal of Athletic Training*, vol. 36, no. 2, pp. 160–169.

Buckwalter, JA & Mankin, HJ 1998, 'Articular cartilage. part I: tissue design and chondrocyte-matrix interactions', *Journal of Bone and Joint Surgery American Volume*, vol. 79, no. 4, pp. 600–611.

Bullough, PG, Munuera, L, Murphy, J & Weinstein, AM 1970, 'The strength of the menisci of the knee as it relates to their fine structure', *Journal of Bone and Joint Surgery British Volume*, vol. 52, no. 3, pp. 564–567.

Burnett, WD, Kontulainen, SA, McLennan, CE, Hazel, D, Talmo, C, Hunter, DJ, Wilson, DR & Johnston, JD 2015, 'Knee osteoarthritis patients with severe nocturnal pain have altered proximal tibial subchondral bone mineral density', *Osteoarthritis and Cartilage*, vol. 23, no. 9, pp. 1483–1490.

Burr, DB 2004, 'Anatomy and physiology of the mineralized tissues: role in the pathogenesis of osteoarthrosis', *Osteoarthritis and Cartilage*, vol. 12, pp. 20–30.

Burr, DB & Gallant, MA 2012, 'Bone remodelling in osteoarthritis', *Nature Reviews Rheumatology*, vol. 8, no. 11, pp. 665–673.

Busija, L, Bridgett, L, Williams, SR, Osborne, RH, Buchbinder, R, March, L & Fransen, M 2010, 'Osteoarthritis', *Best Practice and Research Clinical Rheumatology*, vol. 24, no. 6, pp. 757–768.

Callaghan, MJ, Parkes, MJ, Hutchinson, CE, Gait, AD, Forsythe, LM, Marjanovic, EJ, Lunt, M & Felson, DT 2015, 'A randomised trial of a brace for patellofemoral osteoarthritis targeting knee pain and bone marrow lesions', *Annals of the Rheumatic Diseases*, pp. annrheumdis–2014.

Cappozzo, A, Catani, F, Della Croce, U & Leardini, A 1995, 'Position and orientation in space of bones during movement: anatomical frame definition and determination', *Clinical Biomechanics*, vol. 10, no. 4, pp. 171–178.

Chang, AH, Moisio, KC, Chmiel, JS, Eckstein, F, Guermazi, A, Prasad, PV, Zhang, Y, Almagor, O, Belisle, L, Hayes, K & Sharma, L 2015, 'External knee adduction and flexion moments during gait and medial tibiofemoral disease progression in knee osteoarthritis', *Osteoarthritis and Cartilage*, vol. 23, no. 7, pp. 1099–1106.

Chapman, GJ, Parkes, MJ, Forsythe, L, Felson, DT & Jones, RK 2015, 'Ankle motion influences the external knee adduction moment and may predict who will respond to lateral wedge insoles?: an ancillary analysis from the SILK trial', *Osteoarthritis and Cartilage*, vol. 23, no. 8, pp. 1316–1322.

Chassin, EP, Mikosz, RP, Andriacchi, TP & Rosenberg, AG 1996, 'Functional analysis of cemented medial unicompartmental knee arthroplasty', *Journal of Arthroplasty*, vol. 11, no. 5, pp. 553–559.

Chehab, EF, Favre, J, Erhart-Hledik, JC & Andriacchi, TP 2014, 'Baseline knee adduction and flexion moments during walking are both associated with 5 year cartilage changes in patients with medial knee osteoarthritis', *Osteoarthritis and Cartilage*, vol. 22, no. 11, pp. 1833–1839.

Chen, Y, Wang, T, Guan, M, Zhao, W, Leung, FKL, Pan, H, Cao, X, Guo, XE & Lu, WW 2015, 'Bone turnover and articular cartilage differences localized to subchondral cysts in knees with advanced osteoarthritis', *Osteoarthritis and Cartilage*, vol. 23, no. 12, pp. 2174–2183.

Chiba, K, Uetani, M, Kido, Y, Ito, M, Okazaki, N, Taguchi, K & Shindo, H 2012, 'Osteoporotic changes of subchondral trabecular bone in osteoarthritis of the knee: a 3-T MRI study', *Osteoporosis International*, vol. 23, no. 2, pp. 589–597.

Childs, JD, Sparto, PJ, Fitzgerald, GK, Bizzini, M & Irrgang, JJ 2004, 'Alterations in lower extremity movement and muscle activation patterns in individuals with knee osteoarthritis', *Clinical Biomechanics*, vol. 19, no. 1, pp. 44–49.

Choi, K, Kuhn, JL, Ciarelli, MJ & Goldstein, SA 1990, 'The elastic moduli of human subchondral, trabecular, and cortical bone tissue and the size-dependency of cortical bone modulus', *Journal of Biomechanics*, vol. 23, no. 11, pp. 1103–1113.

Christensen, P, Kjaer, J, Melsen, F, Nielsen, HE, Sneppen, O & Vang, PS 1982, 'The subchondral bone of the proximal tibial epiphysis in osteoarthritis of the knee', *Acta Orthopaedica Scandinavica*, vol. 53, no. 6, pp. 889–895.

Clark, CR & Ogden, JA 1983, 'Development of the menisci of the human knee joint. morphological changes and their potential role in childhood meniscal injury.', *Journal of Bone and Joint Surgery American Volume*, vol. 65, no. 4, pp. 538–547.

Clark, J & Huber, J 1990, 'The structure of the human subchondral plate', *Journal of Bone and Joint Surgery British Volume*, vol. 72, no. 5, pp. 866–873.

Clark, JM 1990, 'The structure of vascular channels in the subchondral plate', *Journal of Anatomy*, vol. 171, pp. 105–115.

Clarke, S, Wakeley, C, Duddy, J, Sharif, M, Watt, I, Ellingham, K, Elson, C, Nickols, G & Kirwan, J 2004, 'Dual-energy X-ray absorptiometry applied to the assessment of tibial subchondral bone mineral density in osteoarthritis of the knee', *Skeletal Radiology*, vol. 33, no. 10, pp. 588–595.

Conaghan, PG, Kloppenburg, M, Schett, G, Bijlsma, JW et al. 2014, 'Osteoarthritis research priorities: a report from a EULAR ad hoc expert committee', *Annals of the Rheumatic Diseases*, vol. 73, no. 8, pp. 1442–1445.

Conaghan, PG & Nelson, AE 2012, *Fast Facts: Osteoarthritis*, Health Press, Oxford, UK.

Creaby, MW, Bennell, KL & Hunt, MA 2012, 'Gait differs between unilateral and bilateral knee osteoarthritis', *Archives of Physical Medicine and Rehabilitation*, vol. 93, no. 5, pp. 822–827.

Creaby, MW, Wang, Y, Bennell, KL, Hinman, RS, Metcalf, BR, Bowles, KA & Cicuttini, FM 2010, 'Dynamic knee loading is related to cartilage defects and tibial plateau bone area in medial knee osteoarthritis', *Osteoarthritis and Cartilage*, vol. 18, no. 11, pp. 1380–1385.

Cross, M, Smith, E, Hoy, D, Nolte, S, Ackerman, I, Fransen, M, Bridgett, L, Williams, S, Guillemin, F, Hill, CL, Laslett, LL, Jones, G, Cicuttini, F, Osborne, R, Vos, T, Buchbinder, R, Woolf, A & March, L 2014, 'The global burden of hip and knee osteoarthritis: estimates from the Global Burden of Disease 2010 study', *Annals of the Rheumatic Diseases*, vol. 73, pp. 1470–1476.

Delp, SL, Loan, JP, Hoy, MG, Zajac, FE, Topp, EL & Rosen, JM 1990, 'An interactive graphics-based model of the lower extremity to study orthopaedic surgical procedures', *IEEE Transactions on Biomedical Engineering*, vol. 37, no. 8, pp. 757–767.

Deluzio, KJ & Astephen, JL 2007, 'Biomechanical features of gait waveform data associated with knee osteoarthritis: an application of principal component analysis', *Gait and Posture*, vol. 25, no. 1, pp. 86–93.

Ding, M, Odgaard, A & Hvid, I 2003, 'Changes in the three-dimensional microstructure of human tibial cancellous bone in early osteoarthritis', *Journal of Bone and Joint Surgery British Volume*, vol. 85, no. 6, pp. 906–912.

Ding, M, Odgaard, A, Linde, F & Hvid, I 2002, 'Age-related variations in the microstructure of human tibial cancellous bone', *Journal of Orthopaedic Research*, vol. 20, no. 3, pp. 615–621.

Doriot, N & Chèze, L 2004, 'A three-dimensional kinematic and dynamic study of the lower limb during the stance phase of gait using an homogeneous matrix approach', *IEEE Transactions on Biomedical Engineering*, vol. 51, no. 1, pp. 21–27.

Driban, JB, Sitler, MR, Barbe, MF & Balasubramanian, E 2010, 'Is osteoarthritis a heterogeneous disease that can be stratified into subsets?', *Clinical Rheumatology*, vol. 29, no. 2, pp. 123–131.

Duncan, H, Jundt, J, Riddle, J, Pitchford, W & Christopherson, T 1987, 'The tibial subchondral plate. a scanning electron microscopic study.', *Journal of Bone and Joint Surgery American Volume*, vol. 69, no. 8, pp. 1212–1220.

Eckstein, F, Hudelmaier, M, Marshall, M & Sharma, L 2009, 'Medial-to-lateral ratio of tibiofemoral subchondral bone area is adapted to alignment and mechanical load', *Calcified Tissue International*, vol. 84, no. 3, pp. 186–194.

Erhart, JC, Mündermann, A, Elspas, B, Giori, NJ & Andriacchi, TP 2008, 'A variable-stiffness shoe lowers the knee adduction moment in subjects with symptoms of medial compartment knee osteoarthritis', *Journal of Biomechanics*, vol. 41, no. 12, pp. 2720–2725.

Erhart-Hledik, JC, Favre, J & Andriacchi, TP 2015, 'New insight in the relationship between regional patterns of knee cartilage thickness, osteoarthritis disease severity, and gait mechanics', *Journal of Biomechanics*, vol. 48, no. 14, pp. 3868–3875.

Farrokhi, S, Tashman, S, Gil, AB, Klatt, BA & Fitzgerald, GK 2012, 'Are the kinematics of the knee joint altered during the loading response phase of gait in individuals with concurrent knee osteoarthritis and complaints of joint instability? A dynamic stereo X-ray study', *Clinical Biomechanics*, vol. 27, no. 4, pp. 384–389.

Faul, F, Erdfelder, E, Buchner, A & Lang, AG 2009, 'Statistical power analyses using G*Power 3.1: Tests for correlation and regression analyses', *Behavior Research Methods*, vol. 41, no. 4, pp. 1149–1160.

Felson, D, Niu, J, Sack, B, Aliabadi, P, McCullough, C & Nevitt, MC 2013, 'Progression of osteoarthritis as a state of inertia', *Annals of the Rheumatic Diseases*, vol. 72, no. 6, pp. 924–929.

Felson, DT 2004, 'Obesity and vocational and avocational overload of the joint as risk factors for osteoarthritis', *Journal of Rheumatology Supplement*, vol. 31, no. 70, pp. 2–5.

Felson, DT 2014, 'Osteoarthritis: priorities for osteoarthritis research: much to be done', *Nature Reviews Rheumatology*, vol. 10, no. 8, pp. 447–448.

Fields, AJ, Eswaran, SK, Jekir, MG & Keaveny, TM 2009, 'Role of trabecular microarchitecture in whole-vertebral body biomechanical behavior', *Journal of Bone and Mineral Research*, vol. 24, no. 9, pp. 1523–1530.

Findlay, DM & Kuliwaba, JS 2016, 'Bone–cartilage crosstalk: a conversation for understanding osteoarthritis', *Bone Research*, vol. 4, p. 16028.

Florea, C, Malo, MKH, Rautiainen, J, Mäkelä, JTA, Fick, JM, Nieminen, MT, Jurvelin, JS, Davidescu, A & Korhonen, RK 2015, 'Alterations in subchondral bone plate, trabecular bone and articular cartilage properties of rabbit femoral condyles at 4 weeks after anterior cruciate ligament transection', *Osteoarthritis and Cartilage*, vol. 23, no. 3, pp. 414–422.

Fregly, BJ, Besier, TF, Lloyd, DG, Delp, SL, Banks, SA, Pandy, MG & D'Lima, DD 2012, 'Grand challenge competition to predict in vivo knee loads', *Journal of Orthopaedic Research*, vol. 30, no. 4, pp. 503–513.

Gök, H, Ergin, S & Yavuzer, G 2002, 'Kinetic and kinematic characteristics of gait in patients with medial knee arthrosis', *Acta Orthopaedica Scandinavica*, vol. 73, no. 6, pp. 647–652.

Goldring, MB & Goldring, SR 2010, 'Articular cartilage and subchondral bone in the pathogenesis of osteoarthritis', *Annals of the New York Academy of Sciences*, vol. 1192, no. 1, pp. 230–237.

Griffin, TM & Guilak, F 2005, 'The role of mechanical loading in the onset and progression of osteoarthritis', *Exercise and Sport Sciences Reviews*, vol. 33, no. 4, pp. 195–200.

Guggenbuhl, P, Bodic, F, Hamel, L, Baslé, MF & Chappard, D 2006, 'Texture analysis of X-ray radiographs of iliac bone is correlated with bone micro-CT', *Osteoporosis International*, vol. 17, no. 3, pp. 447–454.

Hall, M, Bennell, K, Wrigley, T, Metcalf, B, Campbell, P, Kasza, J, Paterson, K, Hunter, D & Hinman, R 2017, 'The knee adduction moment and knee osteoarthritis symptoms: relationships according to radiographic disease severity', *Osteoarthritis and Cartilage*, vol. 25, no. 1, pp. 34–41.

Harrigan, TP, Jasty, M, Mann, RW & Harris, WH 1988, 'Limitations of the continuum assumption in cancellous bone', *Journal of Biomechanics*, vol. 21, no. 4, pp. 269–275.

Heiden, TL, Lloyd, DG & Ackland, TR 2009, 'Knee joint kinematics, kinetics and muscle co-contraction in knee osteoarthritis patient gait', *Clinical Biomechanics*, vol. 24, no. 10, pp. 833–841.

Henriksen, M, Aaboe, J & Bliddal, H 2012, 'The relationship between pain and dynamic knee joint loading in knee osteoarthritis varies with radiographic disease severity. a cross sectional study', *The Knee*, vol. 19, no. 4, pp. 392–398.

Henriksen, M, Simonsen, EB, Alkjær, T, Lund, H, Graven-Nielsen, T, Danneskiold-Samsøe, B & Bliddal, H 2006, 'Increased joint loads during walking–a consequence of pain relief in knee osteoarthritis', *The Knee*, vol. 13, no. 6, pp. 445–450.

Hildebrand, T & Rüegsegger, P 1997a, 'A new method for the model-independent assessment of thickness in three-dimensional images', *Journal of Microscopy*, vol. 185, no. 1, pp. 67–75.

Hildebrand, T & Rüegsegger, P 1997b, 'Quantification of bone microarchitecture with the structure model index', *Computer Methods in Biomechanics and Biomedical Engineering*, vol. 1, no. 1, pp. 15–23.

Hinman, RS, Bowles, KA, Metcalf, BB, Wrigley, TV & Bennell, KL 2012, 'Lateral wedge insoles for medial knee osteoarthritis: effects on lower limb frontal plane biomechanics', *Clinical Biomechanics*, vol. 27, no. 1, pp. 27–33.

Hinman, RS, Payne, C, Metcalf, BR, Wrigley, TV & Bennell, KL 2008, 'Lateral wedges in knee osteoarthritis: What are their immediate clinical and biomechanical effects and can these predict a three-month clinical outcome?', *Arthritis Care and Research*, vol. 59, no. 3, pp. 408–415.

Huang, SC, Wei, IP, Chien, HL, Wang, TM, Liu, YH, Chen, HL, Lu, TW & Lin, JG 2008, 'Effects of severity of degeneration on gait patterns in patients with medial knee osteoarthritis', *Medical Engineering and Physics*, vol. 30, no. 8, pp. 997–1003.

Hudson, D, Royer, T & Richards, J 2007, 'Bone mineral density of the proximal tibia relates to axial torsion in the lower limb', *Gait and Posture*, vol. 26, no. 3, pp. 446–451.

Hulet, C, Sabatier, J, Souquet, D, Locker, B, Marcelli, C & Vielpeau, C 2002, 'Distribution of bone mineral density at the proximal tibia in knee osteoarthritis', *Calcified Tissue International*, vol. 71, no. 4, pp. 315–322.

Hunter, DJ, Gerstenfeld, L, Bishop, G, Davis, AD, Mason, ZD, Einhorn, TA, Maciewicz, RA, Newham, P, Foster, M, Jackson, S & Morgan, EF 2009, 'Bone marrow lesions from osteoarthritis knees are characterized by sclerotic bone that is less well mineralized', *Arthritis Research and Therapy*, vol. 11, no. R11.

Hunter, DJ, Schofield, D & Callander, E 2014, 'The individual and socioeconomic impact of osteoarthritis', *Nature Reviews Rheumatology*, vol. 10, no. 7, pp. 437–441.

Hurwitz, DE, Ryals, AB, Case, JP, Block, JA & Andriacchi, TP 2002, 'The knee adduction moment during gait in subjects with knee osteoarthritis is more closely correlated with static alignment than radiographic disease severity, toe out angle and pain', *Journal of Orthopaedic Research*, vol. 20, no. 1, pp. 101–107.

Hurwitz, DE, Sumner, DR, Andriacchi, TP & Sugar, DA 1998, 'Dynamic knee loads during gait predict proximal tibial bone distribution', *Journal of Biomechanics*, vol. 31, no. 5, pp. 423–430.

Imhof, H, Breitenseher, M, Kainberger, F, Rand, T & Trattnig, S 1999, 'Importance of subchondral bone to articular cartilage in health and disease', *Topics in Magnetic Resonance Imaging*, vol. 10, no. 3, pp. 180–192.

Imhof, H, Sulzbacher, I, Grampp, S, Czerny, C, Youssefzadeh, S & Kainberger, F 2000, 'Subchondral bone and cartilage disease: a rediscovered functional unit', *Investigative Radiology*, vol. 35, no. 10, pp. 581–588.

Johnston, JD, Masri, BA & Wilson, DR 2009, 'Computed tomography topographic mapping of subchondral density (CT-TOMASD) in osteoarthritic and normal knees: methodological development and preliminary findings', *Osteoarthritis and Cartilage*, vol. 17, no. 10, pp. 1319–1326.

Johnston, JD, McLennan, CE, Hunter, DJ & Wilson, DR 2011, 'In vivo precision of a depth-specific topographic mapping technique in the CT analysis of osteoarthritic and normal proximal tibial subchondral bone density', *Skeletal Radiology*, vol. 40, no. 8, pp. 1057–1064.

Jones, RK, Chapman, GJ, Parkes, MJ, Forsythe, L & Felson, DT 2015, 'The effect of different types of insoles or shoe modifications on medial loading of the knee in persons with medial

knee osteoarthritis: A randomised trial', *Journal of Orthopaedic Research*, vol. 33, no. 11, pp. 1646–1654.

Kamibayashi, L, Wyss, UP, Cooke, TD & Zee, B 1995, 'Trabecular microstructure in the medial condyle of the proximal tibia of patients with knee osteoarthritis', *Bone*, vol. 17, no. 1, pp. 27–35.

Karsdal, MA, Christiansen, C, Ladel, C, Henriksen, K, Kraus, VB & Bay-Jensen, AC 2014, 'Osteoarthritis–a case for personalized health care?', *Osteoarthritis and Cartilage*, vol. 22, no. 1, pp. 7–16.

Kaufman, KR, Hughes, C, Morrey, BF, Morrey, M & An, KN 2001, 'Gait characteristics of patients with knee osteoarthritis', *Journal of Biomechanics*, vol. 34, no. 7, pp. 907–915.

Kean, CO, Hinman, RS, Bowles, KA, Cicuttini, F, Davies-Tuck, M & Bennell, KL 2012, 'Comparison of peak knee adduction moment and knee adduction moment impulse in distinguishing between severities of knee osteoarthritis', *Clinical Biomechanics*, vol. 27, no. 5, pp. 520–523.

Khodadadyan-Klostermann, C, von Seebach, M, Taylor, WR, Duda, GN & Haas, NP 2004, 'Distribution of bone mineral density with age and gender in the proximal tibia', *Clinical Biomechanics*, vol. 19, no. 4, pp. 370–376.

Kito, N, Shinkoda, K, Yamasaki, T, Kanemura, N, Anan, M, Okanishi, N, Ozawa, J & Moriyama, H 2010, 'Contribution of knee adduction moment impulse to pain and disability in japanese women with medial knee osteoarthritis', *Clinical Biomechanics*, vol. 25, no. 9, pp. 914–919.

Ko, Su, Ling, SM, Schreiber, C, Nesbitt, M & Ferrucci, L 2011, 'Gait patterns during different walking conditions in older adults with and without knee osteoarthritis - results from the Baltimore Longitudinal Study of Aging', *Gait and Posture*, vol. 33, no. 2, pp. 205–210.

Koo, S & Andriacchi, TP 2007, 'A comparison of the influence of global functional loads vs. local contact anatomy on articular cartilage thickness at the knee', *Journal of Biomechanics*, vol. 40, no. 13, pp. 2961–2966.

Kotlarz, H, Gunnarsson, CL, Fang, H & Rizzo, JA 2009, 'Insurer and out-of-pocket costs of osteoarthritis in the US: Evidence from national survey data', *Arthritis and Rheumatism*, vol. 60, no. 12, pp. 3546–3553.

Kroker, A, Zhu, Y, Manske, SL, Barber, R, Mohtadi, N & Boyd, SK 2016, 'Quantitative in vivo assessment of bone microarchitecture in the human knee using HR-pQCT', *Bone*.

Kulmala, JP, Äyrämö, S & Avela, J 2013, 'Knee extensor and flexor dominant gait patterns increase the knee frontal plane moment during walking', *Journal of Orthopaedic Research*, vol. 31, no. 7, pp. 1013–1019.

Kutzner, I, Trepczynski, A, Heller, MO & Bergmann, G 2013, 'Knee adduction moment and medial contact force–facts about their correlation during gait', *PLoS One*, vol. 8, no. 12, p. e81036.

Landry, SC, McKean, KA, Hubley-Kozey, CL, Stanish, WD & Deluzio, KJ 2007, 'Knee biomechanics of moderate OA patients measured during gait at a self-selected and fast walking speed', *Journal of Biomechanics*, vol. 40, no. 8, pp. 1754–1761.

Lawrence, RC, Felson, DT, Helmick, CG, Arnold, LM, Choi, H, Deyo, RA, Gabriel, S, Hirsch, R, Hochberg, MC, Hunder, GG, Jordan, JM, Katz, JN, Kremers, HM & Wolfe, F 2008, 'Estimates of the prevalence of arthritis and other rheumatic conditions in the United States: Part II', *Arthritis and Rheumatism*, vol. 58, no. 1, pp. 26–35.

Le Pen, C, Reygrobellet, C & Gérentes, I 2005, 'Financial cost of osteoarthritis in France: The "COART" France study', *Joint Bone Spine*, vol. 72, no. 6, pp. 567–570.

Levangie, PK & Norkin, CC 2011, *Joint structure and function: a comprehensive analysis*, FA Davis, Philadelphia, PA.

Levinger, P, Menz, HB, Morrow, AD, Perrott, MA, Bartlett, JR, Feller, JA & Bergman, NB 2012, 'Knee biomechanics early after knee replacement surgery predict abnormal gait patterns 12 months postoperatively', *Journal of Orthopaedic Research*, vol. 30, no. 3, pp. 371–376.

Li, G, Yin, J, Gao, J, Cheng, TS, Pavlos, NJ, Zhang, C & Zheng, MH 2013, 'Subchondral bone in osteoarthritis: insight into risk factors and microstructural changes', *Arthritis Research and Therapy*, vol. 15, no. 6, p. 223.

Lieber, RL 1990, 'Statistical significance and statistical power in hypothesis testing', *Journal of Orthopaedic Research*, vol. 8, no. 2, pp. 304–309.

Lin, ASP, Salazar-Noratto, GE & Guldberg, RE 2015, 'EPIC-μCT imaging of articular cartilage', *Osteoporosis and Osteoarthritis*, vol. 1226, pp. 131–140.

Liu, F, Kozanek, M, Hosseini, A, Van de Velde, SK, Gill, TJ, Rubash, HE & Li, G 2010, 'In vivo tibiofemoral cartilage deformation during the stance phase of gait', *Journal of Biomechanics*, vol. 43, no. 4, pp. 658–665.

Loeser, RF, Goldring, SR, Scanzello, CR & Goldring, MB 2012, 'Osteoarthritis: a disease of the joint as an organ', *Arthritis and Rheumatism*, vol. 64, no. 6, pp. 1697–1707.

Lu, TW & O'Connor, JJ 1999, 'Bone position estimation from skin marker co-ordinates using global optimisation with joint constraints', *Journal of Biomechanics*, vol. 32, no. 2, pp. 129–134.

Madry, H, van Dijk, CN & Mueller-Gerbl, M 2010, 'The basic science of the subchondral bone', *Knee Surgery, Sports Traumatology, Arthroscopy*, vol. 18, no. 4, pp. 419–433.

Madsen, OR, Schaadt, O, Bliddal, H, Egsmose, C & Sylvest, J 1994, 'Bone mineral distribution of the proximal tibia in gonarthrosis assessed *in vivo* by photon absorption', *Osteoarthritis and Cartilage*, vol. 2, no. 2, pp. 141–147.

Mahjoub, M, Berenbaum, F & Houard, X 2012, 'Why subchondral bone in osteoarthritis? the importance of the cartilage bone interface in osteoarthritis', *Osteoporosis International*, vol. 23, no. 8, pp. 841–846.

Makris, EA, Hadidi, P & Athanasiou, KA 2011, 'The knee meniscus: structure–function, pathophysiology, current repair techniques, and prospects for regeneration', *Biomaterials*, vol. 32, no. 30, pp. 7411–7431.

Maly, MR, Acker, SM, Totterman, S, Tamez-Peña, J, Stratford, PW, Callaghan, JP, Adachi, JD & Beattie, KA 2015, 'Knee adduction moment relates to medial femoral and tibial cartilage morphology in clinical knee osteoarthritis', *Journal of Biomechanics*, vol. 48, no. 12, pp. 3495–3501.

Maly, MR, Robbins, SM, Stratford, PW, Birmingham, TB & Callaghan, JP 2013, 'Cumulative knee adductor load distinguishes between healthy and osteoarthritic knees–a proof of principle study', *Gait and Posture*, vol. 37, no. 3, pp. 397–401.

Manal, K, Gardinier, E, Buchanan, T & Snyder-Mackler, L 2015, 'A more informed evaluation of medial compartment loading: the combined use of the knee adduction and flexor moments', *Osteoarthritis and Cartilage*, vol. 23, no. 7, pp. 1107–1111.

Matsui, H, Shimizu, M & Tsuji, H 1997, 'Cartilage and subchondral bone interaction in osteoarthrosis of human knee joint: a histological and histomorphometric study', *Microscopy Research and Technique*, vol. 37, no. 4, pp. 333–342.

McAlindon, TE, Bannuru, RR, Sullivan, MC, Arden, NK, Berenbaum, F, Bierma-Zeinstra, SM, Hawker, GA, Henrotin, Y, Hunter, DJ, Kawaguchi, H, Kwoh, K, Lohmander, S, Rannou, F, Roos, EM & Underwood, M 2014, 'OARSI guidelines for the non-surgical management of knee osteoarthritis', *Osteoarthritis and Cartilage*, vol. 22, no. 3, pp. 363–388.

McKinley, TO, English, DK & Bay, BK 2003, 'Trabecular bone strain changes resulting from partial and complete meniscectomy.', *Clinical Orthopaedics and Related Research*, vol. 407, pp. 259–267.

Messier, SP, DeVita, P, Cowan, RE, Seay, J, Young, HC & Marsh, AP 2005, 'Do older adults with knee osteoarthritis place greater loads on the knee during gait? A preliminary study', *Archives of Physical Medicine and Rehabilitation*, vol. 86, no. 4, pp. 703–709.

Mills, K, Hunt, MA & Ferber, R 2013, 'Biomechanical deviations during level walking associated with knee osteoarthritis: A systematic review and meta-analysis', *Arthritis Care and Research*, vol. 65, no. 10, pp. 1643–1665.

Milz, S & Putz, R 1994, 'Quantitative morphology of the subchondral plate of the tibial plateau.', *Journal of Anatomy*, vol. 185, no. 1, pp. 103–110.

Miyazaki, T, Wada, M, Kawahara, H, Sato, M, Baba, H & Shimada, S 2002, 'Dynamic load at baseline can predict radiographic disease progression in medial compartment knee osteoarthritis', *Annals of the Rheumatic Diseases*, vol. 61, no. 7, pp. 617–622.

Müller, R, Hahn, M, Vogel, M, Delling, G & Rüegsegger, P 1996, 'Morphometric analysis of noninvasively assessed bone biopsies: comparison of high-resolution computed tomography and histologic sections', *Bone*, vol. 18, no. 3, pp. 215–220.

Mündermann, A, Dyrby, CO & Andriacchi, TP 2005, 'Secondary gait changes in patients with medial compartment knee osteoarthritis: increased load at the ankle, knee, and hip during walking', *Arthritis and Rheumatism*, vol. 52, no. 9, pp. 2835–44.

Muratovic, D, Cicuttini, F, Wluka, A, Findlay, D, Wang, Y, Otto, S, Taylor, D, Humphries, J, Lee, Y, Labrinidis, A et al. 2016, 'Bone marrow lesions detected by specific combination of MRI sequences are associated with severity of osteochondral degeneration', *Arthritis Research and Therapy*, vol. 18, no. 54.

Murray, CJ, Vos, T, Lozano, R, Naghavi, M, Flaxman, AD, Michaud, C, Ezzati, M, Shibuya, K, Salomon, JA, Abdalla, S et al. 2013, 'Disability-adjusted life years (DALYs) for 291 diseases and injuries in 21 regions, 1990–2010: a systematic analysis for the Global Burden of Disease Study 2010', *Lancet*, vol. 380, no. 9859, pp. 2197–2223.

Niu, J, Zhang, Y, Torner, J, Nevitt, M, Lewis, C, Aliabadi, P, Sack, B, Clancy, M, Sharma, L & Felson, DT 2009, 'Is obesity a risk factor for progressive radiographic knee osteoarthritis?', *Arthritis Care and Research*, vol. 61, no. 3, pp. 329–335.

Noble, J & Alexander, K 1985, 'Studies of tibial subchondral bone density and its significance.', *Journal of Bone and Joint Surgery American Volume*, vol. 67, no. 2, pp. 295–302.

Paley, D 2002, *Principles of Deformity Correction*, Springer, New York, NY.

Pan, J, Wang, B, Li, W, Zhou, X, Scherr, T, Yang, Y, Price, C & Wang, L 2012, 'Elevated cross-talk between subchondral bone and cartilage in osteoarthritic joints', *Bone*, vol. 51, no. 2, pp. 212–217.

Parfitt, AM, Drezner, MK, Glorieux, FH, Kanis, JA, Malluche, H, Meunier, PJ, Ott, SM & Recker, RR 1987, 'Bone histomorphometry: standardization of nomenclature, symbols, and units: report of the ASBMR Histomorphometry Nomenclature Committee', *Journal of Bone and Mineral Research*, vol. 2, no. 6, pp. 595–610.

Patel, V, Issever, AS, Burghardt, A, Laib, A, Ries, M & Majumdar, S 2003, 'MicroCT evaluation of normal and osteoarthritic bone structure in human knee specimens', *Journal of Orthopaedic Research*, vol. 21, no. 1, pp. 6–13.

Pawson, DJ, Glanzmann, M, Luechinger, R, Müller, R & Stok, KS 2015, 'Quantitative morphometric patterns in cartilage and bone from the humeral heads of end-stage osteoarthritis patients', *Osteoarthritis and Cartilage*, vol. 23, no. 8, pp. 1377–1387.

Perilli, E, Bala, Y, Zebaze, R, Reynolds, KJ & Seeman, E 2015a, 'Regional heterogeneity in the configuration of the intracortical canals of the femoral shaft', *Calcified Tissue International*, vol. 97, no. 4, pp. 327–335.

Perilli, E, Baleani, M, Öhman, C, Baruffaldi, F & Viceconti, M 2007a, 'Structural parameters and mechanical strength of cancellous bone in the femoral head in osteoarthritis do not depend on age', *Bone*, vol. 41, no. 5, pp. 760–768.

Perilli, E, Baruffaldi, F, Bisi, MC, Cristofolini, L & Cappello, A 2006, 'A physical phantom for the calibration of three-dimensional X-ray microtomography examination', *Journal of Microscopy*, vol. 222, no. 2, pp. 124–134.

Perilli, E, Baruffaldi, F, Visentin, M, Bordini, B, Traina, F, Cappello, A & Viceconti, M 2007b, 'MicroCT examination of human bone specimens: effects of polymethylmethacrylate embedding on structural parameters', *Journal of Microscopy*, vol. 225, no. 2, pp. 192–200.

Perilli, E, Parkinson, IH & Reynolds, KJ 2012, 'Micro-CT examination of human bone: from biopsies towards the entire organ', *Annali dell'Istituto Superiore di Sanita*, vol. 48, no. 1, pp. 75–82.

Perilli, E, Parkinson, IH, Truong, LH, Chong, KC, Fazzalari, NL & Osti, OL 2015b, 'Modic (endplate) changes in the lumbar spine: bone micro-architecture and remodelling', *European Spine Journal*, vol. 24, no. 9, pp. 1926–1934.

Perry, J & Burnfield, JM 1992, *Gait analysis: normal and pathological function*, Slack, Thorofare, NJ.

Pham, T, Maillefert, JF, Hudry, C, Kieffert, P, Bourgeois, P, Lechevalier, D & Dougados, M 2004, 'Laterally elevated wedged insoles in the treatment of medial knee osteoarthritis: a two-year prospective randomized controlled study', *Osteoarthritis and Cartilage*, vol. 12, no. 1, pp. 46–55.

Phinyomark, A, Osis, ST, Hettinga, BA, Kobsar, D & Ferber, R 2016, 'Gender differences in gait kinematics for patients with knee osteoarthritis', *BMC Musculoskeletal Disorders*, vol. 17, no. 1, p. 157.

Radin, EL & Rose, RM 1986, 'Role of subchondral bone in the initiation and progression of cartilage damage.', *Clinical Orthopaedics and Related Research*, vol. 213, pp. 34–40.

Rho, JY, Ashman, RB & Turner, CH 1993, 'Young's modulus of trabecular and cortical bone material: ultrasonic and microtensile measurements', *Journal of Biomechanics*, vol. 26, no. 2, pp. 111–119.

Riddle, DL, Stratford, PW & Perera, RA 2016, 'The incident tibiofemoral osteoarthritis with rapid progression phenotype: development and validation of a prognostic prediction rule', *Osteoarthritis and Cartilage*, vol. 24, no. 12, pp. 2100–2107.

Robbins, SM, Wilson, JLA, Rutherford, DJ & Hubley-Kozey, CL 2013, 'Reliability of principal components and discrete parameters of knee angle and moment gait waveforms in individuals with moderate knee osteoarthritis', *Gait and Posture*, vol. 38, no. 3, pp. 421–427.

Roberts, BC, Thewlis, D, Solomon, LB, Mercer, G, Reynolds, KJ & Perilli, E 2016, 'Systematic mapping of the subchondral bone 3D microarchitecture in the human tibial plateau: Variations with joint alignment', *Journal of Orthopaedic Research*.

Rosenberg, M, Mills, C, McCormack, G, Martin, K, Grove, B, Pratt, S & Braham, R 2010, *Physical activity levels of Western Australian adults: findings from the physical activity taskforce adult physical activity survey*, The University of Western Australia, Perth, Australia.

Rousseeuw, PJ 1987, 'Silhouettes: a graphical aid to the interpretation and validation of cluster analysis', *Journal of Computational and Applied Mathematics*, vol. 20, pp. 53–65.

Rutherford, DJ, Hubley-Kozey, CL, Deluzio, KJ, Stanish, WD & Dunbar, M 2008, 'Foot progression angle and the knee adduction moment: a cross-sectional investigation in knee osteoarthritis', *Osteoarthritis and Cartilage*, vol. 16, no. 8, pp. 883–889.

Schipplein, OD & Andriacchi, TP 1991, 'Interaction between active and passive knee stabilizers during level walking', *Journal of Orthopaedic Research*, vol. 9, no. 1, pp. 113–119.

Schmidt, JE, Amrami, KK, Manduca, A & Kaufman, KR 2005, 'Semi-automated digital image analysis of joint space width in knee radiographs', *Skeletal Radiology*, vol. 34, no. 10, pp. 639–643.

Sharma, L, Hurwitz, DE, Thonar, EJ, Sum, JA, Lenz, ME, Dunlop, DD, Schnitzer, TJ, Kirwan-Mellis, G & Andriacchi, TP 1998, 'Knee adduction moment, serum hyaluronan level, and disease severity in medial tibiofemoral osteoarthritis', *Arthritis and Rheumatism*, vol. 41, no. 7, pp. 1233–1240.

Sharma, L, Song, J, Felson, DT, Shamiyeh, E & Dunlop, DD 2001, 'The role of knee alignment in disease progression and functional decline in knee osteoarthritis', *JAMA*, vol. 286, no. 2, pp. 188–195.

Simon, SR, Trieshmann, HW, Burdett, RG, Ewald, FC & Sledge, CB 1983, 'Quantitative gait analysis after total knee arthroplasty for monarticular degenerative arthritis.', *Journal of Bone and Joint Surgery American Volume*, vol. 65, no. 5, pp. 605–613.

Simonsen, EB & Alkjær, T 2012, 'The variability problem of normal human walking', *Medical Engineering and Physics*, vol. 34, no. 2, pp. 219–224.

Smith, AJ, Lloyd, DG & Wood, DJ 2004, 'Pre-surgery knee joint loading patterns during walking predict the presence and severity of anterior knee pain after total knee arthroplasty', *Journal of Orthopaedic Research*, vol. 22, no. 2, pp. 260–266.

Tassani, S & Perilli, E 2013, 'On local micro-architecture analysis of trabecular bone in three dimensions', *International Orthopaedics*, vol. 37, no. 8, pp. 1645–1646.

Thewlis, D, Callary, SA, Fraysse, F & Solomon, LB 2015, 'Peak loading during walking is not associated with fracture migration following tibial plateau fracture: A preliminary case series', *Journal of Orthopaedic Research*, vol. 33, no. 9, pp. 1398–1406.

Thorp, LE, Sumner, DR, Block, JA, Moisio, KC, Shott, S & Wimmer, MA 2006a, 'Knee joint loading differs in individuals with mild compared with moderate medial knee osteoarthritis', *Arthritis and Rheumatism*, vol. 54, no. 12, pp. 3842–3849.

Thorp, LE, Wimmer, MA, Block, JA, Moisio, KC, Shott, S, Goker, B & Sumner, DR 2006b, 'Bone mineral density in the proximal tibia varies as a function of static alignment and knee adduction angular momentum in individuals with medial knee osteoarthritis', *Bone*, vol. 39, no. 5, pp. 1116–1122.

Turner, CH 1998, 'Three rules for bone adaptation to mechanical stimuli', *Bone*, vol. 23, no. 5, pp. 399–407.

Vanwanseele, B, Eckstein, F, Smith, RM, Lange, AK, Foroughi, N, Baker, MK, Shnier, R & Singh, MAF 2010, 'The relationship between knee adduction moment and cartilage and meniscus morphology in women with osteoarthritis', *Osteoarthritis and Cartilage*, vol. 18, no. 7, pp. 894–901.

Wada, M, Maezawa, Y, Baba, H, Shimada, S, Sasaki, S & Nose, Y 2001, 'Relationships among bone mineral densities, static alignment and dynamic load in patients with medial compartment knee osteoarthritis', *Rheumatology (Oxford)*, vol. 40, no. 5, pp. 499–505.

Walter, JP, D'Lima, DD, Colwell, CW & Fregly, BJ 2010, 'Decreased knee adduction moment does not guarantee decreased medial contact force during gait', *Journal of Orthopaedic Research*, vol. 28, no. 10, pp. 1348–1354.

Weidow, J, Tranberg, R, Saari, T & Kärrholm, J 2006, 'Hip and knee joint rotations differ between patients with medial and lateral knee osteoarthritis: gait analysis of 30 patients and 15 controls', *Journal of Orthopaedic Research*, vol. 24, no. 9, pp. 1890–1899.

Weinans, H, Siebelt, M, Agricola, R, Botter, SM, Piscaer, TM & Waarsing, JH 2012, 'Pathophysiology of peri-articular bone changes in osteoarthritis', *Bone*, vol. 51, no. 2, pp. 190–196.

Wen, CY, Chen, Y, Tang, HL, Yan, CH, Lu, WW & Chiu, K 2013, 'Bone loss at subchondral plate in knee osteoarthritis patients with hypertension and type 2 diabetes mellitus', *Osteoarthritis and Cartilage*, vol. 21, no. 11, pp. 1716–1723.

Wilson, JA, Deluzio, K, Dunbar, M, Caldwell, G & Hubley-Kozey, C 2011, 'The association between knee joint biomechanics and neuromuscular control and moderate knee osteoarthritis radiographic and pain severity', *Osteoarthritis and Cartilage*, vol. 19, no. 2, pp. 186–193.

Winter, DA 1984, 'Kinematic and kinetic patterns in human gait: variability and compensating effects', *Human Movement Science*, vol. 3, no. 1-2, pp. 51–76.

Winter, DA 2009, *Biomechanics and motor control of human movement*, John Wiley & Sons, Hoboken, NJ.

Wise, BL, Niu, J, Yang, M, Lane, NE, Harvey, W, Felson, DT, Hietpas, J, Nevitt, M, Sharma, L, Torner, J et al. 2012, 'Patterns of compartment involvement in tibiofemoral osteoarthritis in men and women and in whites and african americans', *Arthritis Care and Research*, vol. 64, no. 6, pp. 847–852.

Yuan, XL, Meng, HY, Wang, YC, Peng, J, Guo, QY, Wang, AY & Lu, SB 2014, 'Bone–cartilage interface crosstalk in osteoarthritis: potential pathways and future therapeutic strategies', *Osteoarthritis and Cartilage*, vol. 22, no. 8, pp. 1077–1089.

Zabala, ME, Favre, J, Scanlan, SF, Donahue, J & Andriacchi, TP 2013, 'Three-dimensional knee moments of ACL reconstructed and control subjects during gait, stair ascent, and stair descent', *Journal of Biomechanics*, vol. 46, no. 3, pp. 515–520.

Zeni, JA & Higginson, JS 2009, 'Differences in gait parameters between healthy subjects and persons with moderate and severe knee osteoarthritis: a result of altered walking speed?', *Clinical Biomechanics*, vol. 24, no. 4, pp. 372–378.

Zeni, JA, Rudolph, K & Higginson, JS 2010, 'Alterations in quadriceps and hamstrings coordination in persons with medial compartment knee osteoarthritis', *Journal of Electromyography and Kinesiology*, vol. 20, no. 1, pp. 148–154.

Zhao, D, Banks, SA, Mitchell, KH, D'Lima, DD, Colwell, CW & Fregly, BJ 2007, 'Correlation between the knee adduction torque and medial contact force for a variety of gait patterns', *Journal of Orthopaedic Research*, vol. 25, no. 6, pp. 789–797.

Zysset, PK, Sonny, M & Hayes, WC 1994, 'Morphology-mechanical property relations in trabecular bone of the osteoarthritic proximal tibia', *Journal of Arthroplasty*, vol. 9, no. 2, pp. 203–216.

Appendix A

Patient Recruitment & Study Allocation

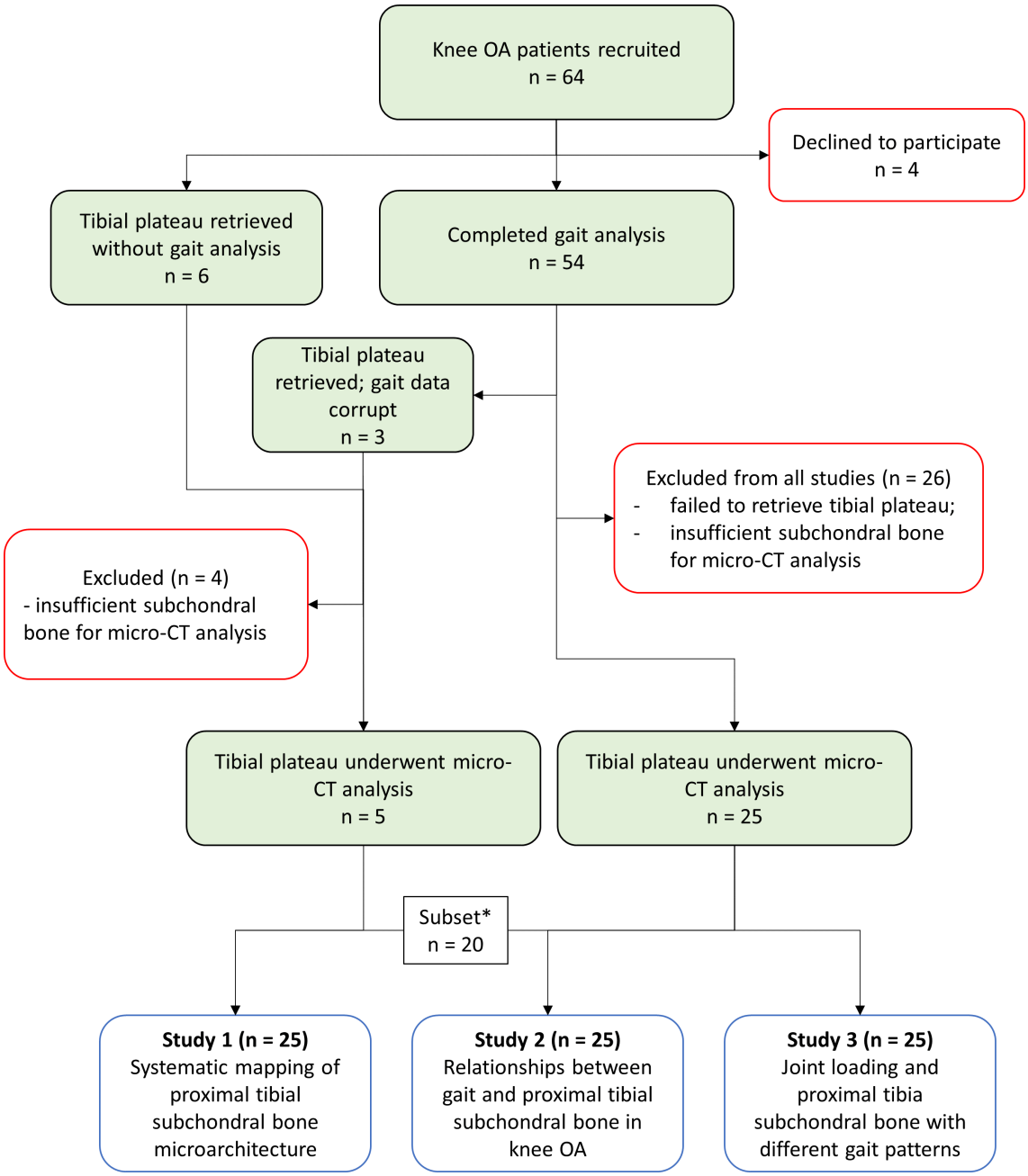

Figure A.1: Flowchart showing patient recruitment and study allocation. Study 1, 2 and 3 were performed in chronological order and so also the patient recruitment. *At the time of Study 1, which looked only at subchondral bone microarchitecture, 20 of the 25 knee osteoarthritis (OA) patients also had undergone gait analysis for Study 2 and 3. Five specimens had no gait data available and as such could not be included in Study 2 and 3. Study 2 and 3 had 5 additional specimens with gait data compared to Study 1